Part One

BISTHIOSEMICARBAZONE LIGANDS

Part Two

PREPARATION AND APPLICATION OF ORGANOTIN POLYMERS

by
Chantelle McRoberts

Graduate Program in Chemistry

Submitted in partial fulfilment
of the requirements for the degree of
Doctor of Philosophy

Faculty of Graduate Studies
The University of Western Ontario
London Ontario
March 1999

Abstract

Part One: Bisthiosemicarbazone Ligands

Several N_2S_2 bisthiosemicarbazone ligands were targeted for chelating ^{99m}Tc. These ^{99m}Tc ligands would be attached to Lisinopril, a receptor specific pharmaceutical, by amidation. In this manner a ^{99m}Tc labelled receptor specific radiopharmaceutical could be prepared, with potential diagnostic application in nuclear imaging.

Several N_2S_2 ligands based on acetylbenzoic acid were prepared. These ligands displayed poor solubility in common organic solvents. As a consequence of the poor solubility, Lisinopril could not be attached to these ligands by amidation. Several N_2S_2 ligands based on pentanedione were also prepared. These ligands displayed much better solubility than the acetylbenzoic acid based compounds. The pentanedione based ligands were prepared by literature procedure and were presumed to be symmetrical compounds. However, characterization of these ligands indicated numerous proton and carbon nonequivalencies in the NMR spectra. A crystal structure determination indicated that a pyrazoline had been synthesized versus the expected linear bisthiosemicarbazone. This pyrazoline formation proved irreversible and bisthiosemicarbazone ligands were abandoned.

Part Two: Preparation and Application of Organotin Polymers

Several novel organotin copolymers have been prepared. These polymers were derived from common copolymer precursors, poly-3 and 4-(2-(dibutylchlorostannyl)ethyl)styrene-co-divinylbenzene-co-styrene. These precursor copolymers were prepared with various loading capacities. As a result, many of the functional derivatives were also prepared with variable loadings. The chlorostannane precursors were converted to organotin oxides, tin carboxylates, tin hydrides, distannanes, and silylstannanes. These

copolymers were prepared for potential solid phase organic chemistry (SPOC) applications. These investigations have provided some insight into the three dimensional copolymer structure.

All of the copolymers prepared have been characterized and preliminary investigation has indicated possible SPOC applications. Tin oxide applications were studied in the most detail. Copolymer-bound tin oxides, as a mixture of stannol and distannoxane, have been shown to catalyze the lactonization of hydroxycarboxylic acids. The polymer-bound catalyst simplifies purification, reducing workup to filtration and trituration. Lactones of 17 and 13 members were successfully prepared, albeit in lesser yields than currently available solution phase organotin reagents. Lactones of 8 and 11 members were not observed with the organotin oxide copolymer.

Keywords: bisthiosemicarbazone, pentanedione, N_2S_2, solid phase organic chemistry, lactonization, hydroxycarboxylic acid

For Wayne and Princess Liddy

Acknowledgements

I will always be grateful to my supervisor and friend, Duncan Hunter. He has provided expert guidance and much needed encouragement during my time at Western. I could not have achieved this milestone without his assistance.

My appreciation goes to members of the Hunter group, both past and present. The original 'core' group deserve special mention, including Len Luyt, Xizhen Zhu, and Cathy Pollock. Cathy, ABBA hasn't been the same since you graduated. Thanks also goes to Robin Martin, who finally saw the light and joined the Hunterites, bringing lots of experience and fancy equipment with him. I will always remember the faculty, staff, and my fellow graduate students fondly. Many people provided assistance during my time in the department. In particular, I am indebted to Ross Davison, Mary Jane Walzak, Dee Jackson, and Bob Berno of Surface Science Western for EDX and XPS analyses. John Vanstone ensured my HPLC was up and running and Ron Maslen was always ready to lend a hand. Thanks to J.J. Vittal for a prompt crystal structure determination and Hilary Jenkins for helping to interpret my results. Special mention goes to Kim Pollard, friend extraordinaire.

I am grateful to Gian Gobbi of Dow Chemical, Hiltrude Grondey of the University of Toronto, and Chris Kirby of the University of Waterloo who collectively ran my solid state NMR samples. The installation of an in-house solid state NMR will certainly be appreciated by the Hunterites!

Finally, I am profoundly grateful to my husband, Wayne, and my family. They have been a constant source of strength and inspiration since I set out on this road.

Table of Contents

List of Tables

List of Figures

List of Abbreviations

ACE	angiotensin converting enzyme
AIBN	azo-bis-isobutyronitrile
CDI	carbodiimide
CNS	central nervous system
COSY	homonuclear correlated spectroscopy
DCC	dicyclohexylcarbodiimide
DEPT	distortionless enhancement by polarization transfer
DMF	N,N-dimethylformamide
DMSO	dimethylsulfoxide
DRIFTS	diffuse reflectance infrared spectroscopy
DVB	divinylbenzene
EDC	(dimethylaminopropyl)ethylcarbodiimide hydrochloride
EDX	energy dispersive xray
EM	effective molarity
EVB	ethylvinylbenzene
HETCOR	heteronuclear correlated spectroscopy
HoBt	hydroxybenzotriazole
HPLC	high performance liquid chromatography
HRMS	high resolution mass spectrometry
IC_{50}	intracellular concentration for 50% binding
LAH	lithium aluminum hydride
LDA	lithium diisopropylamide
LRMS	low resolution mass spectrometry
MAS NMR	magic angle spinning nuclear magnetic resonance
MIBG	m-iodobenzylguandine

PEG	polyethylene glycol
PET	positron emission tomography
PS	polystyrene
RI	refractive index
SPECT	single photon emission computed tomography
SPOC	solid phase organic chemistry
THF	tetrahydrofuran
TLC	thin layer chromatography
TMS	tetramethylsilane
TOCSY	total correlation spectroscopy
TSTU	tetramethylsuccinimidyl tetrafluoroborate
VT	variable temperature

PART ONE

BISTHIOSEMICARBAZONE LIGANDS

Chapter One - Preparation of N_2S_2 Ligands

1.1 Introduction

1.1.1 Nuclear Medicine

Nuclear medicine can be defined as the use of radioactivity for either diagnosis or therapy of various human disease conditions. This area of medical specialization restricts itself to the internalization of radioactivity either by ingestion, injection or inhalation. Typically, radioactive nuclides are introduced into the body as part of a larger radiopharmaceutical. Radiopharmaceuticals are simply pharmaceuticals labelled with a radioactive nuclide in such a manner as to cause minimal interference with the original intended biological activity. Detection of radioactivity within the body is sensitive enough that most pharmaceuticals are administered in sub-therapeutic doses.

Therapeutic nuclear medicine involves the internalization of a radiopharmaceutical and its selective localization within diseased areas such that decay of the radionuclide results in tissue or organ damage. This therapeutic notion, while not yet widely realized, coined the term 'magic bullet' whereby radioactivity could be used to selectively destroy any tumourous growth within the body. Alternatively, a radiopharmaceutical is incorporated into a subject and the distribution, metabolism, and eventual elimination of radioactivity can offer insight into function and physiology with regards to various disease conditions. In this application, diagnostic nuclear medicine holds the promise of increased sensitivity and reduced invasiveness over many conventional techniques. Diagnostic nuclear medicine is much more widely practiced than therapeutic, accounting for approximately 95% of all radiopharmaceuticals produced[1].

Diagnostic nuclear imaging relies heavily on computed tomography to monitor distribution and elimination of radioactivity within the body. These large scintillation cameras provide three dimensional 'maps' of radioactivity within a

test subject. Depending on the type of radionuclide being used, either single photon emission computed tomography (SPECT) or positron emission tomography (PET) is employed. γ- Emitting radionuclides like ^{99m}Tc and ^{123}I use SPECT while positron-emitting nuclides like ^{18}F and ^{68}Ga use PET.

1.1.2 Receptor Specificity

Most pharmaceuticals used in radiopharmaceutical synthesis are receptor specific, meaning they selectively seek and bind to distinct cellular receptors. Radiolabelling these receptor specific pharmaceuticals allows for visualization of the distribution or population of a particular type of receptor. Important for diagnostic purposes, certain disease states result in a preponderance of particular types of cellular receptors. For example, lung granulomatous diseases like sarcoidosis result in an increase in angiotensin converting enzyme (ACE) receptors in lung tissue[2].

A receptor specific pharmaceutical exerts a pharmacological response by binding with a cellular receptor. The structural characteristics of the receptor result in a selective interaction with a complementary molecule. The molecule binding to the receptor active site is classified according to the pharmacological response its binding exerts. An antagonist binds to a receptor and ellicits no biological response. Agonists are those molecules that bind to the receptor and ellicit a biological response. Antagonist or agonist, the binding to the receptor site is selective and discriminatory. Radiolabelling in an obtrusive manner can severely diminish this binding affinity and hence the selectivity of binding. Reduced receptor specificity can lead to non-selective localization of the radiopharmaceutical and hence high background radiation.

IC_{50} values are important indicators for receptor binding specificity in both pharmaceutical and radiopharmaceutical development. An IC_{50} is defined as the concentration of a compound necessary to reduce binding of the native agonist by 50%. A low IC_{50} value, often in the nanomolar range, indicates good

receptor binding affinity for the compound. IC_{50} values for various derivatives of a pharmaceutical will often provide insight towards the favoured radionuclide attachment site. Appropriate attachment sites should result in minimal receptor binding affinity changes upon incorporation of the radionuclide.

1.1.3 Technetium Radiochemistry

Common nuclides for radiolabelling include: ^{13}N, ^{15}O, ^{111}In, ^{11}C, ^{18}F, and various isotopes of iodine. Incorporating ^{123}I and ^{131}I into receptor specific pharmaceuticals is a common approach to radiopharmaceutical synthesis. With a half-life of 13.2 hours, ^{123}I is best suited for diagnosis, while ^{131}I is used for therapeutic applications. Iodine is one of the most clinically used radioisotopes for SPECT nuclear imaging today. Radioisotopes of iodine can be readily incorporated into aromatic ring containing pharmaceuticals by iododestannylation. The iodine isotope binds covalently to the pharmaceutical, contributing only minor changes in overall molecular structure. This typically results in only small changes to receptor binding affinity. Unfortunately ^{123}I and ^{131}I must be produced by a cyclotron or nuclear reactor respectively, limiting both availability and affordability. Ideally, a radiopharmacist would prefer an on-site source of radioactive nuclide for radiopharmaceutical synthesis.

As an alternative to iodine, ^{99m}Tc is well suited for diagnostic imaging procedures. This isotope has a suitably short half-life of 6.02 hours and emission of 140 keV which is appropriate for SPECT imaging. Conveniently, ^{99m}Tc is readily available as the primary decay product of ^{99}Mo. ^{99}Mo, a uranium fission product, decays with a half-life of 67 hours to yield 87% ^{99m}Tc and 13% ^{99}Tc. From the metastable state, ^{99m}Tc decays by γ-emission and internal conversion to the long-lived isotope ^{99}Tc, with a half-life of 2.1×10^5 years. The decay scheme by which ^{99m}Tc is formed and eventually expires is shown in Figure 1.1.

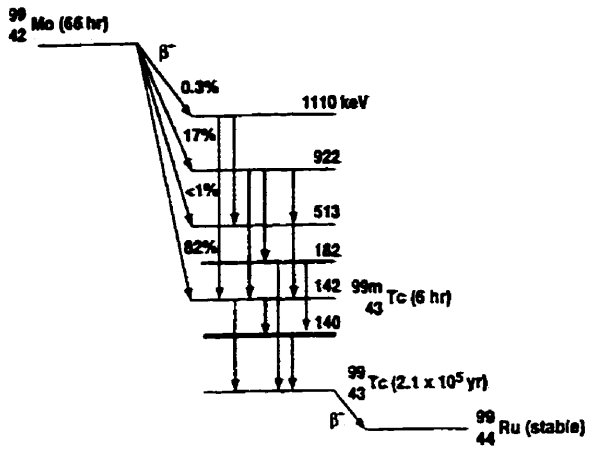

Figure 1.1: Radioactive decay scheme of molybdenum[1]

The availability and affordability of ^{99m}Tc makes it much more convenient for nuclear imaging than ^{123}I and ^{131}I. ^{99m}Tc can be readily prepared from a ^{99}Mo column directly in the radiopharmacy. ^{99}Mo is adsorbed onto silica and upon decay ^{99m}Tc is washed off the column with saline, yielding sodium pertechnetate. With ^{99m}Tc in the +7 oxidation state, reduction to lower oxidation states is necessary for incorporation into radiopharmaceuticals. Even in a lower oxidation state, ^{99m}Tc cannot covalently bond to a pharmaceutical and the metal must be chelated for incorporation. Chelation typically proceeds via electron donating atoms within the chelating molecule, also called a ligand, to give multiple coordinate bonds. The sheer bulk of a chelating group may have adverse effects on the overall structure of the radiopharmaceutical and hence receptor specific binding. The true challenge for the development of receptor specific ^{99m}Tc radiopharmaceuticals lies in the attachment of chelates in a non-obtrusive manner, so as not to disrupt receptor binding affinity.

1.1.4 Receptor Specific Radiopharmaceuticals

Development of radiopharmaceuticals often builds on clinically successful therapeutic drug candidates. With extensive structure activity

research and optimization performed in the drug development stage, much is known about these potential diagnostic imaging agents before radiolabelling is even proposed. The resultant radiopharmaceuticals are administered in sub-therapeutic doses such that no pharmacological effect is observed.

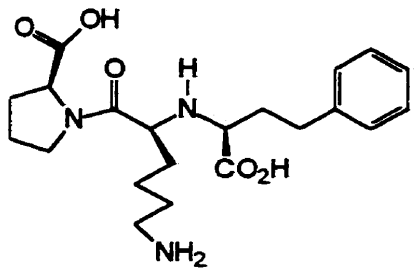

1.1

Lisinopril **1.1** is an angiotensin converting enzyme (ACE) antagonist licensed for therapeutic use by Merck Frosst Pharmaceuticals. This peptidomimetic was originally developed by Patchett and coworkers after extensive structure versus ACE binding affinity studies[3].

The renin-angiotensin system is a major homeostatsis mechanism for regulating arterial pressure[4]. ACE is distributed primarily in the pulmonary vasculature and is involved with two opposing biological molecules, angiotensin II and bradykinin. Angiotensin II and bradykinin provide a control mechanism for arterial pressure. ACE converts angiotensin I to angiotensin II by cleavage of a C-terminal dipeptide. Angiotensin II is a potent vasoconstrictor. ACE is also responsible for the inactivation of bradykinin, which causes vascular dilation. ACE provides a net increase in blood pressure in a two-fold manner, activating a vasoconstrictor and inactivating a vasodilator. Numerous ACE antagonists exist as anti-hypertensive treatments. Lisinopril, a modified dipeptide based on proline and lysine, is one such anti-hypertensive.

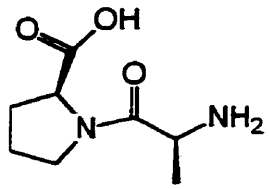

1.2

Lisinopril is a synthetic optimization of Captopril **1.2**, the first ACE inhibitor applied to the clinical treatment of hypertension. The development of Captopril, and ultimately Lisinopril, has allowed much insight into the ACE active site. Numerous structure activity studies have provided valuable information as to the most tolerant location to fix a radionuclide chelate to the pharmaceutical. These studies led researchers to conclude that the S'_1 subsite of the enzyme would dock the lysyl side chain portion of Lisinopril. Derivatization of the lysyl chain of Lisinopril, and subsequent IC_{50} determination yielded only minor losses in binding affinity as shown in Table 1.1.

From these studies it was concluded that the S'_1 pocket of ACE could accommodate considerable changes in steric bulk from the lysyl chain extension. Increasing the bulk of the lysyl chain, as indicated in entries 2-6 of Table 1.1 alters the IC_{50} minimally. Previous studies in this laboratory further confirmed the steric tolerance at the terminal position of the lysine chain. A 3-iodobenzoyl derivative of Lisinopril **1.3** was prepared and demonstrated a stronger binding affinity than Lisinopril itself, with an IC_{50} of 0.6 nm as indicated in entry 7 of the table[5].

Based on these observations, the terminal positon of lysine seemed the most appropriate place to introduce a technetium chelate. It was anticipated the chelate could replace the iodobenzoyl group with minimal effect on the ACE binding affinity. Since the lysine chain of Lisinopril contained a primary amine, linkage to a technetium chelate via amidation appeared practical.

Table 1.1: IC_{50} values for various Lisinopril derivatives

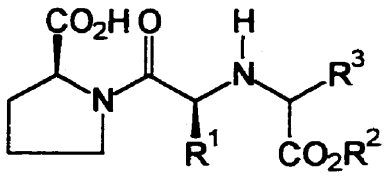

entry	R_1	R_2	R_3	IC_{50} (nM)
1	CH_3	H	*(S)* $(CH_2)Ph$	1.2[3]
2	$(CH_2)_4NH_2$	H	*(S)* $(CH_2)Ph$	1.2[6]
3	$(CH_2)_5NH_2$	H	*(S)* $(CH_2)Ph$	2.8[6]
4	$(CH_2)_4NHCH_3$	H	*(S)* $(CH_2)Ph$	4.6[6]
5	$(CH_2)_4N(CH_3)_2$	H	*(S)* $(CH_2)Ph$	4.5[6]
6	$(CH_2)_4NHC(O)CH_3$	H	*(S)* $(CH_2)Ph$	8.0[6]
7	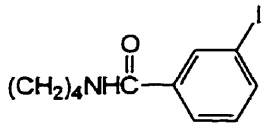 **1.3**	H	*(S)* $(CH_2)Ph$	0.6[5]

Administration of a radiolabelled ACE antagonist could monitor the progress of sarcoidosis based on receptor density within lung tissue or even diagnose this disease once an absolute receptor density was determined. This would be advantageous as sarcoidosis presently requires a biopsy, the physical removal of lung tissue, for diagnosis.

Other receptor specific pharmaceuticals are also available for linkage to a ^{99m}Tc chelate, including MK-329 and tamoxifen. MK-329 is a cholecystokinin receptor anatagonist and could be used as a possible pancreatic imaging agent. Tamoxifen is a estrogen receptor antagonist and could be used as a possible breast and uterine cancer imaging agent. Partial derivatives of both

MK-329 **1.22** and Tamoxifen **1.23** are capable of being conjugated to a ^{99m}Tc ligand via amidation. This research commenced with the arbitrary choice of Lisinopril as the receptor specific bioconjugate. MK-329 and Tamoxifen and their amidation with a ^{99m}Tc ligand were not investigated.

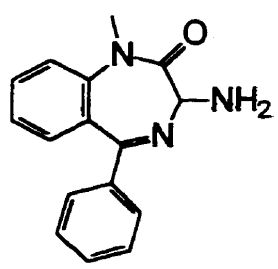

1.22

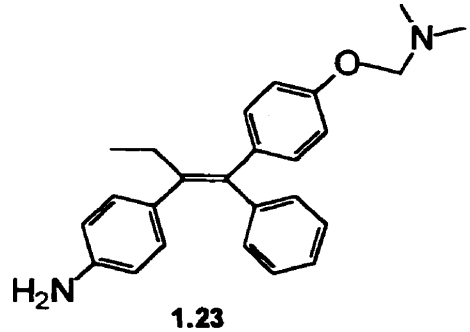

1.23

1.1.5 Existing ^{99m}Tc Radiopharmaceuticals

At present, numerous ^{99m}Tc complexes are used in nuclear medicine as imaging agents. Some examples include ^{99m}Tc-sestamibi **1.24** for myocardial perfusion imaging and ^{99m}Tc-MAG3 **1.25** for renal function studies. These compounds are ^{99m}Tc essential agents, where the technetium complex itself and its three dimensional structure provide only a limited amount of receptor specificity, if any. These chelates, before incorporating ^{99m}Tc, have no receptor selectivity unto themselves making rational development difficult.

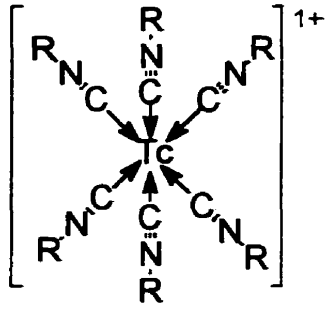

R= $CH_3O-C(CH_3)_2-$

1.24

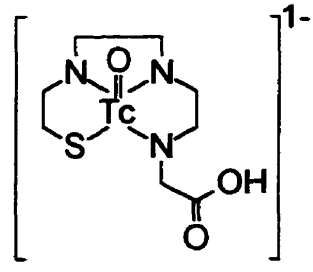

1.25

Radiolabelling small receptor specific pharmaceuticals promises more selective and predictive receptor binding affinity. ^{99m}Tc has also been incorporated within proteins and large macromolecules via non-discriminating attachment of chelators, for example a bleomycin protein has been labelled with ^{99m}Tc using an EDTA chelate **1.26**[7].

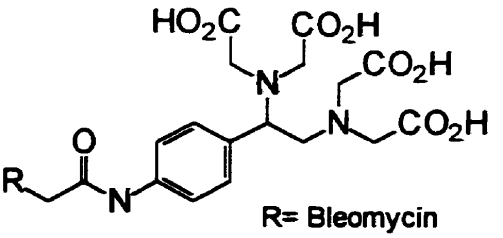

1.26

This labelled protein enjoyed limited success in locating cancerous tumour cells. In general, the sheer bulk of these protein molecules is thought to overcome any negative chelator contributions to binding affinity. Examples of ^{99m}Tc labelled small receptor specific pharmaceuticals, where a chelate can have huge ramifications on binding affinity, are less common in the literature.

Most small receptor specific pharmaceuticals are radiolabelled with ^{123}I. Iodine is easy to incorporate by covalent bond to carbon and its comparatively small size has reduced effects on receptor binding specificty. However, technetium is recognized as a more convenient nuclide for radiolabelling and synthesis of ^{99m}Tc chelated small pharmaceuticals is slowly gaining momentum.

Several reports of receptor specific ^{99m}Tc labelled pharmaceuticals have emerged over the last few years. For instance, 2-nitroimidazole was labelled with a propyleneamine oxime ligand **1.27**[8] for imaging tissue hypoxia.

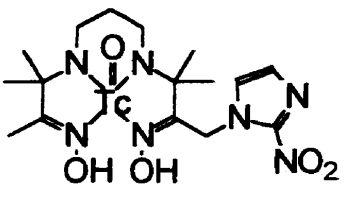

1.27

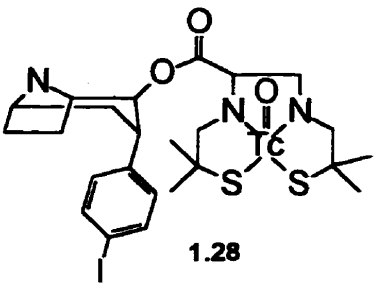

1.28

Dopamine transporter imaging agents for diagnosis of central nervous system (CNS) abnormalities have been reported with ^{99m}Tc labelling of various tropane derivatives **1.28**, **1.29**, **1.30**[9].

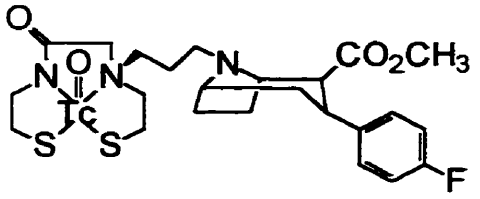

1.29

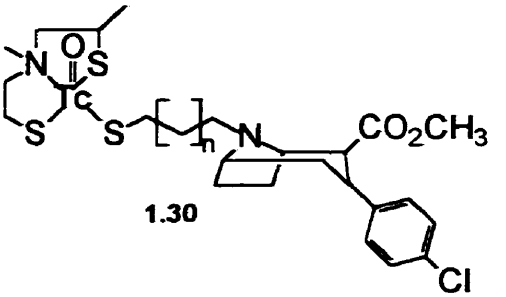

1.30

Even early diagnosis of Alzheimer's disease is being studied[10]. A ^{99m}Tc labelled chrysamine G derivative **1.31** has shown selective binding for neurotic amyloid plaques. The relative density of these amyloid plaques may be an indicator of the onset of Alzheimer's disease. All of these compounds have maintained good receptor specificity in spite of ^{99m}Tc chelator attachment and hold promise as diagnostic tools.

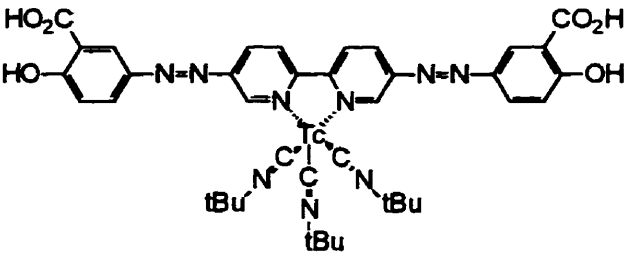

1.31

1.1.6 Project Focus

1.1.6.1 N_2S_2 Chelate Background

The ultimate aim of this research was the preparation of a ^{99m}Tc labelled ACE antagonist, specifically Lisinopril **1.1**, for diagnostic nuclear imaging. Structure activity relationship studies during the development of Lisinopril indicated that the terminal position of the lysyl chain was the most appropriate

position to attach the ^{99m}Tc chelate. Since this terminal position contained a primary amine, linkage of the chelate through an amide was proposed. This necessitated a carboxylate derivative on the ligand that did not participate in ^{99m}Tc chelation, for Lisinopril attachment purposes. Chelation of ^{99m}Tc using a 4-coordinate, 2 nitrogen 2 sulfur system (N_2S_2) was chosen from the outset. Another member of this same research group alternatively focussed on a 4-coordinate, 4 nitrogen system (N4) for the same project aim.

Several N_2S_2 systems had been synthesized and characterized prior to the start of this research project[11]. A survey of the literature is summarized in Table 1.2. All of these ligands are reported to be neutral species. Not all ligands featured a carboxylate moiety for amidation with Lisinopril but provided basic structures which could be further modified for this purpose. Entries 1 and 2 in Table 1.2 contain chiral centres while entry 3 contained a pro-chiral centre. Avoiding chirality in the ligand prior to attachment of the stereospecific Lisinopril would prevent cumbersome purification/resolution steps. As a result, attention centred on entries 4 and 5, the two bisthiosemicarbazone type ligands. These bisthiosemicarbazones **1.32** and **1.16**, as described by Yokoyama, appeared relatively easy to synthesize and lacked a chiral centre.

Bisthiosemicarbazone-based chelators for divalent metals were first described by Petering and Van Giessen[12] as potent anti-tumour agents. Coats went on to describe numerous variations of thiosemicarbazone-based copper (II) chelators[13]. This work was first extended to technetium by Yokoyama[14]. However, there is no indication that Yokoyama investigated covalent attachment of a bithiosemicarbazone N2S2 ligand to a non-peptidal antagonist.

Table 1.2: Existing N_2S_2 Chelates		
Entry		Ligand
1	Fritzberg et al. 1988[11b]	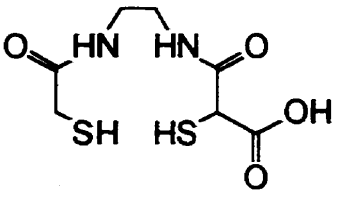
2	Fritzberg et al. 1986[11d]	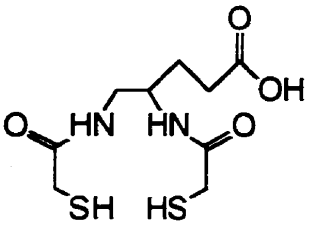
3	Misra et al. 1989[11a]	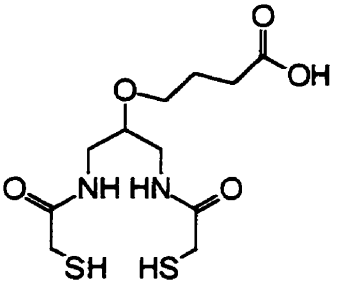
4	Yokoyama et al. 1983[11c] Compound **1.32**	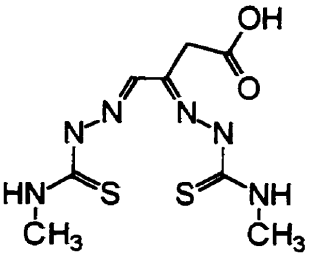
5	Yokoyama et al. 1990[11e] Compound **1.16**	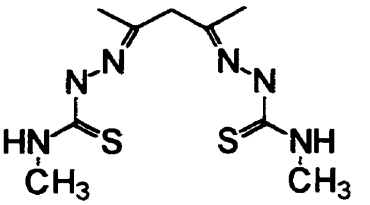

The bisthiosemicarbazone compounds included in Table 1.2 seemed like feasible ligand targets. Compound **1.32** contained a carboxylic acid for covalent attachment of Lisinopril and no chiral centres to complicate purification and characterization. Compound **1.16**, while not containing a carboxylic acid, could be readily derivatized with this functional group.

Delving deeper into the literature surrounding the bisthiosemicarbazone **1.32**, revealed that Yokoyama retracted the synthesis in 1986[15]. He concluded this compound underwent intramolecular cyclization before it could complex with ^{99m}Tc as illustrated in Figure 1.2. The thiosemicarbazide attacked the carboxylate adjacent to the glyoxal, generating a cyclic product. Cyclization could be prevented with insertion of an aromatic spacer between thiosemicarbazide and carboxylate functionalites. The first proposed ligand, based on acetylbenzoic acid, was designed in accordance with these observations.

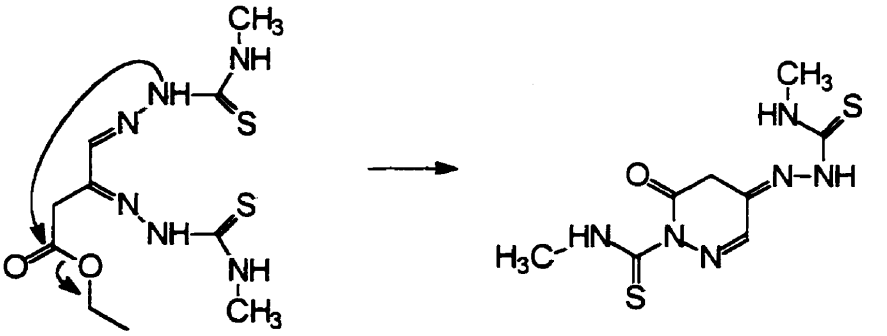

Figure 1.2: Intramolecular cyclization of bis(thiosemicarbazone)

1.1.6.2 Proposed Synthesis of Acetylbenzoic Acid Based N_2S_2 Ligands

The proposed ligand involves the bisthiosemicarbazone of p-carboxyphenylglyoxal and variations thereof. A carboxylic acid provided a site for covalent attachment of Lisinopril prior to radiolabelling with ^{99m}Tc. 4-Acetylbenzoic acid was chosen as the glyoxal precursor. This particular glyoxal precursor had beneficial characteristics. Upon conjugation with Lisinopril, this compound would bear close structural resemblance with the 3-iodobenzoyl

conjugate **1.3** prepared previously in this laboratory[5]. The actual ^{99m}Tc complex replaces the ^{123}I as the radioactive label. In addition, conjugation to the pharmaceutical may require conversion of the acid to an activated ester. The aromatic group could prevent intramolecular cyclization prior to complexing ^{99m}Tc. The proposed synthesis is illustrated in Figure 1.3.

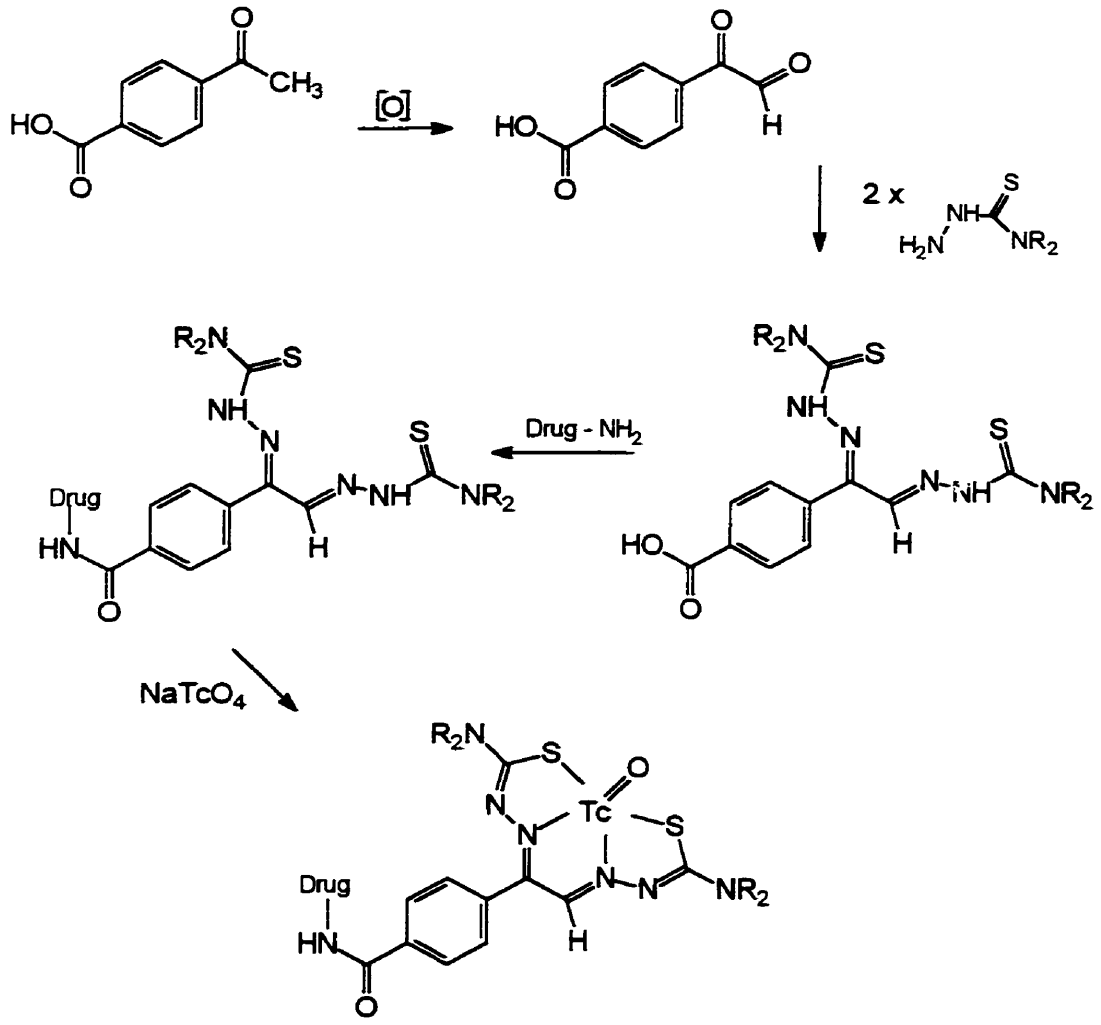

Figure 1.3: Proposed synthesis of acetylbenzoic acid based N_2S_2 ligands

The synthetic scheme requires the oxidation of 4-acetylbenzoic acid to the corresponding glyoxal. This glyoxal is condensed with two equivalents of a thiosemicarbazide derivative. The receptor specific pharmaceutical is attached

via amidation. The entire molecule is then radiolabelled with ^{99m}Tc using pertechnetate. The pertechnetate is reduced to a 6+ state prior to chelation. Typically, technetium prefers a 5+ oxidation state but this would not give a neutral ligand. Yokoyama's thiosemicarbazide based ligands have demonstrated neutrality in the past. In accordance with Yokoyama's ligands, this compound was expected to be overall neutral with technetium in a 6+ oxidation state.

1.1.6.3 Proposed Synthesis of Pentanedione Based N_2S_2 Ligands

The second proposed target ligand involves the bisthiosemicarbazone of pentanedione and variations thereof. Pentanedione must first be alkylated with a short chain carboxylic acid halide to provide a site for amidation with a primary amine containing pharmaceutical. The alkylation of diketones is well documented[16], and was presumed straightforward. Condensation with two equivalents of a thiosemicarbazide would be followed by amidation with Lisinopril yielding a chelated bioconjugate suitable for radiolabelling with ^{99m}Tc as depicted in Figure 1.4.

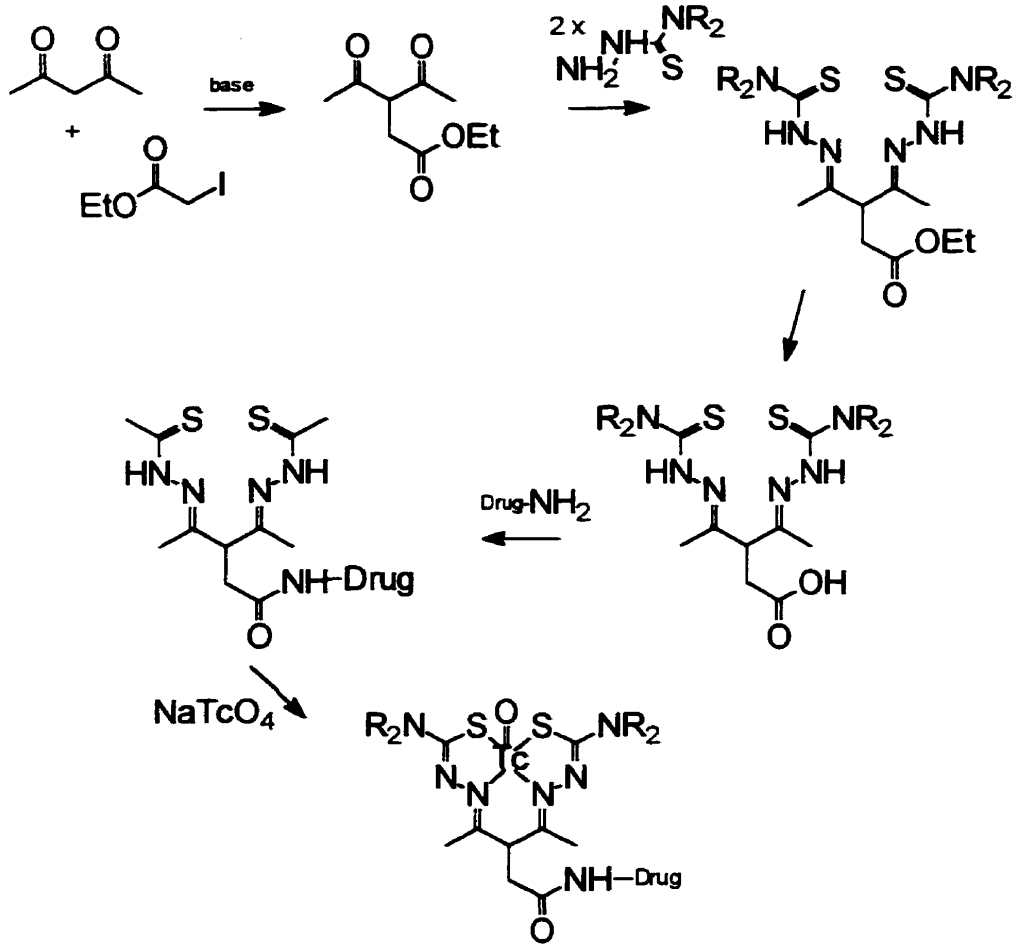

Figure 1.4: Proposed synthesis of pentanedione based N_2S_2 ligands

1.1.7 Coupling Pharmaceutical and Ligand Via Amidation

Countless methods exist for the formation of amide bonds from carboxylic acid and amine precursors. The majority of these methods were initially developed for peptide chemistry but are widely applicable to general synthesis. The direct reaction of a carboxylic acid and amine, without any mediation, will only result in an ammonium salt. However, if the carboxylate carbon is first rendered more electrophilic, an amide can result. All existing amide coupling reagents involve activation of the carboxylate carbon, thus improving the prospects of nucleophilic attack by the amine nitrogen.

Generally, acid anhydrides are more reactive in an electrophilic sense than the corresponding carboxylic acids. Thus, amide coupling reagents activate the carboxylate group by acid anhydride formation. Amide coupling reagents, while all performing the same function, can be divided into two sub-groups based on their mode of activation.

1.1.7.1 Amides Via Acid Anhydrides

The first group of reagents activate the carboxylate group by formation of an acid anhydride of the original carboxylic acid. This group includes carbodiimide reagents as well as thionyl chloride and carbonyldiimidazole. The carbodiimide (CDI) reagents dominate the synthetic field since their cumulative double bond system allows for anhydride formation under relatively mild reaction conditions[17]. CDI reagents include dicyclohexylcarbodiimide(DCC) **1.33**, diisopropylcarbodiimide **1.34**, and the water soluble (dimethylaminopropyl)ethylcarbodiimide hydrochloride (EDC) **1.35**.

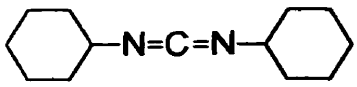

1.33

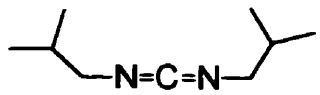

1.34

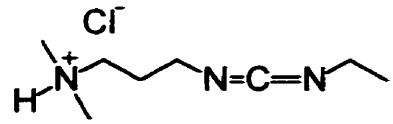

1.35

The proposed route, presented in Figure1.5 for DCC, first gives an O-acylurea. This O-acylurea is attacked by an additional equivalent of carboxylic acid resulting in an anhydride as well as urea and N-acylurea byproducts. For DCC , the dicyclohexylurea byproduct is highly insoluble in common organic solvents and can reportedly be removed by simple filtration. In practice however, the dicyclohexylurea can prove invasive and difficult to remove. The N-acylurea byproduct results from rearrangement of the O-acylurea intermediate. The N-acylurea can represent a significant side reaction,

particularly if the carboxylic acid is used in an equimolar amount relative to the carbodiimide reagent[18]. Alternatively, it is uneconomical to employ an excess of the carboxylic acid reagent relative to the coupling agent. The N-acylurea byproduct is also favoured with long reaction times.

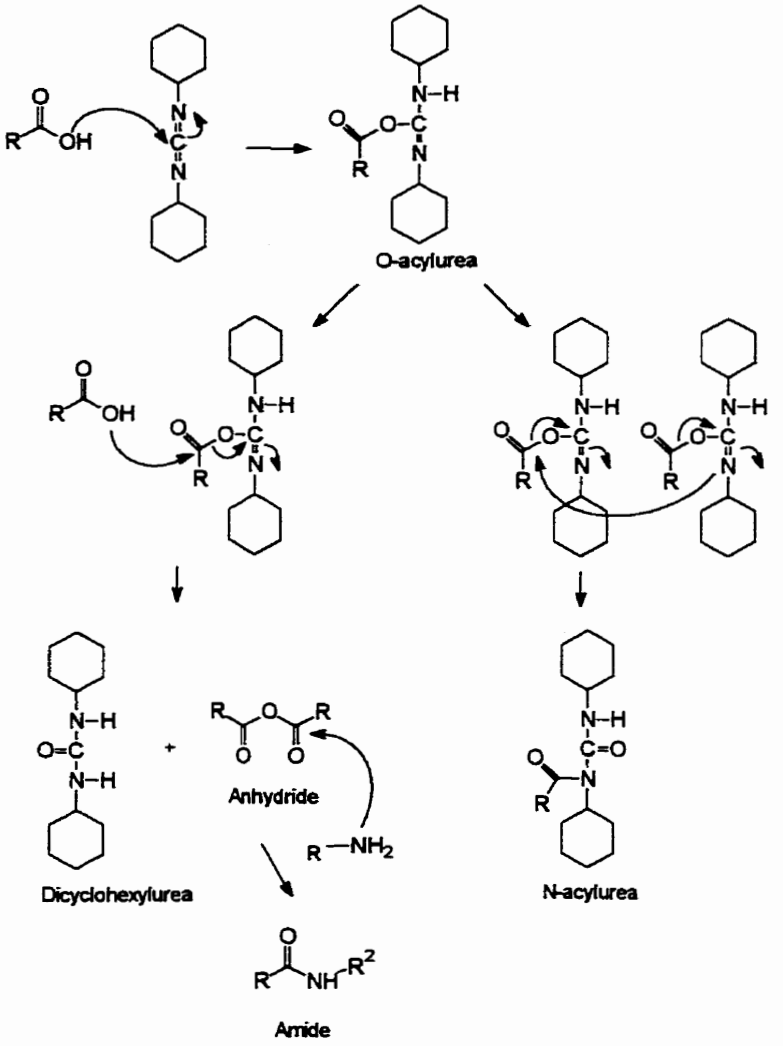

Figure 1.5: Proposed route for amide formation via DCC

1.1.7.2 Amides Via Activated Esters

The second group of amide coupling reagents addresses the N-acylurea byproduct problem associated with CDI mediation. Additives, in combination with CDI reagents, can minimize the N-acylurea by trapping the O-acylurea

intermediate as a mixed anhydride before it can rearrange to the undesirable byproduct. Additives like N-hydroxysuccinimide **1.36** and hydroxy-benzotriazole **1.37** react rapidly with the O-acylurea species yielding an activated ester. This ester is sufficiently reactive to undergo nucleophilic attack by an amine. As in the symmetrical anhydride case, DCC in combination with an additive still results in dicyclohexylurea formation.

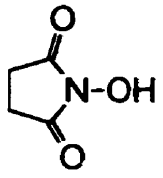

1.36

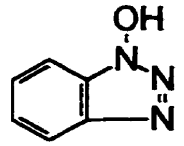

1.37

Other methods, not involving CDI based reagents, also exist for carboxylate activation by ester formation. These non-CDI reagents include ethyl chloroformate **1.38** and 2-succinimido-1,1,3,3-tetramethyl-uroniumtetrafluoroborate (TSTU) **1.42**.

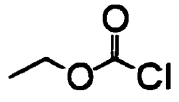

1.38

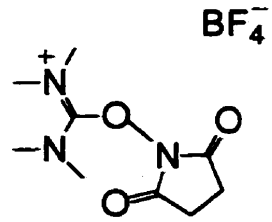

1.42

The carboxylic acid functionality must be deprotonated prior to employing these coupling reagents, usually via triethylamine or diisopropylethylamine. The carboxylate group attacks the coupling reagent to yield an ester, extruding a chloride ion and uronium tetrafluoroborate respectively. The mixed anhydride is thus activated towards nucleophilic attack by the amine, yielding an amide bond. Ethyl chloroformate is

particularly convenient for amide formation since the end products are simply the desired product, carbon dioxide, and ethanol. These end product contaminates are volatile and much easier to remove than the solid ureas encountered with CDI reagents. A proposed route for amide formation via ethyl chloroformate is presented in Figure 1.6.

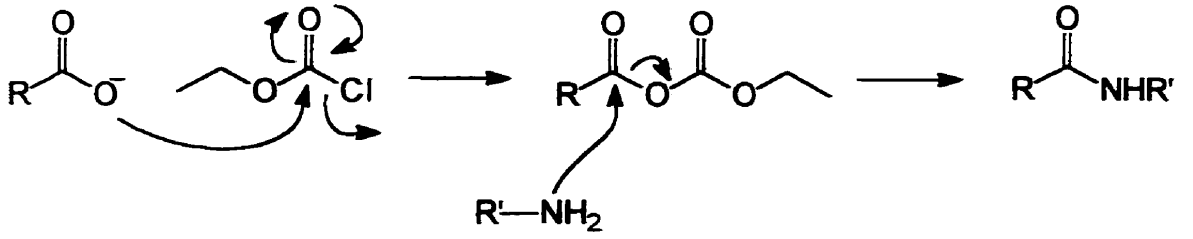

Figure 1.6: Proposed route for amide formation via ethylchloroformate

Many other reagents and methods, too numerous to mention, exist for amide formation. The above mentioned reagents were primarily those considered for amide formation with this project. Reviews on the subject of amide synthesis provide extensive summaries of reagents available[19].

1.2 Results and Discussion

1.2.1 Summary

The objective of this work was to prepare an N_2S_2 bioconjugated chelator for technetium. This chelator would link ^{99m}Tc to Lisinopril **1.1**, a receptor specific pharmaceutical. The linkage required an acid moiety on the chelator for covalent attachment via an amide bond to the pharmaceutical. While this work specifically looked at Lisinopril as the bioconjugate, any receptor specific pharmaceutical containing a primary amine, including MK-329 **1.22** and tamoxifen **1.23** derivatives, would have been suitable.

Several novel N_2S_2 ligands, based on acetylbenzoic acid, have been prepared. ^1H NMR spectroscopic characterization of the ligands incorporating thiosemicarbazide and 4-methylthiosemicarbazide indicated a mixture of two isomers. ^1H NMR characterization of the ligand incorporating 4,4-dimethylthiosemicarbazide indicated only a single isomeric product. All acetylbenzoic acid based ligands displayed poor solubility in common organic solvents. Ligand dissolution often required heating in dilute samples, even for the highly polar dimethylsulfoxide (DMSO). The limited ligand solubility contributed to the failure of amide formation with Lisinopril **1.1**. No amides of Lisinopril and acetylbenzoic acid based N_2S_2 ligands were prepared, despite the variety of amide coupling reagents investigated. Poor ligand solubility and difficulty in preparing any pharmaceutically relevant amide of this ligand led to its demise. This target was abandoned due to the improbability of preparing any bioconjugates that might display sufficient solubility for radiolabelling, biological study, and ultimately use as an imaging agent.

With increased solubility properties in mind, several pentanedione based N_2S_2 ligands were targeted. Various literature methods gave some synthetic success. Although symmetrical products were expected in all cases, characterization of the ligands of thiosemicarbazide, 4-methylthiosemicarbazide, and 4-ethylthiosemicarbazide indicated unexpected

^{1}H and ^{13}C NMR spectral non-equivalencies. A crystal structure determination indicated the ligands had formed a pyrazoline product. The pyrazoline formed through an irreversible, intramolecular cyclization. The irreversibility of this cyclization diminished the usefulness of this N_2S_2 pentanedione based ligand for bioconjugation to Lisinopril **1.1** and radiolabelling with technetium. No alkylation or amidation studies were completed on the pentanedione based ligands once the irreversible cyclization was confirmed.

1.2.2. Acetylbenzoic Acid Based Ligands

1.2.2.1. Design of Ligand

Several N_2S_2 systems have been synthesized and characterized by other researchers as described in Section 1.1.6.1. Bisthiosemicarbazones like those described by Yokoyama were the most suitable targets. These compounds were relatively easy to synthesize and lacked a chiral centre. The lack of a chiral centre avoided a diastereomeric mixture upon attachment of a chiral bioconjugate. The proposed ligands involved the bisthiosemicarbazone of p-carboxyphenylglyoxal and variations thereof. 4-Acetylbenzoic acid was chosen as the glyoxal precursor. The carboxylic acid functionality provided a handle for covalent attachment of a pharmaceutical prior to radiolabelling. The aromatic ring could behave as a spacer between the carboxylate and thiosemicarbazide nitrogen functionalities. The aromatic spacer was incorporated to prevent any intramolecular cyclization within the product as previously illustrated in Figure 1.2.

1.2.2.2. Model Synthesis

Due to the expense of acetylbenzoic acid, acetophenone was used as a model to optimize oxidation conditions. Oxidation of acetophenone was attempted with both oxo-2,2,6,6-tetramethylpiperidinium chloride **1.40**[20] and selenium dioxide[21]. Both of these oxidants are well known in the literature. In

the case of the oxopiperidinium chloride, the ^{1}H NMR spectrum indicated a 36% yield of the desired glyoxal product **1.5**. The ^{1}H NMR spectrum showed a mixture of phenylglyoxal, 2,2,6,6-tetramethylpiperidine, and acetophenone. Yields were determined by ^{1}H NMR spectroscopy with comparison of the methyl on acetophenone to the aldehydic proton of the glyoxal. Phenylglyoxal is known to exist in various states of hydration and this relative yield determination does not take any possible hydration products into account.

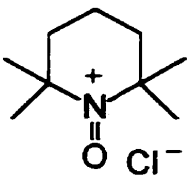

1.40

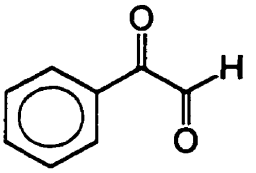

1.5

Selenium dioxide oxidation of acetophenone gave phenylglyoxal **1.5** in presumably quantitative yield as evidenced by the lack of any acetophenone methyl signal in the ^{1}H NMR spectrum. Interestingly, the ^{13}C NMR spectral analysis of **1.5** gave additional carbon signals at 184, 139, 126, 104, and 99.5 ppm. These peaks fall in the expected range for diols and partially hydrated glyoxals. These hydration products were not confirmed or discounted. The one disadvantage with the selenium dioxide oxidation method was the abundance of selenium metal contamination in the final phenylglyoxal product **1.5**. Numerous filtrations through Celite failed to completely remove the contaminant and hence a formal yield has never been determined. Although the oxopiperidinium chloride method gave a more readily purifiable product, selenium dioxide gave the higher yield and was chosen as the oxidant. The acetylbenzoic acid starting material expense dictated the highest yielding method be used. It was assumed that the contaminating metal could be removed in subsequent steps.

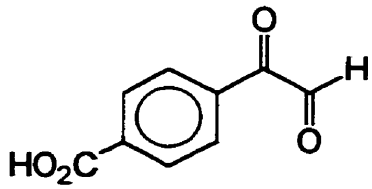

1.8

1.2.2.3. Ligand Syntheses

The selenium dioxide oxidation method was employed with acetylbenzoic acid, yielding *p*-carboxyphenylglyoxal **1.8** in quantitative yield, as judged by the disappearance of all acetylbenzoic acid signals in the crude ^{1}H NMR spectrum. As in the case of phenylglyoxal **1.5**, selenium metal contamination prohibited a formal yield determination. The selenium metal contamination was not deemed detrimental to subsequent synthetic steps and the *p*-carboxyphenylglyoxal was used in its unpurified form for all subsequent reactions.

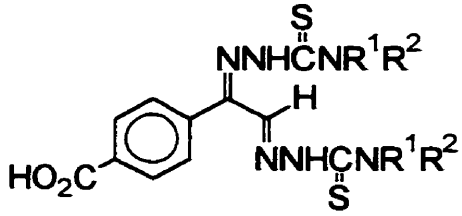

1.9 $R^1, R^2 = H$

1.10 $R^1 = H, R^2 = CH_3$

1.11 $R^1, R^2 = CH_3$

Three acetylbenzoic acid based ligands of thiosemicarbazide were prepared (**1.9**, **1.10**, **1.11**). The thiosemicarbazides differed only in the degree of methylation at the N4-position. The ligands were prepared in purified yields of 42 - 23%. Preparation of the non-methylated *p*-carboxyphenyl-bis(thiosemicarbazone) **1.9** occurred in the highest yield at 42% and the di-methylated *p*-carboxyphenylbis(4,4-dimethylthiosemicarbazone) **1.11** occurred

in the lowest yield at 23%. The low yields are attributable to the poor solubility of the ligands. Inefficient recrystallizations required large volumes of solvents, be it ethanol or methanol, resulting in mediocre yields.

Significant decomposition occurred at melting temperatures for ligands **1.9**, **1.10**, and **1.11**. All three ligands had melting points above 210°C. The combination of low volatility and decomposition made high resolution mass spectrometry (HRMS) exact mass determination difficult. All HRMS for the acetylbenzoic acid based ligands were done by the fast atom bombardment (FAB) method, yielding an M+H molecular ion. No HRMS exact mass was obtained for the non-methylated bisthiosemicarbazone ligand **1.9**. ^{1}H and ^{13}C NMR spectral comparisons with ligands **1.10** and **1.11**, methylated versions for which HRMS exact masses were obtained, confirmed the identity of ligand **1.9**.

All three ligands displayed extremely poor solubility in common organic solvents. The dimethylated *p*-carboxyphenylbis(4,4-dimethylthiosemicarbazone) displayed the best solubility, dissolving in reasonable volumes of THF, DMF, and DMSO. ^{1}H NMR spectroscopic characterization was performed in d_6-DMSO for all ligands. The ^{1}H NMR spectra indicated a mixture of two isomers for the p-carboxyphenylbis(thiosemicarbazone) **1.9** and p-carboxyphenylbis(4-methylthiosemicarbazone) **1.10** ligands. The p-carboxyphenylbis(4,4-dimethylthiosemicarbazone) ligand **1.11** existed as a single isomer in the ^{1}H NMR spectrum.

1.2.2.4 Isomeric Mixtures

Each thiosemicarbazide arm of the N_2S_2 ligands is non-equivalent and thus should result in duplicate amine and amide proton signals. In practice, the ^{1}H NMR spectra of ligands **1.9** and **1.10** were even more complicated. The ^{1}H NMR spectrum for ligand **1.10** is shown in Figure 1.7.

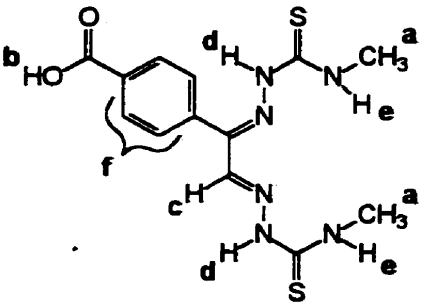

1.10

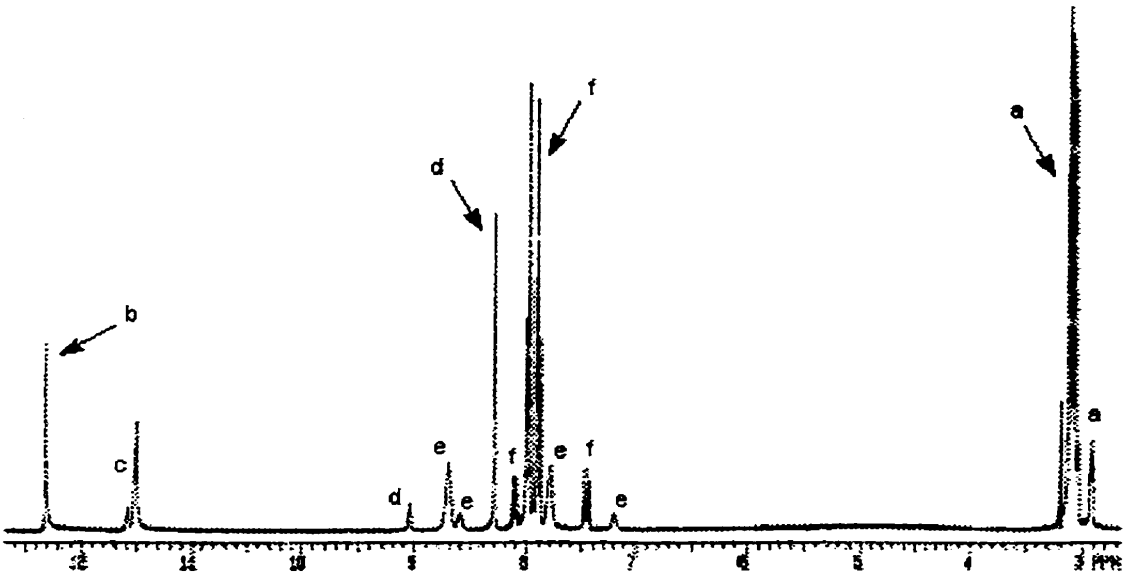

Figure 1.7: ^{1}H NMR of ligand **1.10** at 100°C in d_6-DMSO

The labels on the spectrum coincide with the labels on the compound. Beginning with the methylated secondary amine proton, labelled as 'E', there are four distinct signals in the proton spectrum. Of the four, 2 major multiplet peaks integrated for equal amounts and the remaining 2 minor multiplet peaks integrated equivalently. The major and minor amine multiplets compared to each other in approximately a 4:1 ratio. Conversely the amide protons, labelled as 'D', gave only 2 distinct signals in a non-equivalent ratio. The major signal integrated for 2 protons, as compared to the integration units for the major 'E' signal. The minor 'D' signal integrated for 2 protons as well, based on the

integration units of the minor 'E' signal. Thus, the single amide protons 'D' on each thiosemicarbazide arm of the N_2S_2 ligand were coincident.

Finishing the spectral assignment for Figure 1.7, protons 'A' from the methylated amine are also present in the familiar 4:1 ratio, as are the aromatic protons 'F' and the imine proton 'C'. Based on the integration ratios of major and minor peaks, it was concluded that two isomers of **1.10** exist in an approximate 4:1 ratio. A similar isomeric mixture was observed for the ^{1}H NMR spectrum of ligand **1.9**.

The *p*-carboxyphenylbis(4-methylthiosemicarbazone) ligand **1.10** was studied in detail regarding this isomerization phenomenon. Variable temperature (VT) ^{1}H NMR to 100^{0}C in d_6-DMSO failed to coalesce the ligand to a single isomer although the resolution of both major and minor isomeric signals did improve. ^{13}C NMR spectral analysis including distortionless enhancement by polarization transfer (DEPT) experiments, as well as individual ^{1}H NMR decoupling experiments of both the major and minor isomer proton signals led to the assignments described in the Experimental (Section 1.3). No variable temperature ^{1}H NMR experiments above 100^{0}C were performed.

The isomeric ratio observed in the ^{1}H NMR spectrum for ligands **1.9** and **1.10** may be attributed to syn:anti isomerization at the two newly formed imines in each of the ligands. Syn:anti conversions of imine systems have been observed in the ^{1}H NMR spectra for other molecules[22]. In the N_2S_2 ligand systems, each new imine formed can assume a syn or anti conformation. This could lead to four possible position combinations: syn:syn, anti:syn, syn:anti and anti:anti. Preliminary modelling of ligand **1.9**[23] indicated the most favourable conformation for the external imine nitrogen to be in the anti form. This result seems intuitively correct since the anti form would place the thiosemicarbazide arm of the external imine opposite to the bulk of the molecule, resulting in the least hindered arrangement, as depicted in Figure 1.8.

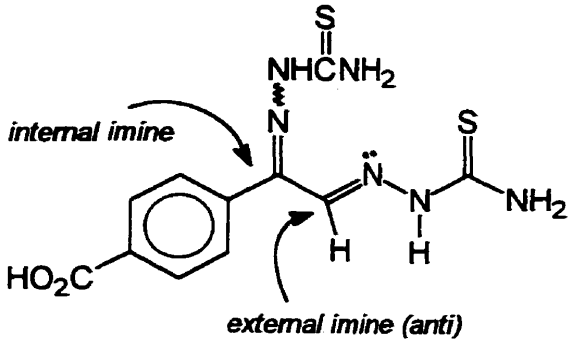

Figure 1.8: External imine fixed in 'anti' conformation for ligand **1.9**

With the external imine fixed in the anti form, the other imine could assume a syn or anti arrangement. Factoring in various rotations about the thioamide bond and carbamate nitrogen bond, six isomers were subjected to semi-empirical geometry optimization[23].

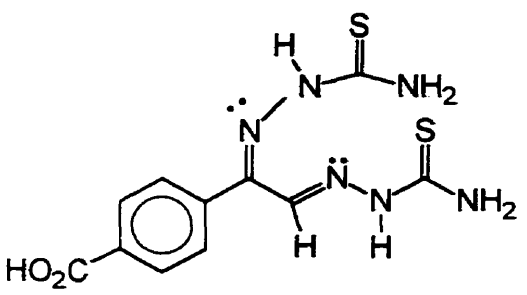

1.9 *anti:anti* (E = -3015.2285)

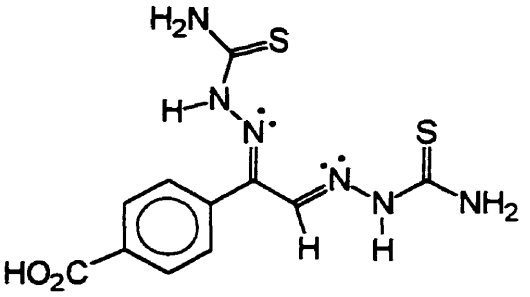

1.9 *syn:anti* (E = -3016.3062)

Figure 1.9: Lowest energy isomers of ligand **1.9**[23]

To this end, 2 isomers, an anti:anti and a syn:anti were found to have the lowest energy of the six possible isomers tested by this method. The energy values associated with these two geometrical isomers of ligand **1.9** are included in Figure 1.9. Based on these geometry optimization studies, the observed ^1H NMR spectra for ligands **1.9** and **1.10** appears to be consistent with anti:syn epimerization at the internal imine position. The two lowest energy

conformations from geometry optimization calculations are so similar in energy that conclusions cannot be made regarding which isomer is present as the major component.

The lack of coalescence in the VT ^{1}H NMR studies at 100^{0}C indicates the isomerization is slow on the NMR timescale and suggests a high energy barrier associated with epimerization for this system. Despite the observed 4:1 isomeric ratio observed in the ^{1}H NMR spectra for ligands **1.9** and **1.10**, ^{13}C NMR spectra for all three ligands gave non-duplicate carbon signals. Specifically, carbon signals were not observed in a 4:1 ratio for each species in the spectrum. This result was curious since ^{13}C NMR spectra typically display increased chemical shift sensitivity relative to ^{1}H NMR spectra.

Not surprisingly, ligands **1.9** and **1.10** also displayed hindered rotation about the thioamide bond. This resulted in non-equivalent protons within each thiosemicarbazide arm for the amines of **1.9** and non-equivalent methyl groups for ligand **1.11**. Non-equivalency due to hindered rotation is well documented in primary and tertiary amide systems[24].

1.2.3. Amide Formation with Acetylbenzoic Acid Based Ligands

1.2.3.1. Model Amides of N_2S_2 Ligands

Effort has focussed on the preparation of amide bonds between the N_2S_2 acetylbenzoic acid based ligands and Lisinopril **1.1**. The high cost and low availability of the Lisinopril bioconjugate necessitated the use of a model amine for investigative amide formation reactions. The model amine, α-phenylethylamine **1.41**, contains a primary amine attached to a chiral centre much like the true bioconjugate. This model amine was inexpensive and spectroscopically straightforward. Amides of α-phenylethylamine, for example **1.12**, conveniently give a distinctive quintet in the ^{1}H NMR spectra due to similar coupling constants for the methyl and amide protons relative to the methine proton, as shown in Figure 1.10. This ^{1}H NMR splitting pattern made

for quick analysis of various amide formation reactions. Amidation reactions primarily focussed on the p-carboxyphenylbis(4-methylthiosemicarbazone) ligand. This ligand was less expensive to prepare than the 4,4-dimethylthiosemicarbazide compound and exhibited a midpoint solubility between the non-methylated and dimethylated ligands.

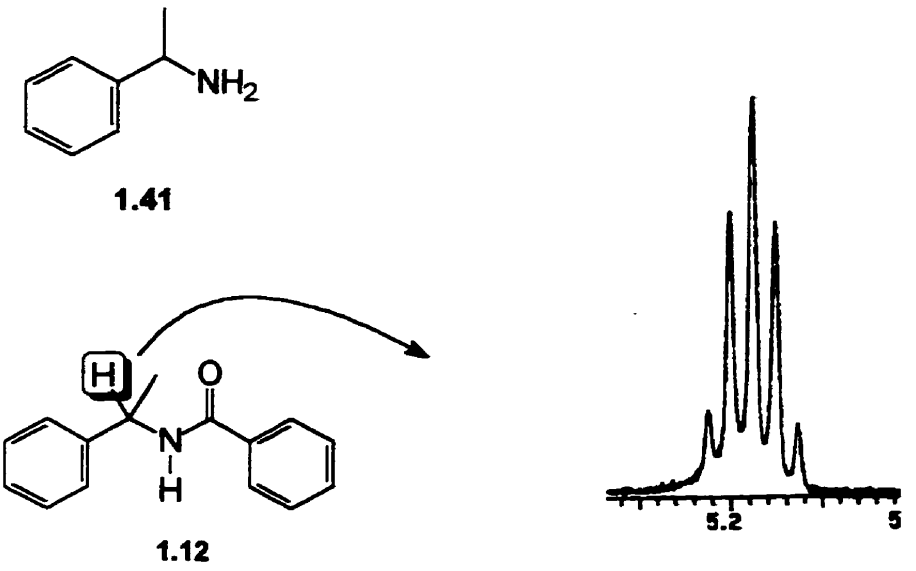

Figure 1.10: Typical amide quintet (^{1}H NMR) from **1.12**

1.2.3.2. Carbodiimide Coupling Reagents

Dicyclohexylcarbodiimide (DCC) is perhaps the most commonly used CDI reagent[25] and so was first investigated for amide formation. Amidation was attempted in different solvents using varying amounts of ligand **1.10**, DCC, and α-phenylethylamine **1.41**. In all instances, no amide formation was observed. ^{1}H NMR analysis of the crude reaction mixtures indicated formation of an amine salt. The amine salt was confirmed by independent synthesis and characterization by ^{1}H NMR spectroscopy. In some instances dicyclohexylurea, a byproduct of DCC coupling reactions, was observed although this may simply be a result of the experimental procedure where excess DCC is quenched with acetic acid[17].

For subsequent investigations, the p-carboxyphenylbis(4-methylthiosemicarbazone) ligand **1.10** was replaced with benzoic acid in an effort to determine the best conditions for DCC mediated amide formation. This series of reactions, for the amide product of benzoic acid and phenylethylamine **1.12** is summarized in the Experimental (Section 1.3). The yields were determined by ^{1}H NMR using benzyl alcohol as an internal standard. The benzylic methylene protons of benzyl alcohol were compared to the quintet integration of the amide products to give a percentage yield for each different set of reaction conditions. Stoichiometric ratios, addition order, and reaction times were varied.

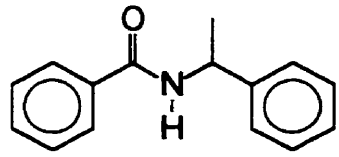

1.12

The optimized conditions from these studies were applied to the p-carboxyphenylbis(4-methylthiosemicarbazone) **1.10** ligand to prepare the amide **1.13**. Unfortunately, no amide formation was observed with the optimized method. In light of this disappointment, other solvents and starting material amounts were used as indicated in Table 1.3. No amide formation was observed under these varied reaction conditions.

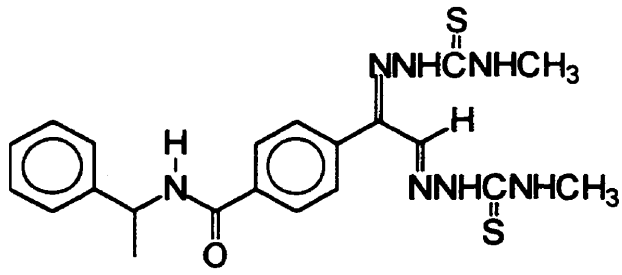

1.13

Table 1.3: Attempted synthesis of amide 1.13	
Solvent	Starting Material Ratios Ligand:DCC:Amine
CH_2Cl_2	1:1:1
THF	1:1:1
CH_2Cl_2 / THF	1:1:1
CH_3CN	2:1:1
Acetone	2:1:1
DMF	2:1:1
$CHCl_3$	2:1:1

It has been reported that both the first carboxylic acid addition to DCC giving the O-acylurea, and the second acid addition to give the acid anhydride are both dependent on solvent polarity[26]. The rate constants for both the O-acylurea and acid anhydride formation rely on breaking the acidic O-H bond of the acid as the rate determining step. Changing solvent polarity changes the relative acid strength and hence the strength of hydrogen bonding. Balcom and Petersen[26] came up with a generalization whereby the reaction would be faster and the anhydride yield better in the solvent for which the acid was only slightly soluble. As explained in Section 1.1.7.1, the acid anhydride is the species which the amine attacks to yield an amide bond.

The experimental results indicate that the solubility of the ligand was playing a role in amide formation. Ideal conditions for amide formation via DCC had been determined by model studies with benzoic acid and α-phenylethylamine **1.41**. These conditions were not compatible with the p-carboxyphenylbis(4-methylthiosemicarbazone) ligand **1.10** and hence no amides were prepared using this carbodiimide coupling reagent.

Carbodiimide coupling reagents in combination with additives such as N-hydroxysuccinimide (NHS) **1.36** were also examined. DCC and NHS were applied with dioxane as solvent to prepare the activated ester of ligand **1.10**. Attempts were made to isolate the succinimidyl ester from the reaction mixture to determine if the activated ester was indeed forming prior to amine addition. Characterization of the resulting crude product gave some spectral evidence for the NHS ester of the ligand but HRMS failed to confirm its synthesis.

1.2.3.3. Other Amidation Methods

While CDI reagents are most commonly used for amidation, many other coupling reagents exist. A survey of the literature reveals many exotic reagents including 2-succinimido-1,1,3,3-tetramethyluronium tetrafluoroborate (TSTU) **1.42**[27], 2-(1-H-bezotriazole-1-yl)-1,1,3,3-tetramethyluronium hexafluorophosphate (HBTU) **1.39**[28], and sulfuryl chloride fluoride **1.43**[29].

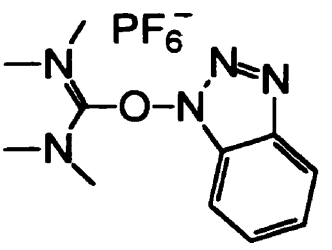

1.39

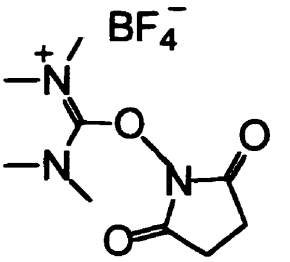

1.42

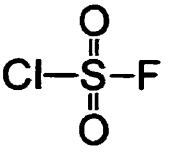

1.43

This study of non-CDI based amidations of p-carboxyphenylbis(4-methylthiosemicarbazone) **1.10** and α-phenylethylamine **1.41** began with the more pedestrian ethyl chloroformate **1.38**[29].

Ethyl chloroformate reacts with the deprotonated carboxylic acid to generate an activated ester. Ethyl chloroformate has several advantages over CDI based reagents. Specifically, the insoluble urea resulting after CDI amidation is eliminated, instead giving volatile byproducts for more convenient purification. Perhaps most important for the N_2S_2 ligand solubility problems,

THF is the favoured solvent system. This is one of the few coupling methods that recommends a polar solvent system like THF.

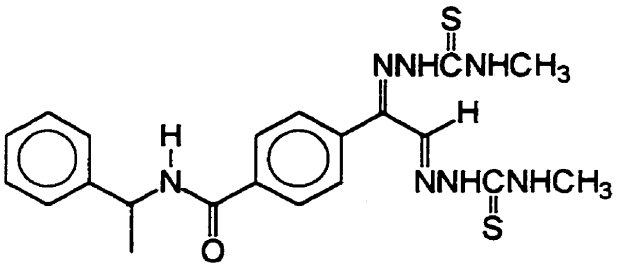

1.13

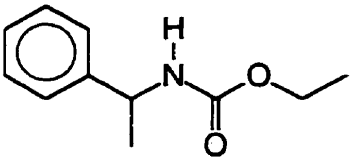

1.44

Reaction of the ligand **1.10** with ethyl chloroformate in the presence of triethylamine, and subsequent addition of α-phenylethylamine **1.41** yielded the desired amide **1.13**. This was the first instance of successful amidation of the p-carboxyphenylbis(4-methylthiosemicarbazone) ligand. The amidation proceeded in low yield with a mixture of products as observed in the ^{1}H NMR spectrum. A mixture of four compounds: the starting ligand **1.10**, the desired amide **1.13**, the amide of ethyl chloroformate **1.44**, and the amine salt, were all present in the ^{1}H NMR spectrum despite purification by preparative layer chromatography. The identity of the amine salt and amide of ethyl chloroformate **1.44** were confirmed by independent synthesis. The ethyl chloroformate amide presumably arose from the incomplete reaction of the coupling reagent with ligand **1.10**. Upon addition of the α-phenylethylamine, nucleophilic attack of ethyl choroformate ensued. This is further confirmed by the presence of unreacted p-carboxyphenylbis(4-methylthiosemicarbazone) **1.10**.

Since the reaction was performed at 0^{0}C, it was felt the low reactivity of the ligand could be addressed. Ethyl chloroformate coupling was deemed a successful candidate for the ligand/Lisinopril amidation. In light of this success, the more exotic coupling reagents were not investigated for model α-phenylethylamine amidation.

1.2.3.4. Model Amides of Lisinopril

Since some success had been realized with model amides of the N_2S_2 ligands, attention turned to Lisinopril **1.1**. We initially required a ^1H NMR diagnostic for successful amide bond formation. Both Lisinopril and the N_2S_2 ligands presented quite complicated ^1H NMR spectra. It was questioned whether conversion from the individual acid and amine moieties to a single amide bond would demonstrate any significant diagnostic peak in the ^1H NMR spectrum.

Conveniently, an amide of Lisinopril and m-iodobenzoic acid, had been previously reported in our laboratory[5]. This synthesis was repeated. m-Iodobenzoic acid was activated as the NHS ester **1.45** and reacted with Lisinopril to yield a bioconjugate amide **1.3** for spectral characterization purposes. The previous report of this synthesis had included only a partial characterization by ^1H NMR although HRMS confirmed its preparation.

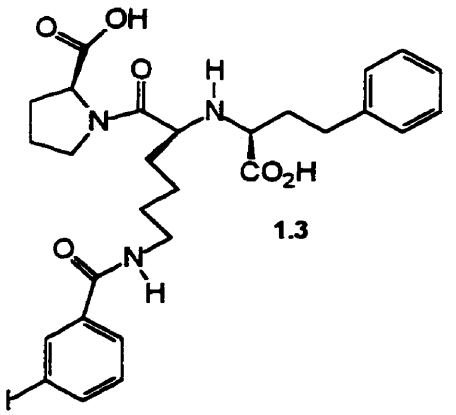

1.3

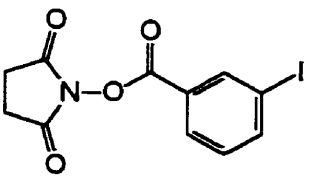

1.45

The spectra resulting from our preparation of this amide were sufficiently complex to make spectral diagnosis of the newly formed amide **1.3** nearly impossible. ^1H NMR characterization of Lisinopril itself became necessary. Lisinopril **1.1** was fully characterized by a combination of ^1H NMR , ^{13}C distortionless enhancement by polarization transfer (DEPT), ^1H-^{13}C heteronuclear correlation (HETCOR) and ^1H-^1H homonuclear correlation

(COSY) spectroscopy.

The ^{1}H NMR assignments concluded from this study are shown in Table 1.4 and coincide to alphabetical labels on structure **1.1**. Assignments for the lysyl side chain were confirmed with ^{1}H-^{1}H total correlation (TOCSY) spectroscopy. The lysyl side chain characterization was most necessary as an amide would presumably alter chemical shifts in this area. The complete characterization, including spectra and an accompanying explanation has been included in Appendix A.

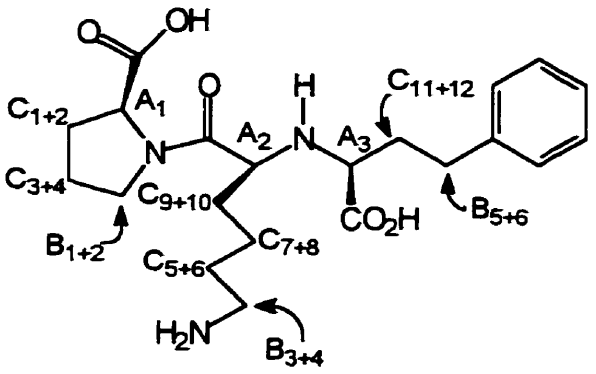

1.1

Table 1.4: ^{1}H NMR characterization of Lisinopril 1.1 in d_4-methanol				
Proton	Chemical Shift (ppm)		Proton	Chemical Shift (ppm)
A_1	1H, m, 4.40		C_{1+2}	1H, m, 2.2 1H, m, 1.95
A_2	1H, m, 4.17		C_{11+12}	2H, m, 2.13
A_3	1H, m, 3.35		C_{5+6} C_{9+10}	4H, m, 1.70
B_{1+2}	2H, m, 3.58			
B_{3+4}	2H, m, 2.95		C_{3+4} C_{7+8}	4H, m, 1.95
B_{5+6}	2H, m, 2.75			

Lisinopril characterization led in turn to the ^{1}H NMR characterization of the m-iodobenzoyl amide product. The ^{1}H NMR spectrum of **1.3** indicated a shift of protons B $_{3+4}$ from 2.95 ppm in Lisinopril to 3.4 ppm in the amide product. This change of 0.45 ppm is reasonable for a methylene group adjacent to a primary amine converting to an amide. This change in protons B $_{3+4}$ was also confirmed by COSY and TOCSY spectroscopy. Since the diagnostic shift of protons B $_{3+4}$ had been determined for amide formation, preparation of the desired amide **1.21**of Lisinopril and the N_2S_2 ligand was attempted.

1.2.3.5. Target Amide of N_2S_2 Ligand and Lisinopril

The ethyl chloroformate amidation method, successful for α-phenylethyl-amine, was applied to p-carboxyphenylbis(4-methylthiosemicarbazone) **1.10** and Lisinopril **1.1**. Although the ligand displayed good solubility in THF, Lisinopril was only slightly soluble in this solvent system. Addition of Lisinopril after initial formation of the ethyl formate activated ester immediately resulted in a suspension. The reaction was left to stir for 2 hours at room temperature and then filtered, re-isolating Lisinopril as a solid. The reaction filtrate yielded an oily solid and its poor solubility prevented purification by recrystallization. ^{1}H NMR spectroscopy indicate a mixture of two compounds, Lisinopril and presumably the desired amide **1.21**. The diagnostic 0.45 ppm shift of protons B $_{3+4}$ from Lisinopril was not apparent.

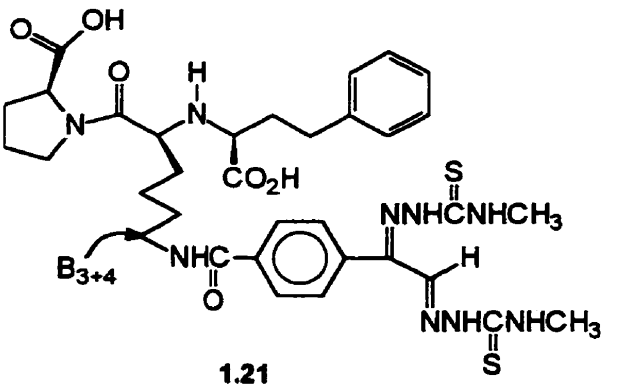

1.21

Poor solubility necessitated spectral analysis in d_6-DMSO versus the amide diagnostic study completed in d_4-methanol. A new peak integrating for 2 protons relative to the ligand was observed at 3.25 ppm. This new peak was neither attributable to Lisinopril or unreacted ligand. This represented a 0.55 ppm shift of protons B_{3+4} in Lisinopril which is still reasonable for a methylene group conversion from amine to amide. The conclusion regarding this new peak as an amide diagnostic was only speculative since the product was never fully purified. HRMS failed to confirm the preparation of the bioconjugate ligand amide **1.21**. Low resolution mass spectrometry (LRMS) indicated the M+H peak for Lisinopril but no larger fragments were observed. This result may be indicative of the involatility of larger fragments like the amide product however it was construed as failure of the amidation method. The scant ^{1}H NMR spectral evidence was presumed to be a coincidental impurity, entirely feasible since the recrystallization and ultimate separation of the amide **1.21** was never realized. This same method was repeated two more times with small additions of DMF to the solvent system to improve solubility and longer reaction times respectively. Neither modification gave as strong evidence for amidation as the initial attempt.

Other amide coupling reagents were applied to the Lisinopril N_2S_2 ligand amide target **1.21** including DCC with HOBt **1.37** and TSTU **1.39**. Neither of these methods indicated formation of the desired amide. The failure of these amidation reactions and thus failure to prepare the target molecule, were attributed to the restricted solubility of both Lisinopril **1.1** and the p-carboxyphenylbis(4-methylthiosemicarbazone) ligand **1.10**. This solubility was deemed 'mutually exclusive' in terms of the amidation methods attempted.

1.2.4. Pentanedione Based Ligands

1.2.4.1 Design of Ligand

Failure to form an N_2S_2 bioconjugate of Lisinopril was attributed in large

part to the poor solubility of the acetylbenzoic acid based ligands. It became obvious that improved solubility would be necessary for the N_2S_2 bioconjugate amidation to proceed. As for the case of the acetylbenzoic acid based ligands, a straightforward synthesis of a non-chiral ligand was desired. Non-chirality in the ligand would prevent diastereomeric mixtures upon bioconjugation. The proposed scheme is presented in Figure 1.11.

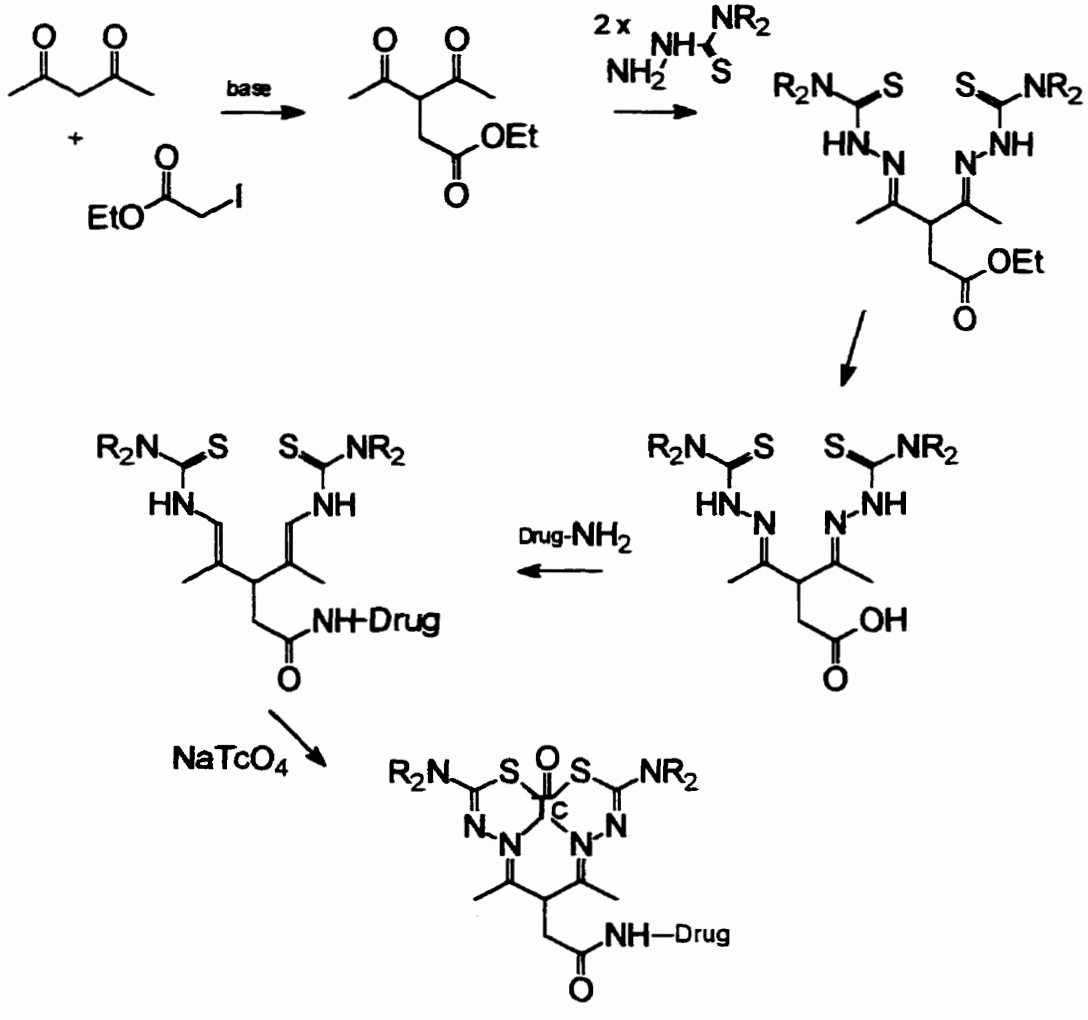

Figure 1.11: Proposed synthesis of pentanedione based N_2S_2 ligands

Bisthiosemicarbazones of pentanedione, with numerous preparations in

the literature including Yokoyama's report of compound **1.16**[11e], were targeted. These molecules would be symmetrical and alkylation with various short chain carboxylic acid halides would provide a route for amidation with the Lisinopril bioconjugate. In addition, chirality would only be introduced into the product upon the attachment of the pharmaceutical due to the symmetrical nature of the alkylated product. It was also proposed that the absence of an aromatic ring, unlike those ligands based on acetylbenzoic acid, would improve the solubility characteristics.

1.2.4.2 Initial Syntheses

Several literature methods existed for preparation of 2,4-bisthiosemicarbamoylpentanediones like **1.16**,**1.17**, and **1.18**. The simplest preparation, reported by Gingras[32] in 1962, mixes two parts thiosemicarbazide and one part dione in refluxing aqueous acid. This preparation has spanned the generations, most recently being applied by El-Asmy in 1989[33]. None of the reports of this direct preparation method, from 1962 to 1989, included NMR spectroscopic characterization of the resultant product. In our hands, direct reaction of thiosemicarbazides with 2,4-pentanedione failed. Specifically, reaction of 2,4-pentanedione with thiosemicarbazide, 4-methylthiosemicarbazide, and 4-ethylthiosemicarbazide in either 0.1N hydrochloric acid or 20% acetic acid resulted in recovery of starting materials. The recovery was confirmed by mixed melting point for the thiosemicarbazide reaction and ^{1}H NMR spectroscopy for the 4-methyl-, and 4-ethylthiosemicarbazide reactions. In light of this preparative failure, several contradictions in the literature became apparent regarding 2,4-bisthiosemicarbamoylpentanedione ligands.

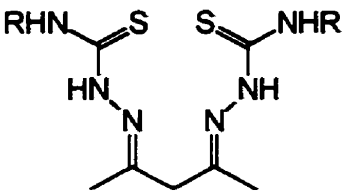

1.16 R=CH3
1.17 R=CH2CH3
1.18 R=H

1.2.4.3. Modified Syntheses

A more extensive literature search revealed a radically different preparation for 2,4-bisthiosemicarbamoylpentanedione ligands **1.16**, **1.17**, and **1.18**. O'Callaghan[34] reported the preparation of pentanedione ligands with various N4-substituted thiosemicarbazides including methyl, ethyl, cyclohexyl and phenyl groups. As illustrated in Figure 1.12, a 1:2 adduct of ethylene diamine and pentanedione **1.14** was prepared and then quantitatively converted to the 1:1 adduct **1.15** with 20% acetic acid. This 1:1 adduct was condensed with two equivalents of a thiosemicarbazide at reflux. A crystalline product precipitated out upon cooling. O'Callaghan characterized each of these products by melting point and elemental composition.

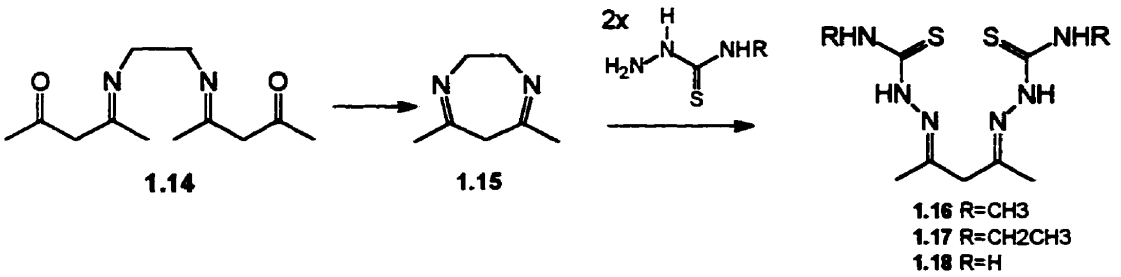

1.14 **1.15**

1.16 R=CH3
1.17 R=CH2CH3
1.18 R=H

Figure 1.12: O'Callaghan's[34] preparation of pentanedione ligands

This same preparation was repeated by Yokoyama with 4-methylthiosemicarbazide[11e] to prepare ligand **1.16** for a technetium chelate. Yokoyama isolated a crystalline product by this method with the same melting point and elemental composition as the original O'Callaghan product. In

addition, this product was characterized by ^{1}H NMR spectroscopy. The assignments from the ^{1}H NMR spectrum are included in Table 1.5.

On close examination, the spectral data did not appear to match the proposed product. The product should be symmetrical with equivalent methyl groups on the dione fragment. In addition, the amide protons of each thiosemicarbazide arm should be equivalent. The spectral data included in Table 1.5 clearly shows separate chemical shifts for each dione methyl group (entries 1 and 2) as well as separate thiosemicarbazide amide protons (entries 4 and 5).

Clearly the product structure assigned to **1.16** was not correct. The mis-identification was further confirmed when Yokoyama radiolabelled this product. Upon incorporation of ^{99m}Tc, two radioactive products were obtained as evidenced by HPLC analysis. Clearly, radiolabelling a symmetrical product should only result in a single radioactive compound.

Table 1.5: Yokoyama's[11e] ^{1}H NMR characterization of 1.16 (d_6-DMSO)

Entry	Chemical Shift (ppm)	Assignment
1	1.74	3H, s, $C\underline{H}_3$
2	1.97	3H, s, $C\underline{H}_3$
3	2.90	6H, d, $NHC\underline{H}_3$
4	6.41	1H, s, $N\underline{H}$
5	7.75	1H, s, $N\underline{H}$
6	8.19	2H, d, $N\underline{H}CH_3$

Yokoyama published a second technetium ligand paper using this 2,4-bisthiosemicarbamoylpentanedione preparation[35]. This paper detailed the synthesis of 2,4-bis(4-methylthiosemicarbamoyl(3,3-dimethylpentanedione))

1.46. Using the same method as the 1990 preparation, a crystalline product was isolated and characterized by melting point, elemental analysis, and ^{1}H NMR spectroscopy. Once again, the spectral data did not fit the proposed symmetrical structure. As with the previous compound, the dione methyl groups were nonequivalent as were the thiosemicarbazide amide protons. It appears that this compound was also mis-identified on the basis of the ^{1}H NMR spectrum. Our own synthetic studies ensued to determine which method, if any, actually led to the synthesis of authentic **1.16**, **1.17**, and **1.18**.

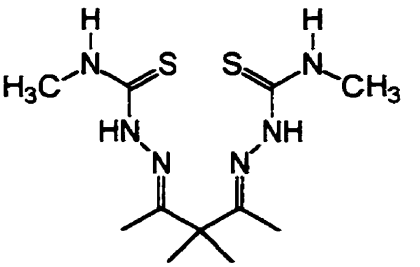

1.46

O'Callaghan's original ethylene diamine mediated synthesis[34] was repeated with thiosemicarbazide, 4-methylthiosemicarbazide, and 4-ethylthiosemicarbazide. In each instance, crystalline product was isolated with melting points similar to the literature. Exact mass determination by HRMS were correct for the anticipated products. Spectroscopic characterization of the experimental products yielded ^{1}H and ^{13}C NMR spectra more complicated than the anticipated symmetrical products would suggest. For example in Figure 1.13, the ^{1}H NMR spectrum ($CDCl_3$) for the 4-methylthiosemicarbazone ligand **1.16** showed 10 sets of signals rather than the anticipated five. As indicated in the spectrum, there was a distinctive AB pattern for the pentanedione methylene protons and non-equivalent methyl protons for both the dione and thiosemicarbazide arms. The spectra obtained for this product were even more complicated than Yokoyama's mis-interpreted ^{1}H NMR data summarized in Table 1.5. Similarly, the ^{13}C NMR spectrum showed nine separate signals

instead of the anticipated five had the product been symmetrical as expected.

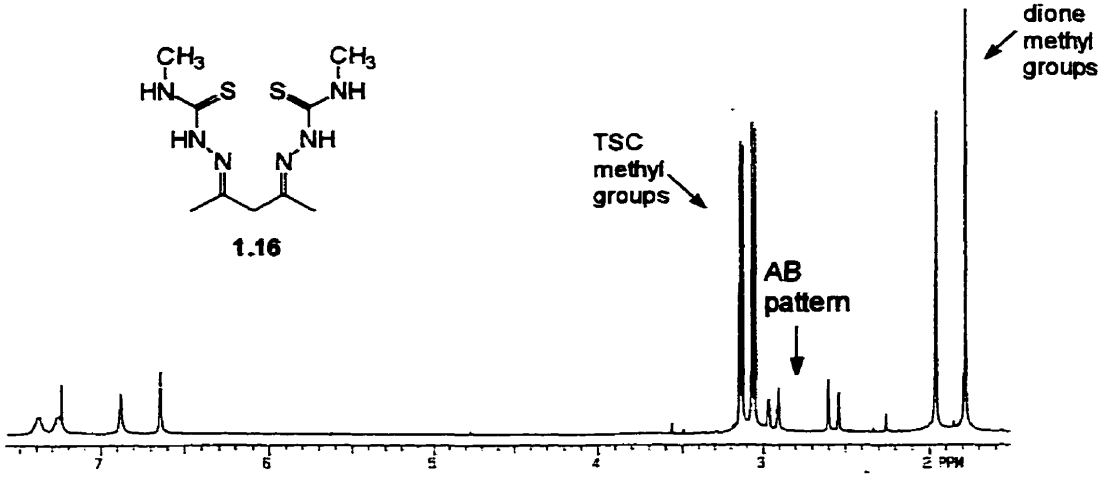

Figure 1.13: ^{1}H NMR spectrum of **1.16** in $CDCl_3$

The pentanedione ligand products of thiosemicarbazide **1.18** and 4-ethylthiosemicarbazide **1.17** showed analogous NMR patterns. Clearly we had not prepared the symmetrical product both O'Callaghan and Yokoyama had presumed. Because of the confusion already present in the literature, we obtained a single crystal X-ray structural determination for the 4-methylthiosemicarbazide pentanedione product **1.16**.

1.2.4.4. Crystal Structure Determination

A single crystal X-ray structure determination, of the product of 4-methylthiosemicarbazide and 2,4-pentanedione mediated by ethylene diamine, revealed an intramolecular cyclization product as depicted in Figure 1.14.

The cyclization would account for the ^{1}H and ^{13}C NMR spectra of this previously assumed symmetrical product. This finding agreed with a published account of a pyrazoline ring forming via yet another preparation method[36]. The crystal structure is shown in Figure 1.15.

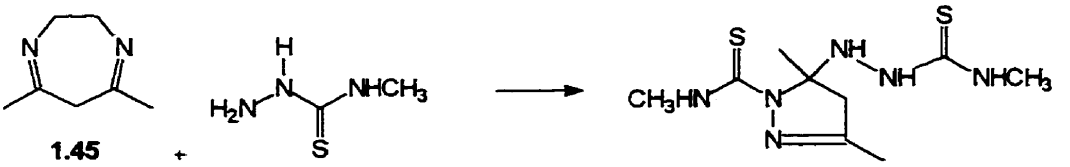

Figure 1.14: Reaction to yield unanticipated pyrazoline product

Experimental details of the X-ray structure determination including tables of positional and thermal parameters, bond distances, bond angles and hydrogen atom coordinates have been filed with the Cambridge Crystallographic Data Centre. A summary is included in Appendix B.

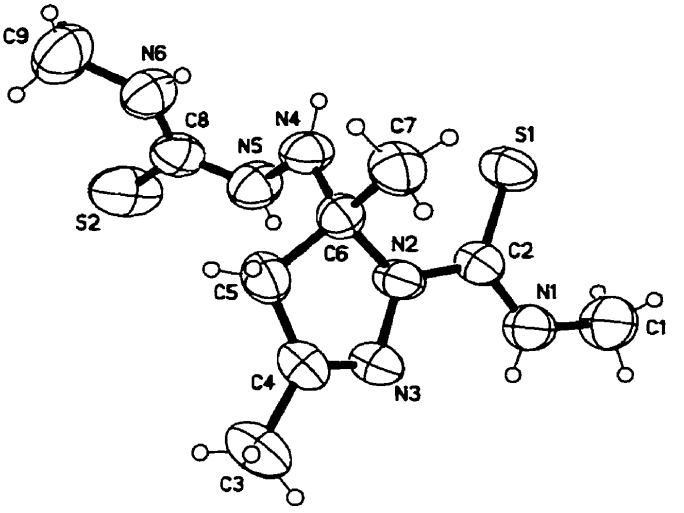

Figure 1.15: Crystal structure of **1.16**

1.2.4.5 Intramolecular Cyclization

In our hands, reaction of 2,4-pentanedione with thiosemicarbazide, 4-methylthiosemicarbazide, and 4-ethylthiosemicarbazide proceeded only with involvement of ethylene diamine as initially reported in 1967 and again in 1990. The products obtained were not the desired 2,4-bisthiosemicarbamoyl-pentanedione ligands but rather pyrazolines possibly formed by intramolecular

attack by the amide nitrogen of the carbazide on the adjacent imine carbon as indicated in Figure 1.16.

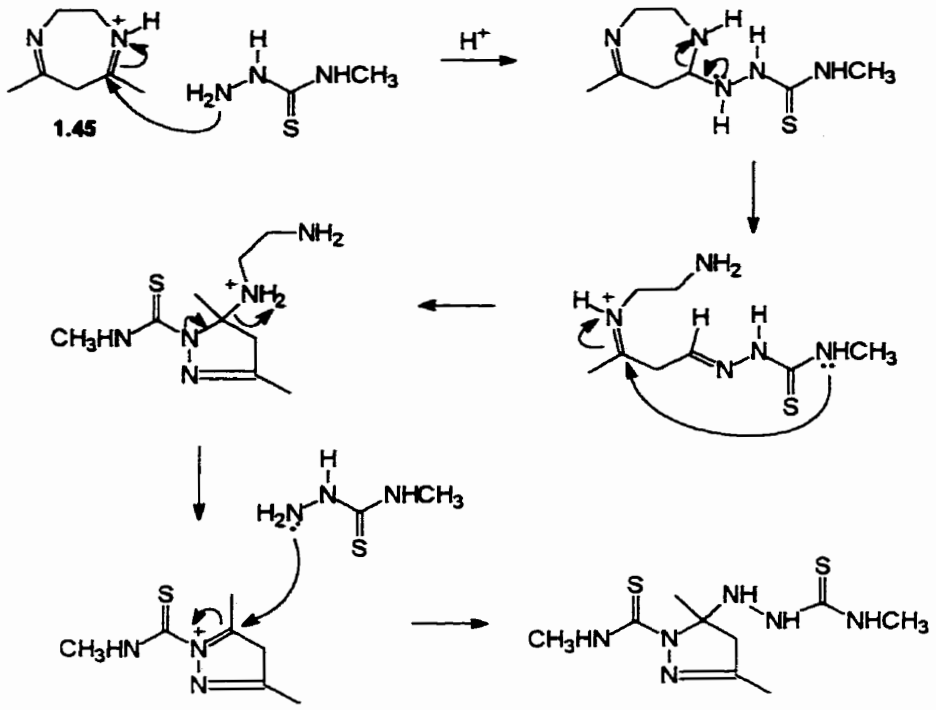

Figure 1.16: A potential route for pyrazoline formation

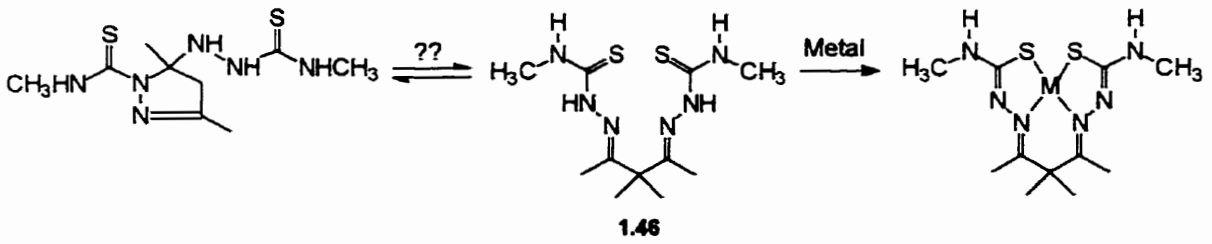

Figure 1.17: Opening the pyrazoline ring by chelation

Attempts were made to determine if the pyrazoline ring might open reversibly and if the open form could be trapped with a metal ion, eventually ^{99m}Tc. The pyrazoline product of **1.16** was refluxed in aqueous zinc acetate solution to open the cyclized ring. It was possible the bisthiosemicarbazone

moeity could open and chelate the divalent zinc metal, as depicted in Figure 1.17. In practice, this led to the reisolation of the bis(4-methylthiosemicarbamoyl)pentanedione pyrazoline product. There is indirect support for the irreversibility of pyrazoline cyclization product via metal chelation. Yokoyama[11e] had unknowingly chelated the pyrazoline product of 4-methylthiosemicarbazide and 2,4-pentanedione with ^{99m}Tc, resulting in two radioactive species as evidenced by HPLC analysis. Presumably the cyclic pyrazoline cyclization remained intact under the action of a chelating metal. Otherwise, a linear thiosemicarbamoylpentanedione ligand would have resulted upon chelation of the technetium metal, yielding only one radioactive product.

Alternatively, an attempt was made to prevent the intramolecular cyclization to a pyrazoline ring. Ligand **1.16** was prepared in the presence of zinc acetate to divert the intramolecular cyclization. This approach anticipated the linear form of the ligand assembling around the divalent zinc metal much like a template effect. Refluxing thiosemicarbazide and pentanedione in 0.1 N hydrochloric acid in the presence of zinc acetate yielded a small amount of crystalline product. The solid was of extremely high melting point with decomposition beginning at 308^{0}C . The material was essentially insoluble in numerous organic solvents including DMF and DMSO making spectral analysis impossible. HRMS failed to confirm the preparation of the N_2S_2 zinc chelate which could be a indication of its poor volatility or its complete absence in the crystalline material isolated. LRMS indicated peaks at lower mass numbers which may correspond to 2,4-pentanedione and 4-methylthiosemicarbazide chelating zinc independently of the N_2S_2 ligand complex. Both pentanedione and thiosemicarbazides can chelate divalent metals independently of each other. No further studies were performed in this regard.

Based on the literature results with the technetium chelation of the pyrazoline product and our own zinc chelation of pyrazoline resulting in reisolated starting material, it appears that the intramolecular cyclization of 2,4-

bisthiosemicarbamoylpentanedione is irreversible.

1.2.4.6 Clarification of the Literature

Attempts to prepare 2,4-bisthiosemicarbamoylpentanediones via literature precedent from 2,4-pentanedione and three different thiosemicarbazides resulted instead in the formation of cyclic pyrazolines. The preparation was attempted with thiosemicarbazide, 4-methylthiosemicarbazide, and 4-ethylthiosemicarbazide, respectively. A single crystal X-ray structure study of the product from 4-methylthiosemicarbazide confirmed the pyrazoline structure. This observation served to correct earlier misassignments of structure. Namely, ethylene diamine mediation leads to pyrazoline cyclization products, not the linear bisthiosemicarbazone N_2S_2 ligands suggested previously[11e,34,35]. Radiolabelling of this irreversible cyclization product would undoubtedly lead to a mixture of products, as previously observed in the literature for a similar compound[11e, 35].

Direct reaction of pentanedione and thiosemicarbazide with acid catalysis leads only to reisolation of starting material, not the linear semicarbazone N_2S_2 ligands suggested in previous reports[32,37]. These findings have been published[38]. The apparent irreversibility of this cyclization resulted in this target N_2S_2 ligand being abandoned prior to any alkylation or amidation studies. The N_2S_2 bioconjugate study, based on thiosemicarbazides, was abandoned. In the acetylbenzoic acid based instance where cyclization is inhibited, solubility prohibits amidation with Lisinopril. The pentanedione ligands are never formed and instead yield cyclized products.

1.3 Experimental

Commercially available starting materials, purchased from Aldrich and Lancaster, were used for the synthetic preparations which follow. All silica and alumina for chromatographic separations was from EM Science. All solvents were obtained from BDH. NMR spectra were recorded on either Varian Gemini XL-200 or XL-300 instruments. All NMR spectral data is given in ppm relative to tetramethylsilane (TMS).

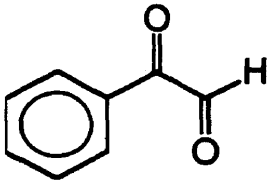

1.5

Preparation of Phenylglyoxal (**1.5**)

Method A: A single-neck flask, fitted with condenser and magnetic stirbar, was charged with acetophenone (427.2 mg, 3.5 mmol), 2,2,6,6,-tetramethyl-oxopiperidinium chloride (674.5 mg, 3.6 mmol) and acetonitrile (50 mL). The orange solution was left to stir for 2 hours until the colour changed to a pale yellow, then refluxed for 1 hour. A white solid precipitated from solution after cooling to room temperature. Filtration, and *in vacuo* concentration of the resultant filtrate yielded an oily product in 36% yield as determined by ^{1}H NMR. Significant amounts of acetophenone and 2,2,6,6-tetramethylpiperidine were also present in the ^{1}H NMR spectrum. No further purification was performed. ^{1}H NMR ($CDCl_3$) crude reaction mixture, tetramethylpiperidine 1.2 -1.8 (m, CH_3 + CH_2); acetophenone 7.4 - 8.2 (m, CH_{AR}), 2.6 (s, CH_3); phenylglyoxal 9.6 (s, CHO), 7.4 - 8.2 (m, CH_{AR}). The relative yield was determined by comparing the ^{1}H NMR spectrum integration for the methyl of acetophenone with the glyoxal aldehydic proton.

Method B: A two-neck flask, fitted with condensor and magnetic stirbar,

was charged with selenium dioxide (164.1 mg, 1.48 mmol), dioxane (10 mL), and water (27μL, 1.5 mmol). The contents were left to stir at 55°C for 30 minutes to aid in the dissolution of selenium dioxide. Acetophenone (147.3 mg, 1.23 mmol) was added and the contents were left to reflux for 16 hours. Selenium metal, as a grey solid, was evident in the reaction flask within 45 minutes of reflux. Upon cooling, multiple filtrations of the selenium metal through Celite yielded an amber oil with a slight suspension. No further purification was performed. The crude ^{1}H NMR spectrum indicated no acetophenone starting material. The yield was assumed quantitative.

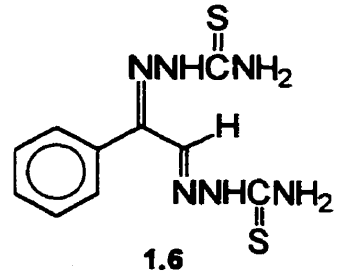

1.6

Preparation of Phenylbis(thiosemicarbazone) (**1.6**)

A two-neck flask fitted with condensor, dropping funnel, and magnetic stirbar, was charged with thiosemicarbazide (161.3 mg, 1.8 mmol), ethanol (absolute, 3.8 mL), and aqueous hydrochloric acid (0.1 M, 6.2 mL). The reaction contents were heated at reflux until the thiosemicarbazide dissolved. The dropping funnel was then charged with phenylglyoxal (154.6 mg, 0.87 mmol) and ethanol (absolute, 2mL). Drop wise addition of the glyoxal to the reaction flask proceeded slowly enough to maintain reflux temperature. The contents were left to reflux an additional hour and then cooled to yield a solid precipitate. Filtration of the precipitate and recrystallization in ethanol (95%) gave 148.6 mg (61%) of product, melting point 252.5 - 255°C with decomposition. The ^{1}H NMR spectrum indicated a mixture of a major and minor isomer in an approximate 4:1 ratio. ^{1}H NMR (d_6-DMSO) Major isomer

11.5 (s, 1H), 8.5 (brs, 2H), 8.05 (brs, 2H), 7.98 (brs, 2H), 7.05 - 7.6 (m, 4H). Minor isomer 11.5 (s, 1H), 11.63 (s, 1H), 8.44 (brs, 2H), 8.0 (brs, 2H), 7.0 - 7.67(m, 4H). ^{13}C NMR (d_6-DMSO) 178.7 (C, C=S), 178.5 (C, C=S), 137.4, 136.8, 135.9 (C, 2X C=N, C_{AR}), 129.2 (C, C_{AR}), 128.6 (CH, C_{AR}), and 126.9 (CH, C_{AR}). Thin film FT-IR indicated no aldehyde or ketone absorbances. HRMS for $C_{10}N_6S_2H_{12}$, calculated 281.0644 (M+H), observed 281.0642.

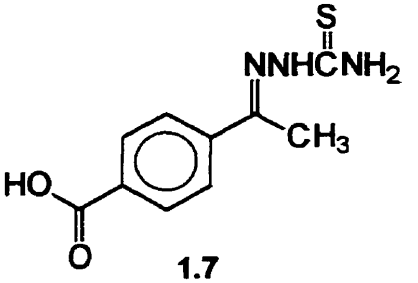

1.7

Preparation of p-Carboxyphenylethyl(thiosemicarbazone) (**1.7**)

This compound was prepared by literature method[13] with minor modifications. A single-neck flask, fitted with condenser and magnetic stirbar, was charged with thiosemicarbazide (67.4 mg, 0.7 mmol), water (4.2 mL), ethanol (absolute, 3 mL), and concentrated hydrochloric acid (700 µL). The reaction was heated to reflux for 5 minutes to dissolve the thiosemicarbazide. Acetylbenzoic acid (102.6 mg, 0.6 mmol) suspended in ethanol (95%, 2 mL) was added to the refluxing reaction dropwise via the top of the condensor. Additional ethanol (95%, 500 µL) was used to wash the sides of the condensor after addition. The reaction was left to reflux an additional 5 minutes. Upon cooling, a pale yellow solid precipitated from solution. Filtration of the solid gave 143 mg of crude product, melting point 248 - 250°C with decomposition. The ^1H NMR and ^{13}C NMR spectra indicated no starting material and so no further purification was performed. ^1H NMR (d_6-DMSO) 12.8 (s, 1H), 10.1 (s, 1H), 8.1 (brs, 1H), 7.6 - 7.9 (m, 4H + 1H), 2.1 (s, 3H). ^{13}C NMR (d_6-DMSO) 179.1 (C, C=O), 167.0 (C, CO_2H), 146.5, 141.7, 130.9 (C, C=N, 2xC_{AR}), 129.1 (CH, C_{AR}), 126.6 (CH, C_{AR}), 13.9 (CH, CH_3). HRMS for $C_{10}N_3O_2H_{11}S$, calculated 238.0650 (M+H) , observed 238.0654.

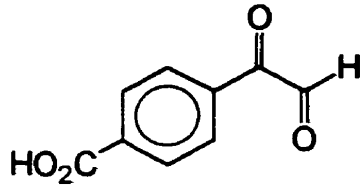

1.8

Preparation of *p*-Carboxyphenylglyoxal (**1.8**)

A two-neck flask fitted with a condenser and magnetic stirbar, was charged with selenium dioxide (1.227 g, 11 mmol), dioxane (20 mL) and water (200 µL, 11 mmol). The reaction flask was heated to aid selenium dioxide dissolution. After 30 minutes, acetylbenzoic acid (212.4 mg, 12.9 mmol) was added and the reaction was left to reflux for 16 hours. The resultant solid selenium metal was removed via filtration through Celite. Decolourization of the filtrate and *in vacuo* concentration yielded an amber oil with solid. No formal yield was determined due to selenium metal contamination however, the ^{1}H NMR spectrum indicated no acetylbenzoic acid starting material as evidenced by the lack of an α-methyl signal at 2.6 ppm. ^{1}H NMR (d_6-DMSO) 7.7-8.0 (m, 4H), no aldehydic proton was visible. ^{13}C NMR (d_6-DMSO) 200.0 (C, C=O), 198.0 (C, C=O), 166.6 (C, CO_2H), 139.8 (C, C_{AR}), 134.5 (C, C_{AR}), 129.4 (CH, C_{AR}), 128.3 (CH, C_{AR}). There were also minor peaks at 184.3, 126.0, 104.2, and 99.5 ppm which may represent hydrated **1.8**. The crude material was used in subsequent reactions without further purification.

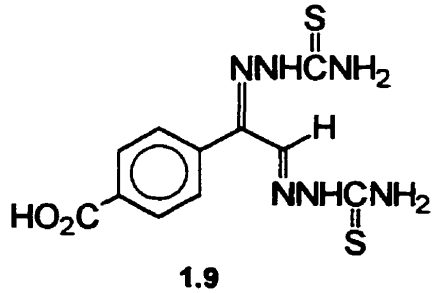

1.9

Preparation of *p*-Carboxyphenylbis(thiosemicarbazone) (**1.9**)

A three-neck flask fitted with condenser, dropping funnel, and magnetic

stirbar, was then charged with thiosemicarbazide (1.3798 g, 15 mmol) and aqueous hydrochloric acid (0.1M, 30 mL). Thiosemicarbazide dissolved with heating the reaction contents to reflux. The dropping funnel was charged with *p*-carboxyphenylglyoxal (3.6632 g crude, maximum 6 mmol) dissolved in ethanol (95%, 15 mL). The *p*-carboxyphenylglyoxal solution was added to the reaction dropwise over 40 minutes. The reaction was left to stir 16 hours at reflux temperature. Upon cooling, a pale yellow solid precipitated from solution. Filtration of the solid and recrystallization in ethanol (absolute) yielded 1.68 g (42.4%) of product, melting point 260-262^{0}C with decomposition. The ^{1}H NMR spectrum indicated a mixture of two isomers in an approximate 4:1 ratio. ^{1}H NMR (d_6-DMSO) Major isomer 12.3 (s, 1H), 11.8 (s, 1H), 8.8 (brs, 2H, NH_2), 8.4 (brs, 2H, NH_2), 8.25 (s, 2H, NH), 7.9 (m, 4H, CH_{AR}). Minor isomer 12.3 (s, 1H), 11.9 (s, 1H), 9.4 (s, 2H, NH), 8.75 (brs, 2H, NH_2), 7.4 (brs, 2H, NH_2), 8.01 (m, 4H, CH_{AR}). ^{13}C NMR (d_6-DMSO) 178.8 (C, C=S), 178.5 (C, C=S), 166.9 (C, CO_2H), 139.9 (C, C_{AR}), 136.6 (C, 2xC=N), 130.9 (C, C_{AR}), 129.4 (CH, C_{AR}), 127.1 (CH, C_{AR}).

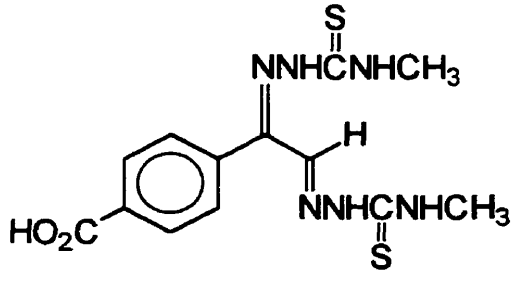

1.10

Preparation of *p*-Carboxyphenylbis(4-methylthiosemicarbazone) (**1.10**)

This compound was prepared in a similar manner to **1.9** with minor variations. A two-neck flask fitted with condenser, dropping funnel, and magnetic stirbar, was charged with 4-methylthiosemicarbazide (1.9173 g, 18.2 mmol) and aqueous hydrochloric acid (0.1M, 30mL). This solution was heated to reflux to dissolve the thiosemicarbazide. The dropping funnel was charged

with *p*-carboxyphenylglyoxal (9.0 mmol) dissolved in ethanol (95%, 15mL). The *p*-carboxyphenylglyoxal solution was added to the reaction dropwise over 35 minutes. An yellow-orange precipitate formed upon initial addition. The reaction contents were refluxed 16 hours following the glyoxal addition. Upon cooling, the solid was filtered and recrystallized in a large volume of methanol to yield 1.13 g (35%) of product, melting point 238 - 242 ^{0}C with decomposition. The ^{1}H NMR spectrum indicated a mixture of two isomers in an approximate 4:1 ratio. ^{1}H NMR (d_6-DMSO) Major isomer 12.3 (s, 1H), 11.78 (s, 1H), 8.85 (q, 1H), 8.25 (brs, 1H), 8.16 (q, 1H), 7.95 (m, 4H), 3.03 (d, 3H), 2.9 (d, 3H). Minor isomer 12.3 (s, 1H), 11.9 (s, 1H), 9.35 (brs, 1H),8.82 (q, 1H), 7.88 (m, 4H), 7.33 (q, 1H), 2.95 (d, 3H), 2.86 (d,3H). ^{13}C NMR (d_6-DMSO) 139.9, 130.9 , 130.1 (C, C=N, 2xC_{AR}), 135.4 (C, C=N), 129.04 (CH, C_{AR}), 126.86 (CH, C_{AR}), 31.45 (CH, CH_3), 31.1 (CH, CH_3). HRMS for $C_{13}N_6S_2O_2H_{16}$, calculated 353.0855 (M+H), observed 353.0855

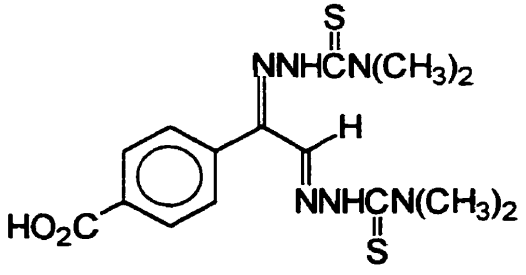

1.11

Preparation of *p*-Carboxyphenylbis(4,4-dimethylthiosemicarbazone) (**1.11**)

This compound was prepared in a similar manner as **1.9** with minor variations. A two-neck flask fitted with condenser, dropping funnel, and magnetic stirbar, was charged with 4,4-dimethylthiosemicarbazide (2.196 g, 18.4 mmol) and aqueous hydrochloric acid (0.1M, 20mL). This solution was heated to reflux to dissolve the thiosemicarbazide. The dropping funnel was charged with *p*-arboxyphenylglyoxal (2.196, 13.4 mmol) dissolved in ethanol (95%, 100mL). The *p*-carboxyphenylglyoxal solution was added to the

reaction dropwise over 25 minutes. After addition, the reaction was left to reflux for 4 hours. Upon cooling, a yellow solid precipitated from solution. The solid was filtered and recrystallized in ethanol (absolute) to give 1.14g (23%) of product, melting point 210 - 214^{0}C with decomposition. ^{1}H NMR (d_6-DMSO) 13.3 (s, 1H), 11.3 (brs, 1H), 8.64 (brs, 2H), 7.8 - 8.04 (m, 4H), 3.42 (s, 6H), 3.32 (s, 6H). ^{13}C NMR (d_6-DMSO) 140.0 (C, C=N), 136.2 and 141.2 (C, C=N, C_{AR}), 130.5 (C, C_{AR}), 129.6 (CH, C_{AR}), 126.13 (CH, C_{AR}), 42.5 (CH, CH_3), 41.2 (CH, CH_3). HRMS for $C_{15}O_2N_6S_2H_{20}$, calculated 381.1168 (M+H), observed 381.1153.

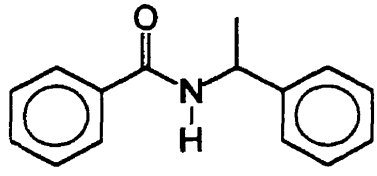

1.12

Preparation of N-(phenylethyl)benzamide: Determining Conditions for Amide Formation via Dicyclohexylcarbodiimide (**1.12**)

Optimized Method: A single-neck flask, equipped with magnetic stirbar, was charged with benzoic acid (220.2 mg, 1.8 mmol), acetonitrile (15 mL) and dicyclohexylcarbodiimide (DCC) (197.0 mg, 0.96 mmol). After stirring the resulting solution for 40 minutes, phenylethylamine (110.2 mg, 0.91 mmol) was dissolved in acetonitrile (10 mL) and added to the reaction flask. After stirring at room temperature for 16 hours, a significant amount of solid dicyclohexylurea (DHU) had precipitated out. The reaction was quenched with acetic acid and the solid removed by filtration. Removal of the solvent *in vacuo* and work-up of the resulting residue yielded 214.8 mg of product still contaminated with small amounts of DHU and the ammonium salt of benzoic acid in a 55:1:6 relative ratio. The yield of amide (86%) was determined using benzyl alcohol as an internal ^{1}H NMR standard. These were considered to be optimized reaction conditions for amide formation using DCC. ^{1}H NMR (d_6-

DMSO) DHU: 5.5 (m, CH_2), 0.6 - 1.8 (m, CH_2); Amide: 7.8 - 7.95 (m, CH_{AR}), 7.2 - 7.6 (m, CH_{AR}), 5.2 (q, RCHNH), 1.5 (d, CH_3); salt: 7.8 - 7.95 (m, CH_{AR}), 7.2 - 7.6 (m, CH_{AR}), 4.2 (m, $RCHNH_3^+$), 1.25 (m, CH_3). MS for $C_{15}H_{15}ON$, calculated 225.1154, observed 225.1158.

Non-Optimized Methods: Preparation of (N-carboxy-2-phenyl)-phenylethylamine was performed in a similar manner to above with differing solvents and reagent ratios. All yields were determined using benzyl alcohol as an internal ^1H NMR standard. Entry 5 included an addition of N-hydroxysuccinimide (NHS) at the same time DCC was added to the reaction flask. No amide was observed by ^1H NMR for entries 1 and 3.

Entry	Solvent System	Reagent Ratio Acid:DCC:Amine	^1H NMR Yield of Amide (%)
1	THF	1:1:1	0
2	THF	2:1:1	20
3	CH_2Cl_2	1:1:1	0
4	CH_2Cl_2	1:3:1	18
5	CH_2Cl_2	1:3:1 + NHS	15
6	CH_2Cl_2	2:3:1	32
7	CH_2Cl_2	2:1:1	82
8	CH_3CN	2:1:1	86
9	$CHCl_3$	2:1:1	70

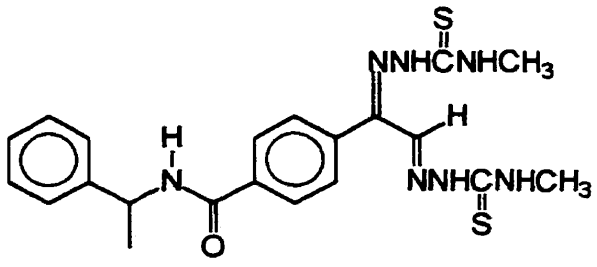

1.13

Preparation of Phenyl-N-carboxyphenylbis(4-methylthiosemicarbazido)ethane (**1.13**)

A single-neck flask, fitted with an argon inlet and magnetic stirbar, was charged with *p*-carboxyphenylbis(4-methylthiosemicarbazone) (231.6 mg, 0.66 mmol) and dry THF (30 mL). The contents of the flask were cooled in an icebath and ethyl chloroformate (63 µL, 0.66 mmol) was added. After stirring for 10 minutes, triethylamine (93 µL, 0.67 mmol) was added. Phenylethylamine (90 mg, 0.74 mmol) was added to the reaction flask after an additional 10 minutes of stirring. The reaction was then left to warm to room temperature. Concentration *in vacuo* and preparative plate chromatography of the resultant residue gave 70 mg (23%) of an oily solid, R_F=0.58 in 8% methanol/ methylene chloride. The ^{1}H NMR indicated a 5:4:2 mixture of the desired amide: amide of ethyl chloroformate: amine salt, as determined by multiplets at 5.2, 4.65, and 4.38 ppm respectively. The ^{1}H NMR shifts for the amide of ethyl chloroformate and the amine salt were confirmed by independent synthesis of these compounds. ^{1}H NMR also indicated some unreacted *p*-carboxyphenyldi(4-methylthiosemicarbazide).

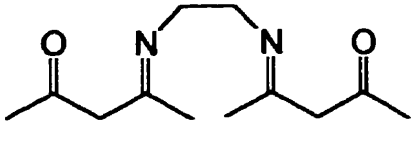

1.14

Preparation of 1,2-Bis(1-methyl-3-oxobutylideneamino)ethane (**1.14**)

This compound was prepared by a literature method[34] with some minor

modifications. A single-neck flask, equipped with magnetic stirbar, was charged with ethylene diamine (3.9 mL, 58 mmol) and water (50 mL). The contents were left to stir for 5 minutes and then 2,4-pentanedione (11.68 mL, 114 mmol) was added. Upon addition, the reaction contents turned yellow. Within 1 hour, a pale yellow solid had precipitated from solution. After 5 hours, the solid was filtered and recrystallized in water to yield 9.0 g (69.3%) of product, melting point 110 - 113^{0}C. ^{1}H NMR ($CDCl_3$) 10.9 (s, 1H), 4.9 (s, 1H), 3.38 (m, 1H), 1.88 (s, 3H), 1.85 (s, 3H). HRMS for $C_{12}N_2O_2H_{20}$, calculated 224.1524, observed 224.1516.

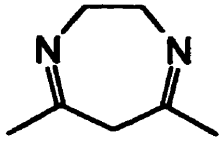

1.15

Preparation of 2,4-Pentanediimine ethane: 1:1 Adduct of Pentanedione and Ethylene Diamine (**1.15**)

1,2-bis(1-methyl-3-oxobutylideneamino)ethane was converted to the 1:1 adduct of pentanedione and ethylene diamine via literature procedure[34]. The conversion was carried out in 20% acetic acid at room temperature for 24 hours. Neutralization of the reaction with aqueous sodium hydroxide (50% by wt) and extraction into diethylether yielded a yellow oil in essentially quantitative yield. A ^{1}H NMR ($CDCl_3$) spectrum indicated only the 1:1 adduct as judged by the dione methyl equivalency at 1.9 ppm versus the non-equivalencies observed for these same protons in **1.14**. This compound was used in subsequent reactions without further purification.

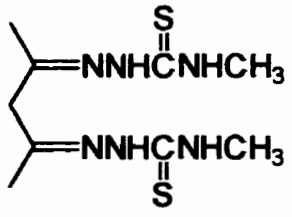

1.16

Attempted Preparation of 2,4-Bis(4-methylthiosemicarbamoyl)pentanedione (**1.16**)

This compound was prepared according to literature method[34] with minor modifications. A single-neck flask, fitted with condensor and magnetic stirbar, was charged with 2,4-pentanediimine ethane **1.15** (1.0084 g, 8.13 mmol) and aqueous methanol (50%, 50 mL). The contents were left to stir until homogeneous and then 4-methylthiosemicarbazide (1.700 g, 16.2 mmol) was added to the reaction. The contents were heated to reflux for 1 hour. After sitting at room temperature for 24 hours, colourless crystals precipitated from the brown solution. The solid was filtered and recrystallized in aqueous methanol (50%) to yield 1.5001 g (35%) of product, melting point 174 - 176^{0}C. ^{1}H NMR ($CDCl_3$) 7.25 (brq, 1H), 6.85 (s, 1H), 6.63 (s, 1H), 3.15 (d, 3H), 3.07 (d, 3H), 2.97 and 2.59 (CH_AH_B, 2H, J=18 Hz), 1.98 (s, 3H), 1.8 (s, 3H). ^{13}C NMR ($CDCl_3$) 183.7 (C, C=S), 175.5 (C, C=S), 153.5 (C, C=N), 85.0 (C), 47.2 (CH, CH_2), 30.9 (CH, CH_3), 30.2 (CH, CH_3), 23.5 (CH, CH_3), 16.2 (CH, CH_3). HRMS for $C_9N_6S_2H_{18}$, calculated 274.1034, observed 274.1032.

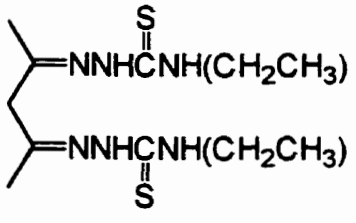

1.17

Attempted Preparation of 2,4-Bis(4-ethylthiosemicarbamoyl)pentanedione (**1.17**)

This compound was prepared in a similar manner as 2,4-bis(4-methylthiosemicarbamoyl)pentanedione **1.16** with the exception of the recrystallization. Crude melting point 120 - 135^{0}C with decomposition. Crude ^{1}H NMR ($CDCl_3$) 7.3 (m, 1H), 7.2 (m, 1H), 6.82 (brs, 1H), 6.65 (brs, 1H), 3.6 (m, 4H), 2.95 and 2.59 (CH_AH_B, 2H), 1.98 (s, 3H), 1.8 (s, 3H), 1.25 (t, 6H). ^{13}C NMR ($CDCl_3$) 183.5 (C, C=S), 175.0 (C, C=S), 153.0 (C, C=N), 85.0 (CH, CH_2), 47.2 (CH, CH_2), 23.7 (CH, CH_3), 16.3 (CH, CH_3), 14.66 (CH, CH_2), 14.35 (CH, CH_2). HRMS for $C_{11}N_6S_2H_{22}$, calculated 302.1351, observed 302.1344.

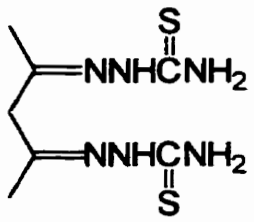

1.18

Attempted Preparation of 2,4-Bis(thiosemicarbamoyl)pentanedione (**1.18**)

This compound was prepared in a similar manner as 2,4-bis(4-methylthiosemicarbamoyl)pentanedione **1.16** with the exception of the recrystallization. Crude melting point 135 - 137^{0}C. Crude ^{1}H NMR (CD_3OD) 4.85 (s, 4H), 2.95 and 2.8 (CH_AH_B, 2H), 2.0 (s, 3H), 1.82 (s, 3H), no signal was observed for the amide protons on nitrogen. HRMS for $C_7N_6S_2H_{14}$, calculated 246.0721, observed 246.0724.

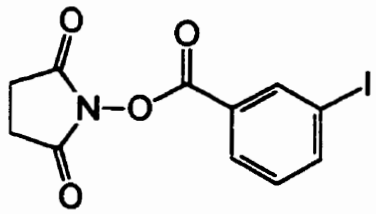

1.19

Preparation of N-hydroxysuccinimidyl-3-iodobenzoate (**1.19**)

This compound was prepared according to literature precedent[5]. Recrystallization in a mixture of dichloromethane and diethyl ether gave 759 mg (53%) of product, melting point 139 - 143°C. ^{1}H NMR ($CDCl_3$) 8.44 (m, 1H), 8.08 (m, 1H), 7.95 (m, 1H), 7.25 (m, 1H), 2.9 (s, 4H).

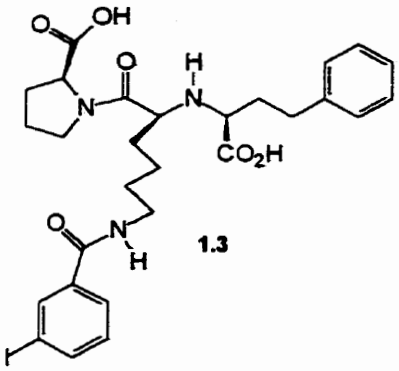

1.3

Preparation of the Amide of *m*-Iodobenzoic Acid and Lisinopril (**1.3**)

This compound was prepared according to literature precedent[5]. Purification via sephadex column resulted in 289.5 mg (66%) of product, melting point 129 - 130°C. ^{1}H NMR (CD_3OD) 8.2 (brs, 1H), 7.8 - 7.9 (m, 2H), 7.1 - 7.3 (m, 6H), 4.55 (m, 1H), 4.3 (m, 1H), 3.65 (m, 2H), 3.45 (m, 1H), 3.4 (m, 2H), 2.8 (m, 2H), 2.28 (m, 1H), 2.12 (m, 2H), 2.0 (m, 5H), 1.65 (m, 4H). All spectral assignments were made with the assistance of TOSCY and COSY, HETCOR, and other NMR spectra, included in Appendix A. HRMS for $C_{28}N_3O_6H_{34}I$, calculated 636.1574, observed 636.1574.

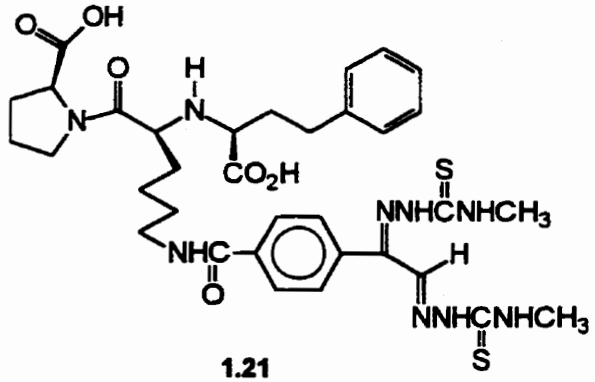

1.21

Attempted Preparation of the Amide of Lisinopril and p-Carboxyphenylbis(4-methylthiosemicarbazone) (**1.21**)

A two-neck flask, fitted with argon inlet, stopper and magnetic stirbar, was charged with *p*-carboxyphenylbis(4-methylthiosemicarbazone) (98.9 mg, 0.28 mmol), THF (dry, 35 mL), and triethylamine (78 µL, 0.56 mmol). The resulting solution was left to stir with cooling in an icebath (0^0C). After 45 minutes, ethyl chloroformate (267 µL, 0.28 mmol) was added. After an additional 2 hours of stirring under argon at 0^0C, Lisinopril (107.9 mg, 0.28 mmol) was added resulting in a suspension. The reaction was left to warm to room temperature. Filtration of the solid and concentration of the resultant filtrate yielded an oily solid product. Limited solubility prevented purification via recrystallization. The solid was purified by washing with water to remove any triethylamine, isolating 119.7 mg of product. The precipitate was dried to yield 15.7 mg of a solid, melting point 138 - 144^{0}C. ^{1}H NMR of the precipitate indicated Lisinopril. ^{1}H NMR of the filtrate product indicated a combination of both ligand and Lisinopril signals but no aldehyde signal from the ligand was apparent. A new peak was visible at 3.2 ppm and this signal, in combination with the peak at 2.75 ppm integrated for 2 hydrogens. This was interpreted as a combination of amide and original Lisinopril amine in a ratio of 3:2. No further purification was performed. ^{1}H NMR (d_6-DMSO) 12.05 (brs, 1H), 9.4 (m, 1H), 8.7 (m, 1H), 8.4 (m, 1H), 8.2 (m, 1H), 7.9 - 8.05 (m, 4H), 7.3 - 7.1 (m, 5H), 4.24 (m, 1H), 3.6 (m, 1H), 3.52 (m, 2H), 3.3 (m, 1.2H), 3.05 (m, 6H), 2.75 (m, 0.8H), 2.6 (m, 2H), 2.2 - 1.4 (m, 12H). HRMS for $C_{34}N_9O_6S_2H_{45}$ failed to confirm the preparation of the desired product.

1.4 References

1. Saha, G. Fundamentals of Nuclear Pharmacy 4th Edition, **1998**, Springer, New York.
2. Lieberman, J., *J. Am. Med.* **1975**, *5*, 365.
3. Patchett, A.A.; Harris, E.; Tristram, E.W.; Wyvratt, M.J.; Wu, M.T.; Taub, D.; Peterson, E.R.; Ikeler, T.J.; TenBroeke, J.; Payne, L.G.; Ondeyka, D.L.; Thorsett, E.D.; Greenlee, W.J.; Lohr, N.S.; Hoffsomer, R.D.; Joshua, H.H.; Ruyle, W.V.; Rothrock, J.W.; Aster, S.D.; Maycock, A.L.; Robinson, F.M.; Hirschmann, R. *Nature* **1980**, *288*, 280.
4. Atkkinson, A.B.; Robertson J.I.S. *Lancet* **1979**, *Oct 20*, 836.
5. Quiquero, V. Radiotracers for the Angiotensin System Ph.D. Thesis **1993**, University of Western Ontario, London.
6. Wyvratt, M.J.; Patchett, A.A. *Med. Res. Rev.* **1985**, *5*, 483.
7. DeReimer, L.H.; Meares, C.F. *J. Med. Chem.* **1979**, *22*, 1019.
8. Linder, K.E.; Chan, Y.W.; Cyr, J.E.; Malley, M.F.; Nowotnik, D.P.; Nunn, A.D. *J. Med. Chem.* **1994**, *37*, 9.
9. (a) Tamagnan, G.; Gao, Y.; Baldwin, R.M.; Zoghbi, S.S.; Neumeyer, J.L. *Tetrahedron Lett.* **1996**, *37*, 4553. (b) Meltzer, P.C.; Blundell, P.; Jones, A.G.; Mahmood, A.; Garada, B.; Zimmerman, R.E.; Davison, A.; Holman, L.; Madras, B.K. *J. Med. Chem.* **1997**, *40*, 1835. (c) Meegalla, S.; Plossi, K.; Kung, M.P.; Chumpradit, S.; Stevenson, A.D.; Frederick, D.; Kung, H.F. *Bioconj. Chem* **1996**, *7*, 421.
10. Han, H.; Cho, C.G.; Lansbury Jr., P.T. *J. Am. Chem. Soc.* **1996**, *118*, 4506.
11. (a) Misra, K.; Virzi, F.; Hnatowich, D.J.; Wright, G. *Tetrahedron Lett.* **1989**, *30*, 1885. (b) Fritzberg, A.R.; Abrams, P.G.; Beaumier, P.L.; Kasina, S.; Morgan, C.; Rao, T.N.; Reno, J.M.; Sanderson, J.A.; Srinivasan, A.; Wilbur, D.S.; Vanderheyden, J. *Proc. Natl. Acad. Sci USA*

1988, *85*, 4025. (c) Yokoyama, A.; Arano, Y.; Hosotani, T.; Yamada, A.; Horiuchi, K.; Yamamoto, K.; Torizuka, K.; Ueda, N.; Hazue, M. *Nucl. Med. Biol. Adv. Proc. 3rd World Congress* **1983**, 1097. (d) Fritzberg, A.R.; Abrams, P.L.; Kasina, S.; Morgan, C.; Reno, J.M.; Srinivasan, A.; Wilbur, D.S.; Scroff, R.W.; Vanderheyden, J. *J. Nucl. Med.* **1986**, *27*, 957. (e) Arano, Y.; Yabuki, M.; Yahata, T.; Horiuchi, K.; Yokoyama, A. *Chem. Pharm. Bull.* **1990**, *38*, 3099.

12. Petering H.G.; VanGeissen, G.J. *J. Med. Chem.* **1968**, *1*, 695.
13. Coats, E.A.; Milstein, S.R.; Holbein, G.; McDonald, J.; Reed, R.; Petering, H.G. *J. Med. Chem.* **1976**, *19*, 131.
14. Yokoyama, A.; Terauchi, Y.; Horiuchi, K.; Tanaka, H.; Odori, T.; Morita, R.; Mori, T.; Torizuka, K. *J. Nucl. Med.* **1976**, *17*, 816.
15. Arano. Y.; Yokoyama, A.; Magata, Y.; Saji, H.; Horiuchi, K.; Torizuka, K. *Int. J. Nucl. Med. Biol.* **1986**, *12*, 431.
16. (a) Yoffe, S.T.; Vatsuro, K.V.; Kugutcheva, E.E.; Kabachnik, M.I. *Tetrahedron Lett.* **1965**, *10*, 593. (b) Clark, H.A.; Miller, J.M. *J.C.S. Perkin I* **1977**, 1743.
17. Detar, D.F.; Silverstein, R. *J. Am. Chem. Soc.* **1966**, *88*, 1013.
18. Williams, A.; Ibrahim, I.T. *Chem. Rev.* **1981**, *81*, 589.
19. Zabicky, J. The Chemistry of Amides **1970**, Interscience, New York.
20. (a) Golubev, V.A.; Miklyush, R.V. *J. Org. Chem. U.S.S.R.* **1972**, *8*, 1376. (b) Hunter, D.H.; Racok, J.S.; Rey, A.W.; Zea Ponce, Y. *J. Org. Chem.* **1988**, *53*, 1278. (c) Hunter, D.H.; Barton, D.H.R.; Motherwell, W.J. *Tetrahedron Lett.* **1984**, *25*, 603.
21. Blatt Organic Synthesis Collective Volume II **1943**, 509.
22. Lambert, J.B.; Shurvell, H.F.; Lightner, D.A.; Cooks, R.G. Organic Structural Spectroscopy **1998**, Prentice-Hall, Upper Saddle River.
23. Hyperchem Molecular Visualization Software **1994**, using MM+ molecular mechanics with Polak-Ribiere convergency for geometry optimization.

24. Silverstein, R.M.; Bassler, G.C.; Morrill, T.C. Spectrophotometric Identification of Organic Compounds 5th Edition, **1991**, John Wiley and Sons, New York.

25. Kurzer, F.; Douraghi-Zadeh, K. *Chem. Rev.* **1967**, *67*, 107.

26. Balcom, B.J.; Petersen, N.O. *J. Org. Chem.* **1989**, *54*, 1922.

27. Bannwarth, W.; Knorr, R. *Tetrahedron Lett.* **1991**, *32*, 1157.

28. Knorr, R.; Trzeciak, A.; Bannwarth, W.; Gillessen, D. *Tetrahedron Lett.* **1989**, *30*, 1927.

29. Olah, G.A.; Narang, S.C.; Garcia-Luna, A. *Synth. Comm.* **1980**, 661.

30. Terao, S.; Shiraishi, M. *J.C.S. Perkin I* **1982**, 2909.

31. Arano, Y.; Yabuki, M.; Yahata, T.; Horiuchi, K.; Yokoyama, A. *Chem. Pharm. Bull.* **1990**, *38*, 3099.

32. Gingras, B.A.; Suprunchuk T.; Bayley, C.H. *Can. J. Chem.* **1962**, *40*, 1053.

33. El-Asmy, A.A.; Al-Ansi, T.Y. *Synth. React. Inorg. Met. Org. Chem.* **1989**, *19*, 309.

34. O'Callaghan, C.N.; Twomey, D. *J. Chem. Soc. (C)* **1967**, 2400.

35. Arano, Y.; Yabuki, M.; Jones, A.G.; Yokoyama, A. *Chem. Pharm. Bull.* **1991**, *39*, 104.

36. Zelenin, K.N.; Tomchin, A.B.; Solod, O.V.; Malov, M.Y. *Khim. Geterot. Soed.* **1986**, *1*, 128.

37. El-Asmy, E.A.; Morsi, M.A.; El-Shafei, A.A. *Trans. Met. Chem.* **1986**, *11*, 494.

38. Hunter, D.H.; McRoberts, C.; Vittal, J.J. *Can. J. Chem.* **1998**, *76*, 524.

PART TWO

PREPARATION AND APPLICATION OF ORGANOTIN POLYMERS

Chapter 2 - Preparation and Characterization of Organotin Polymers

2.1 Introduction

2.1.1 Solid Phase Organic Chemistry

The concept of organic synthesis using reagents covalently bound to a solid support was first introduced in the early 1960s. Employing a suitably functionalized polymer, a reagent is attached and further derivatized while on the insoluble resin. This heterogeneous approach to synthesis has its roots in Merrifield's pioneering peptide work[1]. Moving beyond peptides, the application of solid phase organic chemistry (SPOC) to general organic synthesis has rapidly expanded. The growth in the literature regarding SPOC has been practically exponential since 1992 and is summarized in recent reviews by Balkenhohl[2] and Hermkens[3] respectively.

2.1.1.1 Advantages and Disadvantages

In principle, solid phase organic synthesis has many benefits over conventional solution phase techniques. Tethering a molecule to an insoluble support prior to derivatization can save time, effort, and most importantly money. For conventional serial synthesis, the majority of time is spent with separation and purification of target molecules. The most dramatic benefit of SPOC is that isolation and purification is performed by simple filtration of the polymer-bound product away from reagents and byproducts. Since isolation is so straightforward, excess reagents can be used to drive reactions to completion. Filtration removes these reagents and immediately ceases the reaction, providing the product in exceptional purity ready to be cleaved from the polymeric support. The excess reagents washed from the polymer with each synthetic step may be recycled, as can the solid support following cleavage of the product. Tethering reagents to solid supports can also reduce their inherent toxicity, making handling and purification safer and easier. In

some instances, as attested by Laszlo[4], greater reaction selectivities and rates have been observed with solid phase tethered reagents. Faster reactions translate to milder conditions for organic transformations.

Not all reactions when applied to SPOC display faster rates or selectivity. Reactions can slow dramatically under heterogeneous conditions due to slow permeation of reagents through the solid phase. In addition, SPOC synthesis is limited to small quantities of product. Depending on the solid support employed, linkage and cleavage will add additional steps to a synthetic route. The application of new reactions to SPOC can require extensive optimization time. Reaction conditions are not necessarily transferable between solution and solid phase synthesis and some reaction conditions may never be applicable to solid phase. Most importantly, SPOC precludes easy analysis without prior cleavage of the product from the solid support. TLC analysis to judge reaction completion is impossible, as is conventional FT-IR and NMR characterization.

For many organic preparations, the advantages out-weigh the disadvantages. Consequently, solid phase organic chemistry has become a viable synthetic alternative for small molecule synthesis.

2.1.2 Solid Phase Organic Chemistry - The Past

In 1963, Merrifield[1] published the first account of solid phase synthesis. Merrifield prepared peptides using a chloromethylated polystyrene support **2.1**. The support, a styrene/divinylbenzene copolymer, was functionalized with methyl chloromethylether in the presence of zinc chloride. The chloromethyl group, the linker in this example, was esterified with a *t*-butyloxycarbonyl (*t*-BOC) protected amino acid. Deprotection followed by reaction with additional *t*-BOC protected amino acids occurred sequentially, yielding a peptide. At each step, the solid support was washed to remove byproducts and unreacted reagents. The approach was so novel and generally applicable that Merrifield's

contributions were recognized with the 1984 Nobel Prize in chemistry. The synthetic scheme from Merrifield's original publication is shown in Figure 2.1. This iterative process has been automated and peptide synthesizers have become commonplace in protein chemistry.

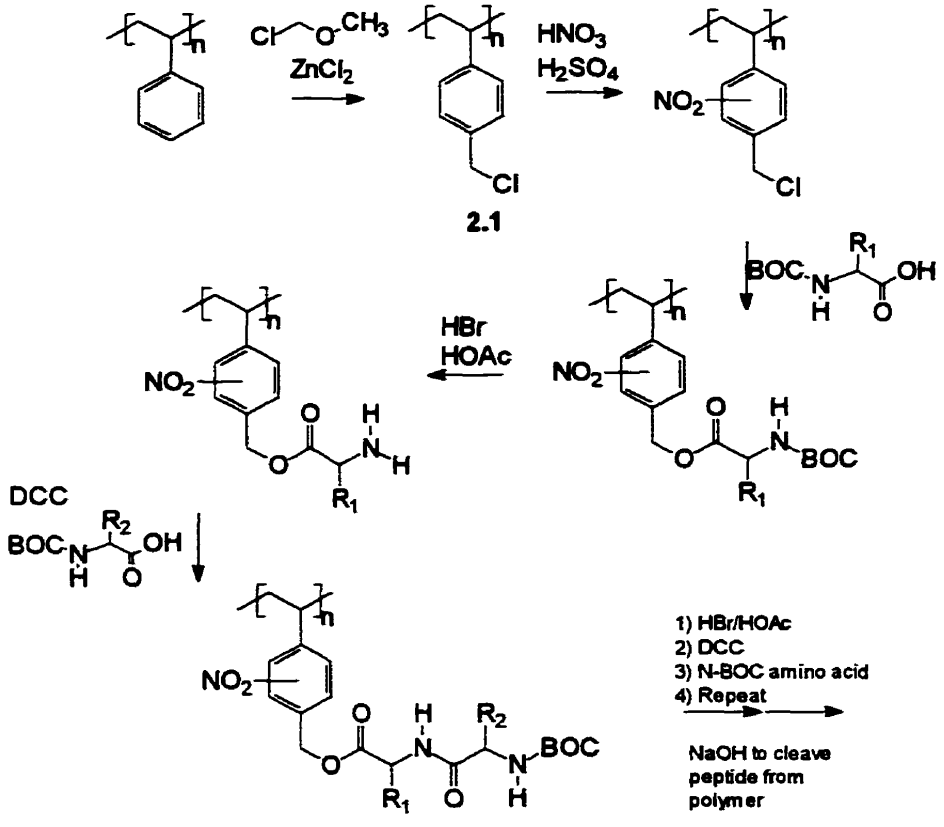

Figure 2.1: Merrifield's solid phase peptide synthesis route

Solid phase peptide synthesis quickly evolved to the point where large libraries of various sequences could be prepared simultaneously. This was welcome news for molecular biology and biochemistry. Unfortunately, peptides and peptidomimetics can be poor drug candidates relative to small organic molecules. There existed a great desire to expand the field of SPOC to the same level as automated peptide synthesis.

General organic synthesis involves demanding reaction conditions

including large temperature ranges, inert atmospheres, and aggressive reagents. As such, the leap from solid phase peptide synthesis to small organic molecule synthesis has not been trivial. A few reports of SPOC using functionalized polystyrene[5] surfaced following Merrifield's discovery but the approach was not widely embraced until recently.

2.1.3 Solid Phase Organic Chemistry - The Present

Organic chemists are rapidly accepting the practicality of synthesis on solid supports. SPOC has matured to the point where routine organic transformations can be carried out using well-documented reaction conditions. In some instances, the chemistry has become so routine as to be automatable. Fuelled by pharmaceutical research, SPOC has become the cornerstone of combinatorial chemistry.

Combinatorial chemistry allows for simultaneous synthesis of large numbers of compounds. As defined by Czarnik and DeWitt[6], it is a "new sub-field of chemistry with the goal of synthesizing very large numbers of chemical entities by condensing a small number of reagents together in combinations defined by a given reaction sequence". The technique is typically automated and although not restricted to SPOC, solid phase methods predominate.

Bunin and Ellman[7] reported the first combinatorial method for solid phase synthesis of a benzodiazepine library. Over seven synthetic steps, a library of ten compounds were each obtained in greater than 90% yield. The researchers used the inherent benefits of SPOC, namely excess reagents to drive each step to completion and simple purification between steps. The generalized synthetic scheme shown in Figure 2.2 uses a polystyrene support much like the Merrifield resin. Bunin and Ellman used common organic reagents and commercially available alkylating agents to build their diverse library.

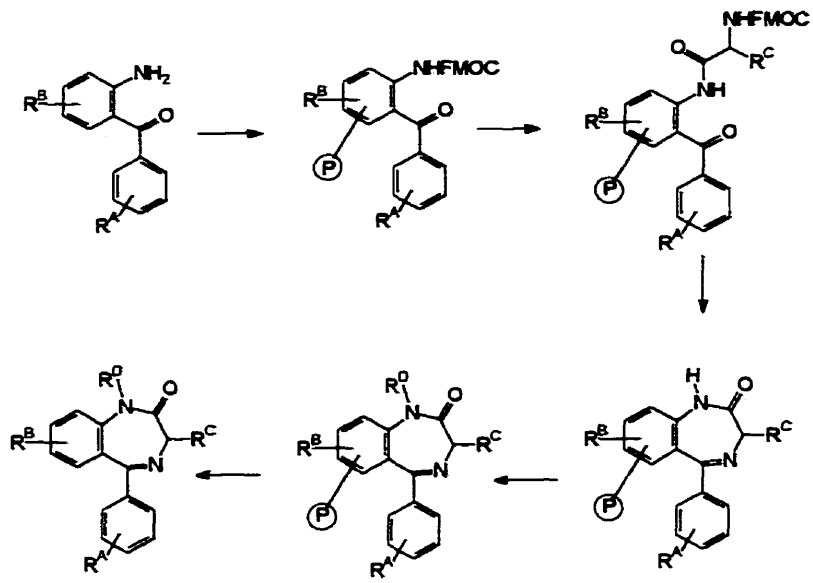

Figure 2.2: Ellman's benzodiazepine synthesis

This report signalled the official birth of combinatorial chemistry. Other researchers were quick to follow, making diverse and biologically relevant libraries of organic compounds using SPOC. Presently, nearly every pharmaceutical company is funding in-house combinatorial research[8]. These techniques have rapidly matured such that multiple organic synthesizers can churn out thousands of compounds once solid phase reaction conditions are determined. The advent of combinatorial chemistry has created a renewed interest in solid supports and SPOC compatible syntheses. Pharmaceutical research and development was the primary motivator for resurgence in SPOC interest. With the creation of high speed biological assays, new compound synthesis had become the bottle-neck of the drug discovery process. SPOC, as it relates to combinatorial chemistry, represented a method to make compound synthesis more timely and cost-effective.

2.1.4 Solid Phases Available

As the interest in SPOC has grown, the variety of solid supports available has expanded. The majority of supports are polystyrene-based (PS). Polystyrene resins used for SPOC are typically crosslinked with 1 - 2% divinylbenzene (DVB) to render them insoluble in most organic solvents. Polystyrene has good thermal stability and swellability in a large range of solvents. Swellability ensures the polymer pores enlarge, making them permeable to organic reagents. In this respect, the polymer interior is as accessible as the polymer surface during reaction. Swellabilty is expressed as a volume or weight increase of the resin following an organic solvent soak. Occasionally, polystyrene is grafted with polyethylene glycol (PEG) to alter its swellabilty and wetability.

For historical reasons, Merrifield resin predominates in SPOC applications. A few commercially available resins, compiled from a supplier catalogue[9], are given in Table 2.1. The linker group represents the functionality on the target molecule following cleavage from the solid support. The functional group is the site on the support where linkage occurs. Linkage would typically be made via an ester or amide derivative as with entries 1-3. An ether linkage would be necessary for entry 4 in the table. Ethers are less common linker modes for SPOC. Existing SPOC resins typically range in loading capacity from 0.1 mmol/g to 1.0 mmol/g resin. Loading capacity is a measure of the number of functional groups available for linking reagents onto the solid support per gram of resin. Resins can be prepared either by functionalizing existing polymers, like chloromethylation of polystyrene in the presence of zinc chloride, or by copolymerizing appropriately functionalized monomers with the basic resin monomers.

Many commercially available supports are limited by ester or amide linkage to the resin. Esters and amide linkers have poor stability under acidic conditions and so reduce the range of reactions available. In addition, the final

product must contain an carboxylic acid derivative from the former linkage site further reducing synthetic variability. A real need exists for a resin that allows for wide variability in the target molecule functionality following cleavage from the insoluble resin. Inevitably, no solid phase will ever be suitable for all synthetic applications since SPOC encompasses such a large range of reaction conditions. A variety of resins and linker strategies will be necessary to comprehensively cover the entire spectrum of known organic transformations.

Table 2.1: Commercially available resins for SPOC

Entry	Resin	Type	Functional Group	Linker Group
1	Merrifield	PS	CH_2-Cl	RCO_2H
2	Wang	PS/PEG	CH_2-OH	RCO_2H
3	Rink Amide	PS/PEG	NH_2	RCO_2H
4	Novosyn TG	PS/PEG	R-OH	R-OH

2.1.5 Organotin Reagents

The synthetic versatility of organotin reagents is well documented and several exhaustive reviews exist[10]. The most common organotin reagents include trialkyltin halides and trialkyltin hydrides. Some commonly observed transformations for these reagents are included in Figure 2.3.

Tin halides can be hydrolysed to stannols to give esterification catalysts. Reaction with a lithiated aromatic provides a simple route to arylstannanes. Nucleophilic attack gives a wide variety of organotin reagents including tin alkoxides and tin amines. Reduction to a trialkyltin hydride gives a free radical initiator for cyclizations and ring enlargements. Tin hydrides can also hydrostannylate unsaturated carbon bonds or be reduced to stannyl anions. Stannyl anions provide a route to trialkylarylstannanes as well as distannanes. Distannanes have applications as free radical initiators.

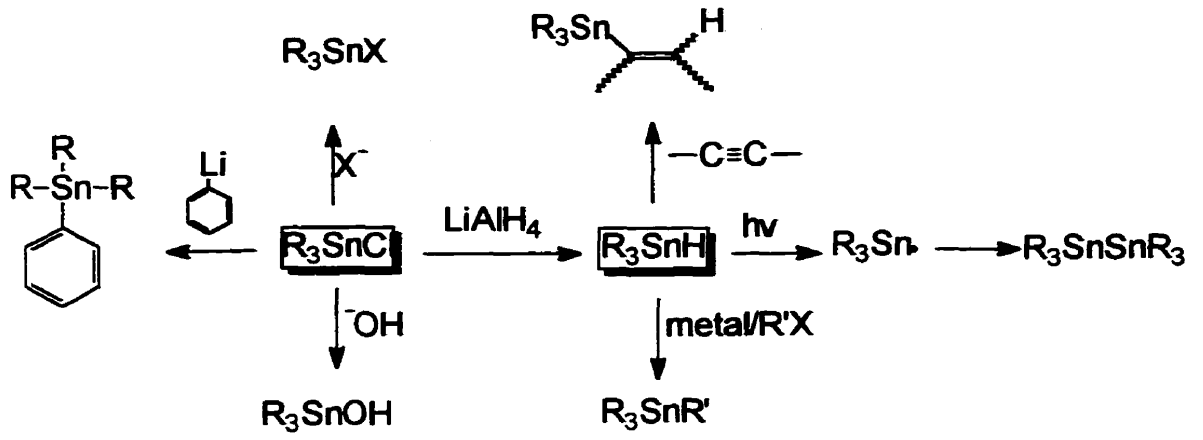

Figure 2.3: Common transformations for organotin halides and hydrides

Trialkylarylstannanes display notable reactivity in electrophilic aromatic substitution reactions. The trialkylstannyl functionality makes for an excellent leaving group allowing for *ipso*-substitution under mild reaction conditions. A variety of *ipso*-substitutions for a trialkylarylstannane are summarized in Figure 2.4. The reactivity of the sp^2 carbon-tin bond, attributed to the β-effect, allows for introduction of a wide variety of functional groups on the aromatic ring.

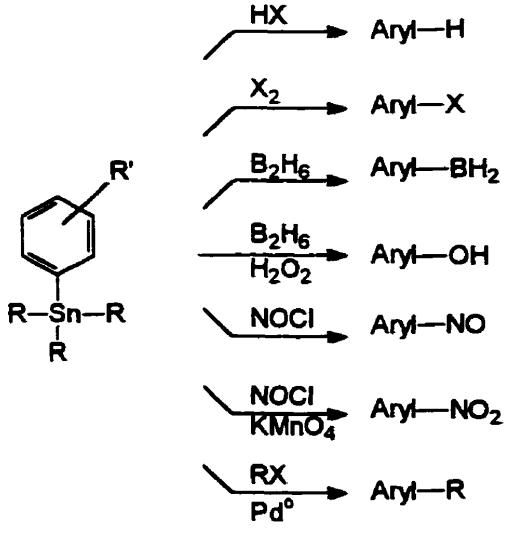

Figure 2.4: Electrophilic aromatic substitution of arylstannanes

2.1.6 Organotin Functionalized Solid Supports

Despite the synthetic versatility of organotin reagents, they are not routinely applied to pharmaceutical synthesis[11]. Organotin reagents are generally quite toxic[10a] and quantitative removal of organotin impurities from reaction mixtures is difficult. The toxicity of organotin reagents also makes for worker safety and waste disposal problems.

In 1990, Neumann first tried to alleviate the pitfalls of organotin reagents by preparing a polystyrene-supported organotin hydride[12]. The supported organostannane was prepared using both of the conventional methods for solid support functionalization. The first preparation method is illustrated in Figure 2.5. Hydrostannylation of divinylbenzene (DVB) with di-*n*-butylchlorostannane **2.11** gave the functionalized monomer **2.2**. Copolymerization of this monomer **2.2** with additional DVB, in the presence of azoisobutyronitrile (AIBN), resulted in polymer **2.3**. Subsequent reduction of **2.3** with di-*n*-butylaluminum hydride yielded the tethered organostannane **2.4** with 1.5 mmol/g loading.

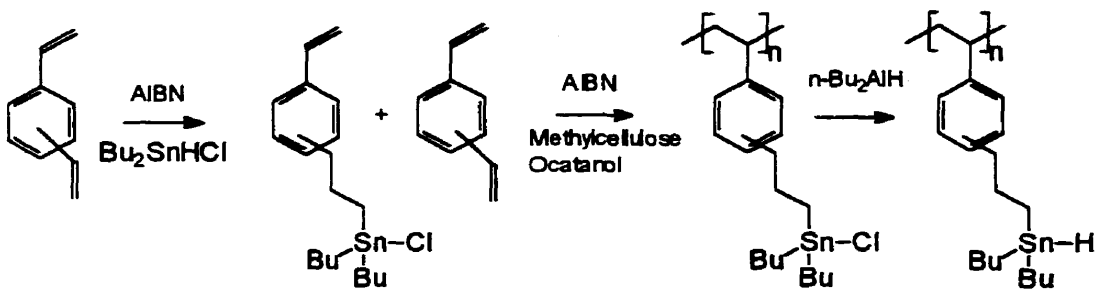

Figure 2.5: Preparation of a polystyrene supported organotin hydride

Alternatively, Neumann prepared **2.4** by chloromethylating polystyrene, converting it to the phosphonium salt, and vinylating with formaldehyde in the manner of a Wittig reaction. As illustrated in Figure 2.6, the vinyl group could then be hydrostannylated with di-*n*-butylchlorostannane **2.11** to yield **2.3** and

then reduced to the polymer-bound tin hydride **2.4**. Neumann found this method to yield 0.9 mmol/g loading.

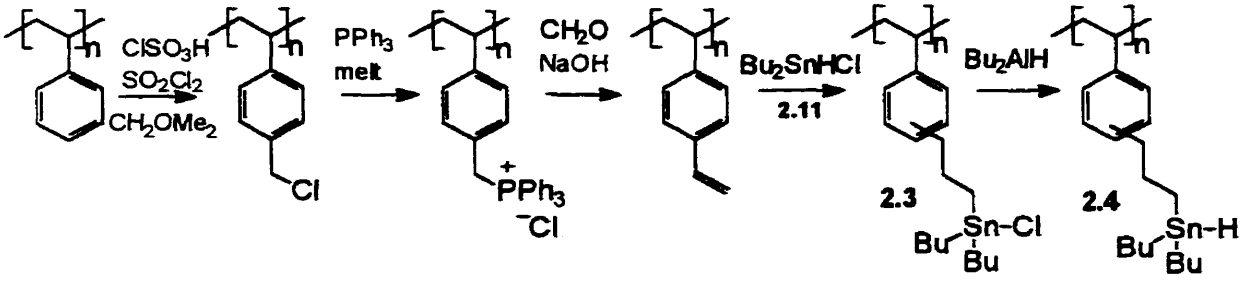

Figure 2.6: Alternate preparation of a polystyrene supported organotin hydride

Neumann set out to show that this immobilized organotin hydride could be used for the free radical cyclization of 5-hexenylbromide. The tethered reagent displayed a reactivity similar to solution phase tri-n-butyltin hydride. By linking organostannane to a polystyrene support, Neumann was able to effect the free radical reaction and remove all traces of tin impurity by simple filtration.

Following the successful application of a solid phase organotin hydride to free radical cyclization, Neumann went on to illustrate dehalogenations, deaminations[13], and dehydroxylations[14]. Reactivity rates were generally 50 - 100% of the reaction rates observed with solution phase reagents and the solid phase organotin reagent could be recycled several times. By 1992, Neumann had applied the solid phase organostannane reagent **2.4** to the Geise reaction, a radical coupling of organohalides with electron deficient olefins[15]. Neumann also illustrated the practicality of ring enlargement reactions for the preparation of methyl- and benzotropones using the solid phase tin hydride[16].

A solid supported organodistannane on the same polystyrene scaffold was prepared from the polymer-tethered di-*n*-butylchlorostannane intermediate **2.3**[17]. As illustrated in Figure 2.7, compound **2.3** was reduced in the presence of magnesium anthralide to link proximal tin sites on the polymeric backbone.

Optimization of this procedure later used lithium naphthalide as the reducing agent to yield 0.95 mmol/g - 1.1 mmol/g loading of the distannane **2.6**[18]. This solid phase organodistannane allowed for stannyl radical formation in the absence of organotin hydride as a hydrogen donor. This reagent was applied to radical cyclizations and performed in much the same manner as non-polymer bound organodistannanes with the exception of easy purification.

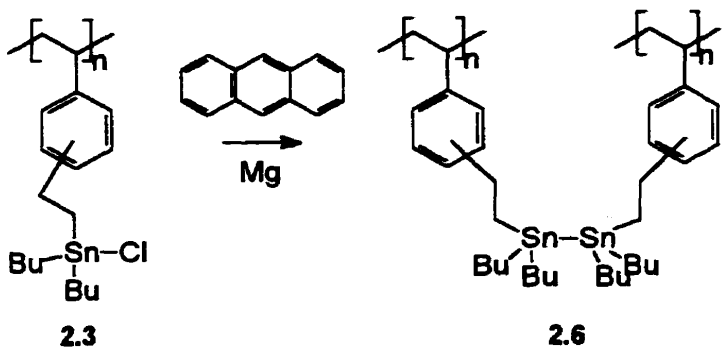

2.3 **2.6**

Figure 2.7: Neumann's preparation of a organodistannane

The polymer-tethered di-*n*-butylchlorostannane intermediate **2.3** was applied to a solid phase variation of Stille coupling[19] as illustrated in Figure 2.8. The di-*n*-butylchlorostannane **2.3** was converted to a tethered di-*n*-butylalkylstannane **2.7** by Grignard reagent. Subsequent reaction with an organic halide in the presence of a palladium catalyst yielded the cross coupled product. The product was released into the reaction solution and the tin impurities remained on the polymeric support. Stille reagents, like **2.7**, could also be prepared from the hydrostannylation of terminal alkynes with polymer-bound organostannane **2.4**.

Neumann died in August 1993, shortly before his Stille coupling account was published. With the exception of Junggebauer's optimization of polymer-bound distannane[18], no further applications of these organotin functionalized polystyrenes were published. During the last decade of his research career, Neumann reconfirmed the versatility of organostannanes. He addressed

purification and toxicity concerns by tethering the reagent to an insoluble support and developed a reagent widely applicable to organic synthesis.

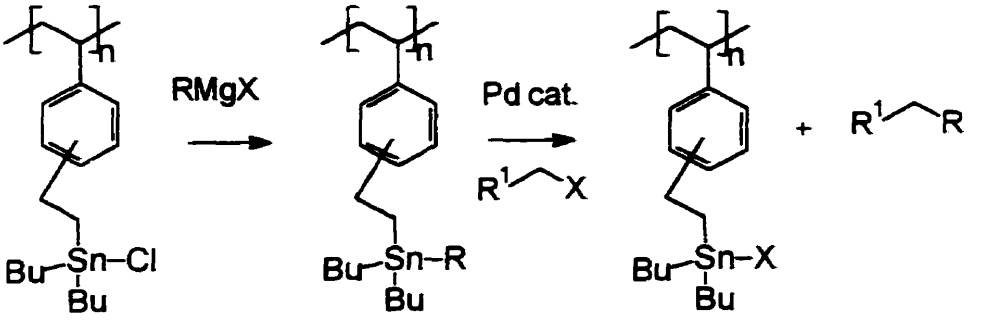

2.3 2.7

Figure 2.8: Solid phase Stille type coupling

The idea of tethering organostannane reagents to a solid support was not novel. Several other researchers had attempted to prepare similar compounds. These attempts included a polystyrene-tethered tin dihydride **2.8**[20] and a silica tethered silyl-alkylstannane **2.9**[21]. Neither of these solid phase reagents displayed sufficient reactivity for practical application.

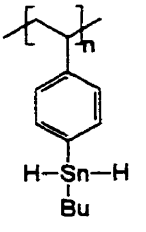

2.8

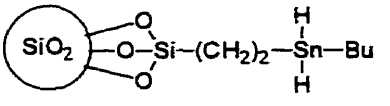

2.9

2.1.7 Applications of Organotin Functionalized Supports

In recent years, our laboratory has developed solid phase methods for radiopharmaceuticals preparation. To date, these syntheses have employed Neumann's polymer-tethered di-*n*-butylchlorostannane reagent **2.3**. Various pharmaceuticals, with aromatic rings in their skeletons, have been attached to

the solid phase as arylstannanes. The sp^2 bond of the arylstannane is highly activated towards *ipso*-substitution thus making a versatile solid phase linker. This approach allows for a variety of functional groups on the pharmaceutical following polymer cleavage.

2.1.7.1 Radiopharmaceutical Synthesis

Preparing various arylstannanes on the polystyrene scaffold and subsequent cleavage from the polymer with radioactive electrophiles represents an excellent method for no carrier-added radio-halogenation. No carrier-added radiolabelling gives high specific activity in the resultant radiopharmaceutical as well as high radiochemical yields. Only the desired radioactive product is released from the polymer allowing for simple isolation and purification. This represents a vast improvement over other available radiolabelling methods. Our research interest focussed on the attachment of existing pharmaceuticals to Neumann's polystyrene scaffold and subsequent radiolabelling by *ipso*-substitution of the sp^2 arylstannane bond with radioiodine.

Culbert[22] attempted the first iodination of polymer-tethered *p*-bromoarylstannane. The arylstannane was a model for N-isopropyl-*p*-amphetamine, an established radiopharmaceutical for monitoring brain perfusion[23]. As illustrated in Figure 2.9, the polymer-tethered *p*-bromoarylstannane was prepared by lithiation of *p*-dibromobenzene and reaction with **2.3**. The tin-aryl bond was then successfully cleaved from the support with $Na^{131}I$ using N-chlorosuccinimide as an oxidizing agent for the radioiodine. Culbert went on to attach (^{131}I)-N-isopropyl-4-bromoamphetamine to **2.3** and subsequently radioiodinated to yield N-isopropyl-*p*-iodoamphetamine, the authentic brain perfusion imaging agent, in 44% radiochemical yield.

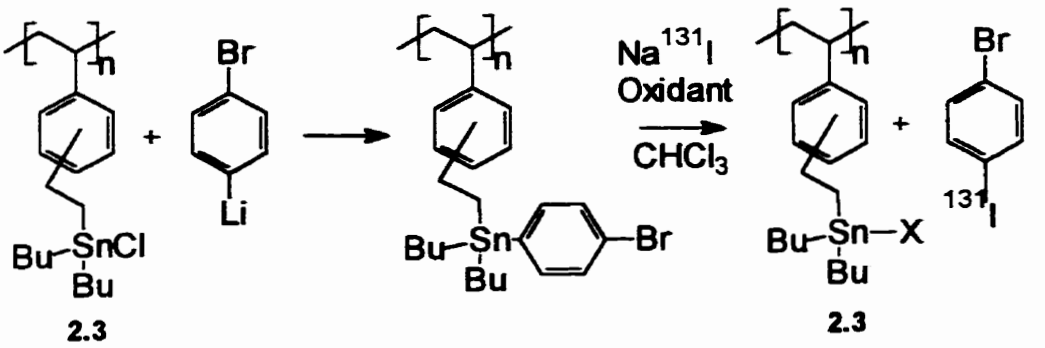

Figure 2.9: Culbert's initial arylstannane iodination

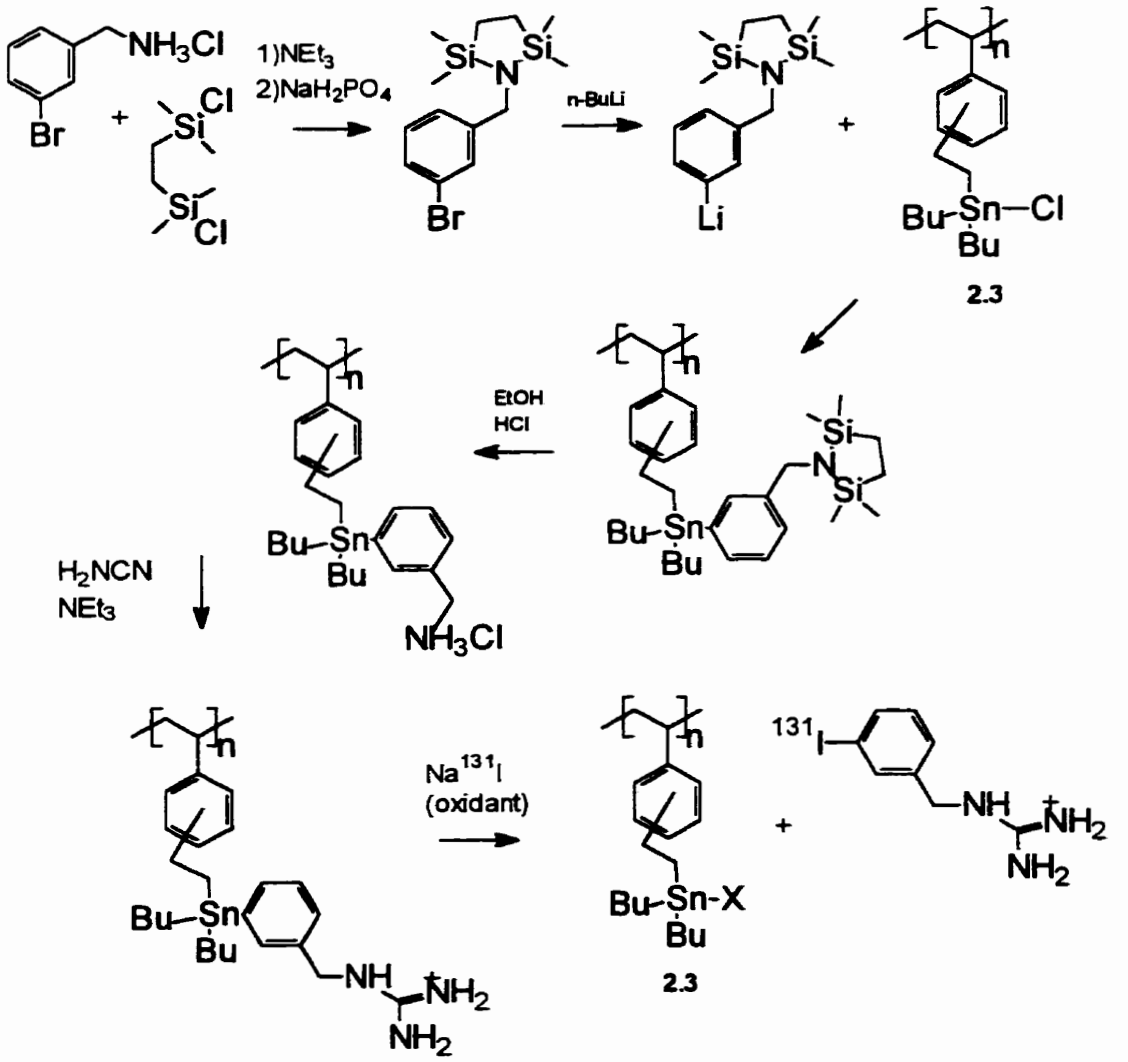

Figure 2.10: Synthesis of MIBG

A myocardial therapeutic and imaging agent, *m*-iodobenzylguanidine (MIBG), has been prepared via the di-*n*-butylchlorostannane solid phase **2.3**[24]. After optimization by Zhu[25], this established radiopharmaceutical was prepared in greater than 90% radiochemical yield. MIBG was prepared according to Figure 2.10. The *p*-bromobenzylammonium chloride was first protected then lithiated. Reaction of this lithiated species with the chlorostannane polymer furnished the arylstannane. Further modification was performed on the aromatic ring after tethering to the polystyrene support.

2.1.7.2 General Organic Synthesis with Arylstannanes

Existing solid phase supports, like Merrifield and Rink Amide, have restrictions on the types of functional groups that can be present on the target molecule following cleavage. Specifically, these resins are limited to carboxylic acid derivatives. The versatility of the arylstannane linker could remove some of the functional group restrictions associated with SPOC. The preparation of radiopharmaceuticals using an organostannane insoluble support has gradually progressed into general solid phase organic synthesis. Based on existing solution phase organotin chemistry, a wide variety of functional groups can be prepared upon arylstannane cleavage. The functional groups available upon cleavage have been previously summarized in Figure 2.4. Aromatic rings figure prominently in many biologically active compounds. Since the arylstannane bond represents such a versatile linker to the solid support, energy has focussed on preparing polymer-supported aromatic rings with a wide variety of functional groups.

Pollock[26] has investigated protic conditions for cleavage of various polymer-tethered arylstannanes. These studies also examined the accessibility of interior active sites within the polymer matrix as a function of protic reagent employed. This research has provided insight regarding reaction conditions appropriate for the organostannane polymers. Ideally, these organostannane

polymers, like **2.3**, will be used with SPOC for combinatorial applications. To this end, our laboratory continues to expand the repertoire of reactions available on this solid phase.

Janabi[27] and Manning[28] have investigated novel ways to attach aromatic carboxylic acid derivatives to polymer **2.3** without using problematic lithiated intermediates. Tethering a aromatic carboxylic acid derivative to the polymer as an arylstannane would allow for varied chemistry on the solid phase. Marzinzik[29] has discussed that aromatic aldehydes grafted on a solid phase are pivotal branch points for combinatorial synthesis. After transformation of the aldehydes to α,β-unsaturated ketones, various polymer-bound heterocycles are accessible including pyrazoles, pyridines, and dihydropyrimidines. The varied functional groups available following cleavage from the organotin solid support would further expand the combinatorial variability of this approach.

2.1.8 Applications for Other Polymer-Bound Organotin Functionalities

The bulk of our research interest has concentrated on preparation of polymer-supported arylstannanes. Subsequent reactions while attached to the solid phase have provided insight into reaction conditions compatible with polystyrene-tethered organostannanes. Quantitative characterization of the cleavage products has revealed the reactivity of the polystyrene-tethered arylstannanes relative to conventional solution phase reagents. To date, research had been restricted to organostannane polymers with the maximal obtainable loading capacity. Moving beyond arylstannanes, we wished to explore other polymer-bound organotin functionalities.

Polystyrene-supported di-n-butylstannanes **2.4** and tetra-n-butyldistannanes **2.6** have been reported by Neumann[13] but only radical type reactions using these polymers have been explored. As discussed in Section 2.1.5, trialkyltin hydrides are precursors to a variety of functional groups. In solution phase, deprotonation with a strong base leads to the trialkylstannyl

anion. This anion can react with trialkysilylchloride to yield a silylstannane[30]. Silylstannanes are known to form mixtures of products upon reaction with aryl- or alkyl-electrophiles in the presence of a palladium catalyst according to the scheme in Figure 2.11[31]. Cyanocuprate catalysts are also known to effect a similar coupling[32].

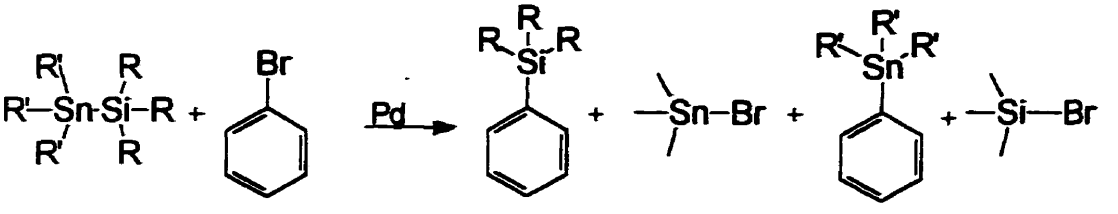

Figure 2.11: Palladium catalyzed coupling with silylstannanes

Mori[31] has discussed factors which can alter arylstannane versus arylsilane formation in solution phase silylstannane palladium coupling reactions. We wished to prepare silylstannanes on the organotin solid support. If successful, palladium catalyzed coupling studies would determine if tin versus silicon selectivity reflected that of the solution phase reagents. If tin incorporation can be favoured, this method could potentially represent a high yielding preparation of arylstannanes for pharmaceutical precursors that circumvents protecting group chemistry and lithiated intermediates.

Solution phase distannanes are also known to couple aryl- and alkyl-electrophiles in the presence of palladium[33]. Tin versus silicon selectivity could be avoided in this novel approach to arylstannanes, offering an advantage over silylstannanes. As illustrated schematically in Figure 2.12, applying this approach to a solid support means only 50% of the available tin sites would be present as arylstannanes.

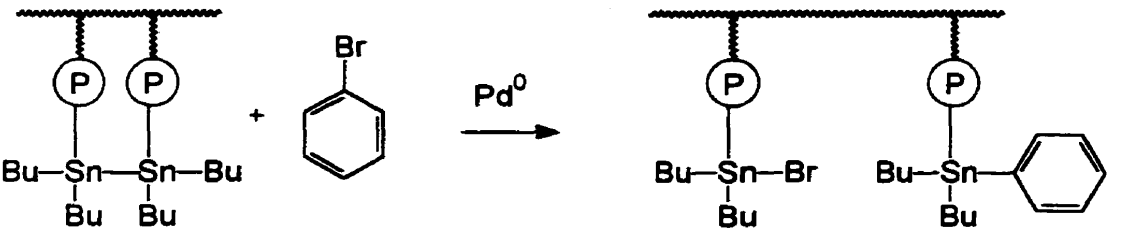

Figure 2.12: Schematic of palladium catalyzed coupling with polymer bound distannanes

Since both tin sites of the distannane are linked to the polymer, a mixture of aryl-tin and electrophile-tin would result. This could lead to product mixtures in subsequent transformations, possibly negating the positive aspects of SPOC. The resultant product mixtures would be dependent on the reactivity of the electrophile-tin species byproduct from the distannane palladium coupling. Despite this potential disadvantage, distannanes with various loading capacities are of interest. Distannanes require tin sites to be in close vicinity within the polymer matrix. It was suggested this functional group may provide insight into the proximity of tin sites along the polymeric backbone.

Polystyrene-tethered di-*n*-butylchlorostannanes **2.3** can be readily hydrolysed with aqueous base to give tin-oxygen species. Solution phase tin oxides are known to mediate esterifications, transesterifications, and deesterifiactions[34]. We wished to determine the type of tin oxide functionality present after hydrolysis of the chlorostannane polymer **2.3**. Ideally this tin oxide could be applied to esterification type reactions. The polystyrene-bound tin oxide could possibly also be applied as a solid phase protecting group for carboxylic acids. In addition, attachment of the tin oxide species to a solid support may be used to alter intramolecular versus intermolecular esterifications of bifunctional molecules.

2.1.8.1 Proposed Project

To date, only maximal loading chlorostannane polymers have been prepared. We wished to alter the polymer composition to see how bulk properties, tin distribution, and reactivity would be effected. Polystyrene-based di-*n*-butylchlorostannane copolymers of various loading capacities and crosslinking abilities were to be prepared and characterized. These copolymers would then be converted to tin hydrides, distannanes, silylstannanes, tin oxides and tin carboxylates. With the exception of tin hydrides and distannanes, the other functional groups represent novel preparations. These polymer-bound tin functional groups would be examined to determine whether the reactivity reflected that of solution phase reagents. We were also interested in the effect loading capacity would have on the reactivity of various functional groups. We would examine the various functional groups under reduced loading capacities to better understand the three dimensional structure of the solid phase matrix. These new polymer-bound functional groups would be fully characterized. Ideally, applications to SPOC could be tested to demonstrate the wide utility of this polymer system.

2.2 Results and Discussion

2.2.1 Summary

Four different poly(monomer-**2.2**-co-styrene-co-divinylbenzene) compounds have been prepared. These copolymers differ in the proportions of the three different monomers used for their preparation. One of the four copolymers has also been prepared with reduced amounts of divinylbenzene as a crosslinking agent. These polymers were characterized by solid state NMR spectroscopy, EDX analysis, infrared spectroscopy and wet chemistry techniques.

Following characterization, the di-*n*-butylchlorostannane copolymers were transformed into various organotin functional groups. Hydrolysis to stannols and distannoxanes gave information regarding the three dimensional structure of the polymer matrix. These functional groups also have applications in solid phase organic chemistry (SPOC) as esterification catalysts. The practical SPOC application of polymer-bound stannols and distannoxanes has been discussed in Chapter three. The reduction of the chlorostannane copolymers to distannanes also gave some information regarding the polymer structure. Distannanes can be applied to SPOC arylstannane preparation.

Further expanding the copolymer-bound organotin functional groups available, conversion to tin carboxylates, tin hydrides and silylstannanes was attempted with mixed results. The tin carboxylates were investigated as solid phase protecting groups for carboxylic acids, well documented applications in solution phase chemistry. Silylstannanes, and the tin hydrides required for their preparation, were also investigated. Only preliminary applications of silylstannane were investigated.

The research discussed in this chapter has served to expand our knowledge of the di-*n*-butylchlorostannane copolymer preparation, characterization and reactivity. These studies will further our attempts to apply the di-*n*-butylchlorostannane polymers to SPOC.

2.2.2 The Polymerization

The copolymers investigated in this study were prepared by emulsion polymerization, as detailed by Neumann[12]. Minor adjustments were made, particularly with the reduced loading and reduced crosslinking copolymers. These small changes were made in an attempt to maximize copolymer loading capacities and simplify preparation. All the copolymers were prepared with monomer **2.2** resulting from the hydrostannylation of DVB, presumably with di-*n*-butylchlorostannane **2.11**. Di-*n*-butylchlorostannane is prepared by *in situ* conproportionation as shown in Figure 2.13.

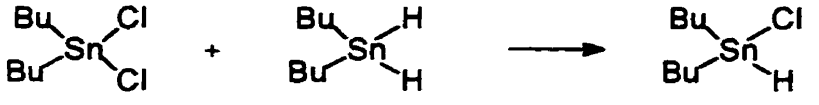

2.10 **2.11**

Figure 2.13: Disproportionation to yield di-*n*-butylchlorostannane

Solution phase ^{119}Sn NMR spectral studies have indicated that the disproportionation of **2.10** and di-n-butyldichlorostannane gives di-*n*-butylchlorostannane **2.11** as the major species with a signal at -46.3 ppm as indicated in Figure 2.14.

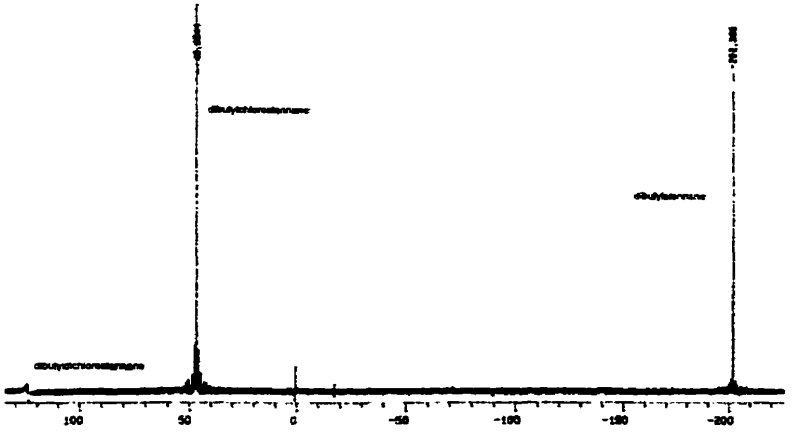

Figure 2.14: ^{119}Sn NMR spectrum of di-*n*-butylchlorostannane

Compound **2.10** and di-n-butyldichlorostannane are reacted in the presence of DVB at or below ambient temperature, as Neumann's procedure dictates. DVB can be hydrostannylated with **2.11** to yield the desired monomer **2.2**. However, di-*n*-butylstannane **2.10** can also hydrostannylate DVB directly to yield **2.18** as indicated in Figure 2.15. Solution phase ^{1}H NMR spectroscopic analysis of a reaction aliquot from monomer preparation, included in Figure 2.16 did not indicate any of the undesired monomer **2.18** as evidenced by the lack of a tin hydride signal at 4.7 - 5.0 ppm. No attempt was made to interpret the aromatic or butyl regions of the spectrum. Ethylvinylbenzene, as indicated on the spectrum, is present in about 22% yield relative to DVB.

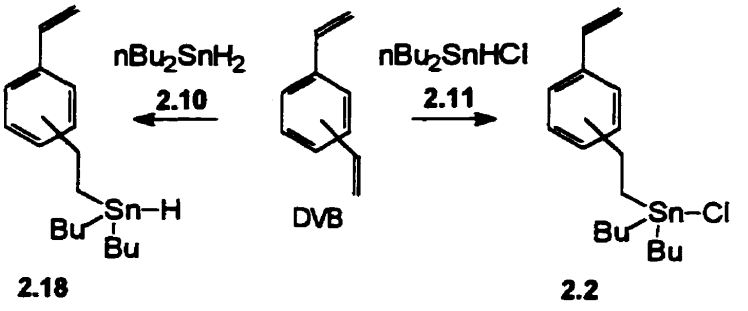

Figure 2.15: Two Possible Monomers Formed with DVB

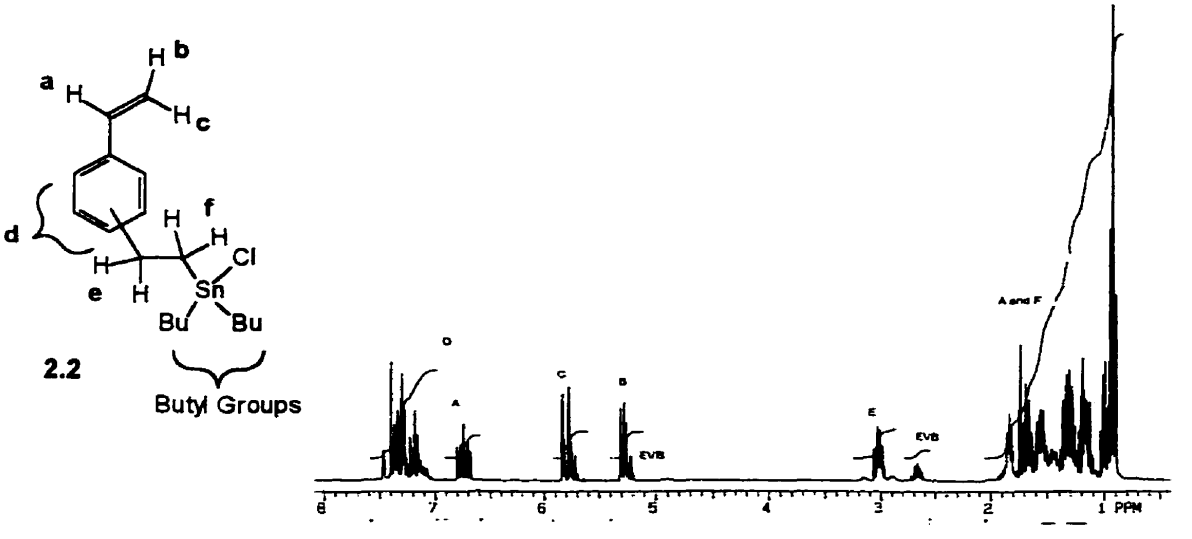

Figure 2.16: ^{1}H NMR spectrum aliquot from monomer **2.2** preparation

The monomer **2.2** is polymerized by addition of more DVB and free radical initiator followed by heating in a two phase system to yield the solid support **2.3** with a single tin species as confirmed by MAS solid state ^{119}Sn NMR spectroscopy. It is interesting to note that MAS solid state ^{119}Sn NMR spectroscopy only indicated a chlorostannane species, even though polymerization involved heating at reflux in the presence of water. Under these reaction conditions, no hydrolysis of the chlorostannane has occurred.

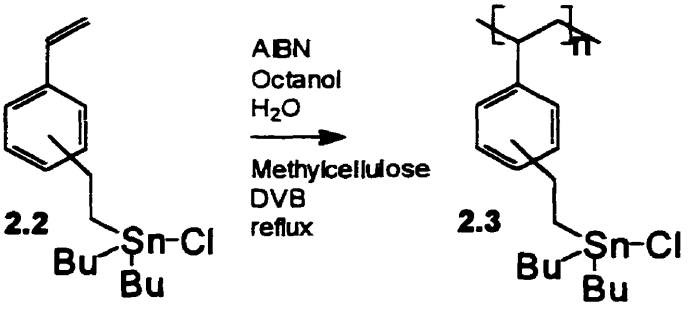

Figure 2.17: Polymerization step

2.2.3 Preparation and Characterization of High Loading Polymers

Four copolymers were prepared in this study and are best distinguished in terms of loading capacity and degree of crosslinking. Loading capacity is a measure of the moles of functional groups per gram of polymer. For the purpose of this discussion, a high loading polymer refers to the maximum loading capacity attainable, prepared by using **2.2** as the sole monomer. Less than optimally loaded copolymers, termed medium and low loading capacity, will be discussed in the next section.

It should be realized that the structural representation for the chlorostannane copolymer **2.3** is an oversimplification. It ignores the inclusion of 20 mol% of DVB in the polymerization mixture. In addition, this representation doesn't account for further changes in monomer proportions during the polymerization since copolymer yields of only 50-65% (by weight)

were obtained. Ignoring this factor, a hypothetical loading capacity can be determined by assuming that the monomer and DVB are incorporated into the polymer in the same proportions as they were initially present. For example, copolymer **2.3A** was prepared with 6.5 g DVB and 89 g (225 mmol) of functionalized monomer. Hypothetical maximum loading capacity was determined as 225 mmol / (6.5 g + 89 g), which equals 2.35 mmol/g.

Di-*n*-butylchlorostannane functionalized polystyrene with high loading capacity and 20 mol% crosslinking **2.3A** was the most studied copolymer system. In our hands, we have prepared copolymers of 1.80 - 1.56 mmol/g loading. This represents a range of 78 - 68% of hypothetical loading capacity, calculated above. Reasons for this less than optimal loading include the approximately 20% contamination of technical grade divinylbenzene (DVB) with ethylvinylbenzene (EVB). EVB may have been hydrostannylated to yield the non-polymerizable intermediate **2.20**. It is unknown if hydrostannylation of this compound occurs but the yield and loading calculations were made assuming that EVB had not been hydrostannylated. The ^{1}H NMR spectrum included in Figure 2.16 suggest no hydrostannylation of EVB since small peaks perhaps due to the vinyl groups of EVB were observed at 5.7 and 5.2 ppm. Purification of the DVB prior to polymerization has been attempted however it is non-trivial and has only occasionally been used for copolymer preparation. No purification of DVB was done for this study.

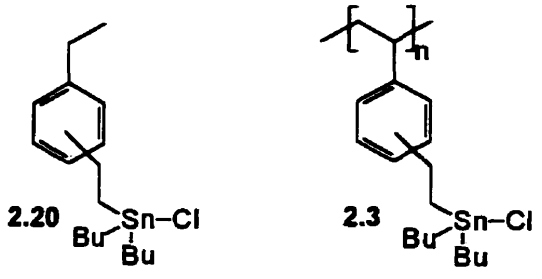

Loading capacities are determined by Mohr analysis[35]. The chlorostannane copolymer was hydrolysed in sodium hydroxide and aqueous

ethanol. The liberated chloride from this procedure was then titrated with standardized silver nitrate solution. EDX analysis has indicated that tin and chlorine are present in close to equimolar amounts and so the amount of chloride liberated is also a measure of the amount of tin present within the polymer. An example EDX analysis has been included in Figure 2.18 for polymer **2.3A**.

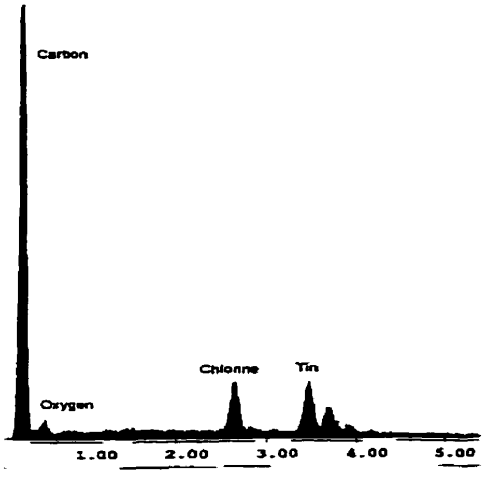

Figure 2.18: EDX analysis for elemental composition of **2.3A**

Discrepancies from maximal loading could arise from incomplete hydrolysis prior to Mohr titration. This would lead to artificially low loading capacity values. These concerns have been addressed by MAS solid state ^{119}Sn NMR spectroscopy. Analysis of the polymer prior to hydrolysis indicated only a single chlorostannane species in the NMR spectrum. A spectrum following hydrolysis and Mohr titration indicated no chlorostannane species remaining. Thus, complete reaction had occurred and loading capacity values are accurate. The before and after solid state ^{119}Sn NMR spectra have been included in Figure 2.19.

Practically speaking, sub-optimal loading capacities are acceptable if all tin species are present as the same type and reactivity. Most solid phases used in SPOC applications range from 0.1 - 1.0 mmol/g loading[9]. In our

polymer system, even 68% of maximal tin loading is substantially higher than many commercially available solid supports.

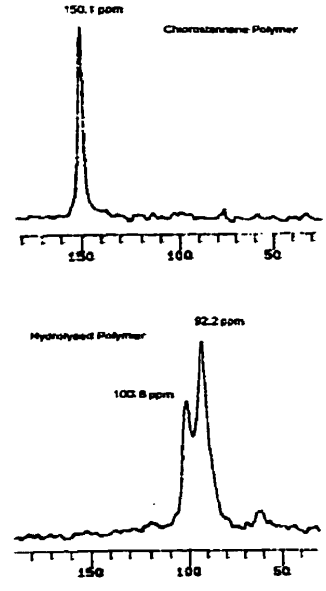

Figure 2.19: ^{119}Sn NMR spectra before (top) and after (bottom) hydrolysis of **2.3A**

EDX analysis should yield the elemental composition for the copolymer with 68% of maximal loading (1.56 mmol/g). Presuming a representative distribution of chlorostannane species in the area being analyzed, this composition is shown in Table 2.2 along with the calculated composition.

EDX analysis always included oxygen. This oxygen was not chemically bound to the organotin copolymer as evidenced by the single chlorostannane species in MAS solid state ^{119}Sn NMR studies. Analysis of the 1.56 mmol/g high loading resin, after correcting for oxygen, gives an elemental composition very close to calculated.

The error associated with low atom percent values in EDX analysis can be as high as 10%. Thus, within experimental error, tin and chlorine are present in equal amounts. This finding agrees with the MAS solid state NMR data. The elemental composition observed from EDX analysis for **2.3A** supports a random distribution of chlorostannane species through-out the copolymer matrix.

Table 2.2: Elemental composition from EDX analysis of high loading copolymer (1.56 mmol/g)		
Element	Theoretical Atom %	Experimental Atom %
Carbon	95.3	95.59
Tin	2.35	2.45
Chlorine	2.35	2.71

2.2.4 Altering Loading Capacity and Degree of Crosslinking

Following the preparation of high loading chlorostannane functionalized polystyrene **2.3A**, we investigated how reduced crosslinking and reduced loading would effect bulk polymer properties. Consequently, three novel copolymers were prepared. Two of these had reduced loading capacity (**2.3B** and **2.3C**) and the third had reduced loading and reduced crosslinking (**2.3D**).

The preparative procedures differed only slightly from the method for preparing the high loading capacity polymer. Styrene was copolymerized with the functionalized monomer **2.2**, and divinylbenzene as outlined in Figure 2.20. By varying the proportions of each compound, different loading capacity and crosslinking copolymers were produced. The proportions used for each preparation are indicated in Table 2.3.

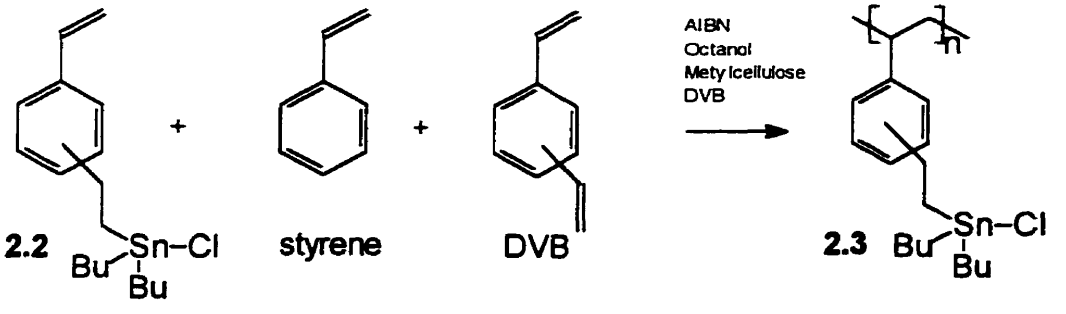

Figure 2.20: Preparation of reduced loading capacity copolymer

Copolymer **2.3B**, termed a medium loading polymer, incorporated chlorostannane monomer and styrene in equimolar amounts and thus should have half the loading capacity as the high loading polymer. Polymers **2.3C** and **2.3D** were low loading polymers, incorporating approximately one tenth the chlorostannane monomer. Crosslinking was kept constant at 20 mol % DVB for **2.3B** and **2.3C**. DVB crosslinking was reduced in **2.3D** to 3 mol % which is more typical for commercial polystyrene-co-divinylbenzene resins.

Table 2.3: Relative monomer proportions for reduced loading and reduced crosslinking copolymers

Polymer Type	Monomer **2.2** (mol %)	Styrene (mol %)	DVB (mol %)
High loading, high crosslinking **2.3A**	80	0	20
Medium loading, high crosslinking **2.3B**	40	40	20
Low loading, high crosslinking **2.3C**	8	72	20
Low loading, low crosslinking **2.3D**	10	87	3

All three copolymers were characterized by MAS solid state ^{119}Sn NMR spectroscopy, EDX analysis, FT-IR spectroscopy, and Mohr analysis. MAS solid state ^{119}Sn NMR spectroscopy indicated a single tin species, chlorostannane, for all three copolymers. From EDX analysis it was concluded that equimolar amounts of tin and chlorine were present in each copolymer. FT-IR analysis using a DRIFTS accessory gave aromatic overtones in the low loading copolymers, indicative of styrene incorporation in the polymeric backbone.

Hydrolysis with sodium hydroxide in aqueous ethanol and Mohr titration of the resultant free chloride indicated loading capacities of 1.1 mmol/g, 0.24 mmol/g, and 0.04 mmol/g for **2.3B**, **2.3C**, and **2.3D** respectively. These

numbers respectively represent approximately 46%, 10% and essentially 0% loading of maximum calculated. The lack of hydrolysis of **2.3D** indicated that the chlorostannane groups are inaccessible to sodium hydroxide reagent. Polymer **2.3D**, unlike the other copolymers, did not noticeably swell in aqueous ethanol, the hydrolysis solvent. At low crosslinking levels, this polymer seems to have suffered from irreversible pore collapse. Hydrolysis in a different solvent system was not investigated. MAS solid state ^{119}Sn NMR spectroscopy confirmed that hydrolysis was unsuccessful for copolymer **2.3D**. Only chlorostannane functional groups were present following the hydrolysis procedure.

Since loading capacity was reduced in all these copolymers, the chlorostannylated monomer would become diluted in the polymer backbone. Multiple EDX analyses of the same copolymers indicated significant variability in absolute composition as presented in Table 2.4, although relative amounts of tin and chlorine remained close to equivalent.

Table 2.4: Multiple EDX analyses of reduced loading copolymers

Polymer Type	Chlorine (atom %)	Tin (atom %)	Ratio Cl/Sn
Medium loading, high crosslinking **2.3B**	1.23	1.38	0.89
	0.84	0.94	0.89
	1.03	1.05	0.98
Low loading, high crosslinking **2.3C**	0.32	0.37	0.86
	0.36	0.43	0.84
Low loading, low crosslinking **2.3D**	0.31	0.33	0.93
	0.26	0.28	0.92

At low atom percents, EDX analysis errors can be as high as 20%.

Consequently, it is difficult to conclude if the variability is a function of the analysis technique or the non-random distribution of tin within the copolymer. Other methods were required to comment on the homogeneity of the chlorostannane copolymers with reduced loading capacity.

2.2.5 Structural Studies

With high loading copolymers, Neumann[18] concluded that as much as 97% of available chlorostannane functional groups could be converted to distannanes. This finding suggests the tin sites are flexible within the polymer matrix and are in close enough proximity so as to react with each other. With such a rigid, highly crosslinked copolymer matrix, this result was surprising.

In addition, our own studies regarding hydrolysis of chlorostannanes with sodium hydroxide in aqueous ethanol resulted in varying amounts of distannoxanes depending upon the copolymer loading capacity. Like the distannanes, formation of distannoxanes would require the hydrolysed tin species to be in close proximity within the polymer and be flexible enough to react with one another. These two copolymer-bound organotin functional groups were used for indirect studies on the distribution of tin species within the polymer matrix. These functional groups were also targeted for potential SPOC applications. These SPOC applications will be discussed later in this Chapter.

2.2.5.1 Preparation of Polymer-Bound Distannoxanes and Stannols

Mohr analysis to determine loading capacity of the chlorostannane copolymers required hydrolysis in basic aqueous ethanol to liberate chloride. Analysis of the resultant copolymers by MAS solid state ^{119}Sn NMR spectroscopy following hydrolysis indicated two tin signals at 92 and 101 ppm respectively. In solution phase, hydrolysis of tri-*n*-butylchlorostannane is found to yield tri-*n*-butylstannol[10b] in equilibrium with hexa-*n*-butyldistannoxane as indicated in Figure 2.21.

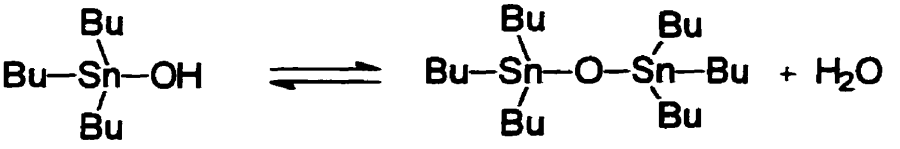

Figure 2.21: Solution phase distannoxane/stannol equilibrium

This equilibrium has been reconfirmed by solution phase ^{119}Sn NMR spectroscopic studies. Anhydrous hexa-*n*-butyldistannoxane, in $CDCl_3$, gives almost exclusively a signal at 93.0 ppm in the ^{119}Sn NMR spectrum. There is a small amount of a second signal at 104.7 ppm as well. In d_6- benzene the distannoxane gives a signal at 84.7 ppm, illustrating a significant solvent dependence. After treating hexa-*n*-butyldistannoxane with water and re-analyzing in $CDCl_3$, the peak at 104.7 ppm becomes much larger at the expense of the distannoxane species at 93.0 ppm. Presumably the peak at 104.7 is due to the tri-*n*-butylstannol compound.

The chemical shifts observed in the solution phase NMR spectrum closely reflect those species seen in the MAS solid state ^{119}Sn NMR spectra. A NMR spectrum of the hydrolyzed chlorostannane polymer **2.3A** is included in Figure 2.22. After comparison to the solution phase studies, the MAS solid state NMR peak at 101 ppm was assigned as di-*n*-butylstannol functionalized polystyrene. The peak at 92 ppm was assigned to the distannoxane species. Similar assignments had been made by Dumartin[36] who had prepared a polystyrene-bound distannoxane **2.22** as a complex mixture and assigned its chemical shift at +83 ppm. Dumartin does not pre-swell his polystyrene-based supports prior to MAS solid state ^{117}Sn NMR analysis. The ten ppm difference between this chemical assignment and our own may simply be due to solvent dependence, much like moving from benzene to chloroform in solution phase NMR studies.

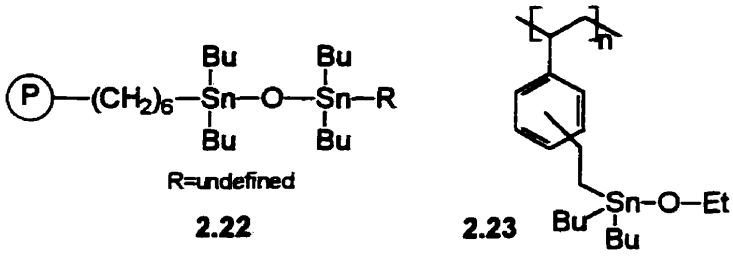

2.22 **2.23**

No established chemical shift data for tri-*n*-butylstannol was found in the literature. Although the equilibrium has been well documented, there was a remote possibility that the second species, at 101 ppm could be something other than the expected stannol. Another reasonable possibility was formation of the tin alkoxide of ethanol **2.23** under the hydrolysis reaction conditions. This possibility was quickly eliminated since the solution state ^{119}Sn NMR chemical shift of this tin alkoxide has been assigned at +76 ppm[37]. In addition, tin alkoxides are reported to be hydrolytically unstable and would not survive on the solid support without extensive precautions. Thus, the hydrolysed copolymer species were assigned conclusively as stannol and distannoxane.

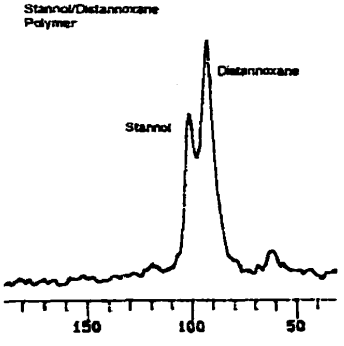

Figure 2.22: MAS solid state^{119}Sn NMR spectrum of distannoxane/ stannol copolymer **2.3B**

All copolymers **2.3** indicated a mixture of stannol and distannoxane in the MAS solid state ^{119}Sn NMR spectrum. An example of the medium loading capacity copolymer, following hydrolysis, is shown in Figure 2.22. Stannol was

thought to represent polymer-bound species that were in isolation, unable to react with adjacent tin sites, whereas distannoxanes species resulted from tin sites that were in close enough proximity to react. The relative intensities of the stannol species versus distannoxane in the solid state NMR spectrum was thought to be useful for conclusions regarding the proximity of tin sites. Thus, the relative amounts of distannoxane to stannol, for the various loading capacity polymers, were compared as summarized in Table 2.5. These relative peak intensities, taken from the solid state ^{119}Sn NMR spectra, are only approximate due to the overlap of each signal. The decrease in the relative amount of distannoxane to stannol is not directly proportional to the decrease in copolymer loading capacity.

To ensure the relative amounts of copolymer-bound distannoxane and stannol were truly attributable to a proximity effect, copolymer **2.3A** was hydrolysed at room temperature overnight and then analysed by MAS solid state ^{119}Sn NMR spectroscopy. The same sample of copolymer **2.3A** was then refluxed in benzene for 24 hours with azeotropic removal of water and analyzed by solid state ^{119}Sn NMR spectroscopy. No change in the relative amounts of polymer-bound distannoxane and stannol was observed. This implies that the relative amounts of distannoxane and stannol are determined by the proximity of adjacent tin species within the copolymer matrix.

Table 2.5: Polymer-bound distannoxane:stannol ratio as a function of copolymer loading capacity

Copolymer Type	Loading Capacity	Distannoxane: Stannol ratio	mmol Distannoxane/ mmol Stannol (calc'd)
2.3A	High 1.6 mmol/g	3.0	0.6 / 0.4
2.3B	Medium 1.1 mmol/g	2.0	0.37 / 0.37
2.3C	Low 0.24 mmol/g	0.5	0.04 / 0.16

Clearly the relative amount of distannoxane decreased as copolymer loading capacity was reduced. This supports the conclusion that the chlorostannane monomer was randomly diluted when styrene was included during polymerization in the reduced loading preparations.

2.2.5.2 Preparation of Polymer-Bound Distannanes

Neumann has reported that chlorostannane functionalized polystyrene **2.3** can be reduced with lithium naphthalide to yield polymer-bound distannane **2.6**[18]. This distannane product was prepared under anhydrous conditions and characterized by tin gravimetry and distannane iodometry. No solid state ^{119}Sn NMR spectral studies were done on this distannane system.

Our own solution phase ^{119}Sn NMR spectral studies on commercially available hexa-*n*-butyldistannane identified the distannane tin chemical shift at -80 ppm. Dumartin's solid state ^{117}Sn NMR spectral studies on a complex mixture of polymer-bound species identified a distannane at -83 ppm[36]. The chemical shift of Neumann's polystyrene-bound distannane was expected to be similar.

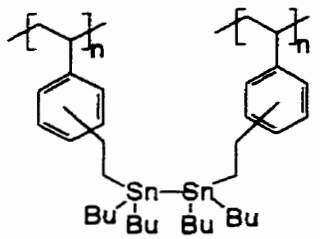

2.6

The preparation of distannanes **2.6A**, **2.6B**, and **2.6C** was attempted with the various loading copolymers **2.3A**, **2.3B**, and **2.3C** respectively. The reduced crosslinking copolymer **2.3D** was not used in this study due to its poor swelling properties. During distannane preparation, precautions were taken to shield the products from light. No such precautions were outlined in the original preparation however there was concern over the stability of the distannane

products. The copolymers **2.6A**, **2.6B**, and **2.6C** were analyzed by FT-IR spectroscopy immediately following preparation. As expected, no new peaks attributable to Sn-Sn were apparent in the FT-IR spectra. The most important observation was that these products differed from the distannoxane/stannol copolymers in the 1600-1450 cm^{-1} region and contained no peak due to Sn-H stretching in the 1800 cm^{-1} region.

EDX analysis for elemental composition was performed 3 days after preparation. No chlorine was evident in products **2.6B** and **2.6C** which supported complete reduction of the chlorostannane species. Product **2.6A** contained approximately 1:10 chlorine to tin (0.28:2.77 atom %) indicating about 90% reduction. Oxygen was present in all samples in approximately the same amount (7.68 - 8.72 atom %).

There was a significant delay prior to MAS solid state ^{119}Sn NMR analysis. Approximately 9 - 12 days following preparation, the copolymers **2.6A**, **2.6B**, and **2.6C** were analyzed by MAS ^{119}Sn NMR spectroscopy. Polymers **2.6A** and **2.6C** indicated the presence of a single tin species at +83 ppm. This NMR chemical shift is not appropriate for a distannane product expected at -80 ppm but instead more closely coincides with a tin oxygen species, possibly distannoxane or tin peroxide.

The MAS solid state ^{119}Sn NMR spectrum for polymer **2.6A** has been included in Figure 2.23. Although resolution is poor, it is obvious that only a single tin species is present. Copolymer **2.6B** gave the same signal as the predominant species with minor peaks at -78 and -88 ppm. The minor peaks were poorly resolved and no attempt was made to quantify the relative intensities.

The delay in obtaining NMR spectra may have been sufficient for the air oxidation of the distannane species according to Figure 2.24. Commercially available hexa-alkyldistannanes are known to undergo air oxidation to yield distannoxanes via a bis(stannyl)peroxide intermediate. The peroxide

decomposes to distannoxane at room temperature[38].

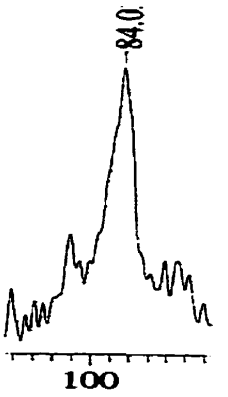

Figure 2.23: MAS solid state ^{119}Sn NMR spectrum of **2.6A** as a neat powder

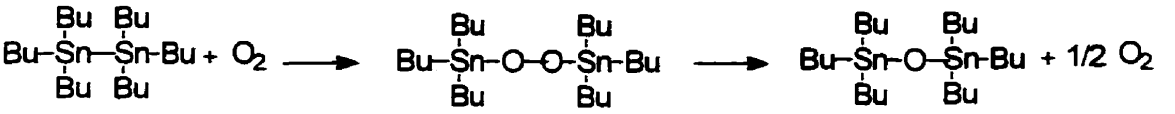

Figure 2.24: Formation and decomposition of bis(stannyl)peroxides

Interestingly, a single tin oxygen species was prepared as the major product for all three copolymers despite the wide variability in tin loading capacity. The tin-oxygen species cannot simply be a result of the hydrolysis of the original tin chlorine bond from chlorostannane **2.3A**. It has been shown that hydrolysis leads to mixtures of distannoxane/stannol in the NMR spectrum, not a single product. We are confident that reduction did occur, as evidenced by the EDX analysis with the absence of chlorine.

It is thought that the distannane species has been prepared and air oxidized to the distannoxane prior to NMR analysis. Although a bis(stannyl)peroxide is a possible product from the oxidation of a distannane, the analogous solution phase bis(tributyltin)peroxide is reported to decompose completely at room temperature within 24 hours[39]. If the tin peroxide reactivity is at least that of the solution phase species than no peroxide would have survived to be analyzed by NMR 12 days following preparation. The tin species

ultimately resulting from air oxidation of distannane is a single tin-oxygen species. If the species is truly a distannoxane then the tin sites must be in close enough proximity to yield one oxidation product exclusively. Alternatively, the tin sites must be flexible within the copolymer to enable the formation of the distannoxane product exclusively.

Neumann reported no difficulties with polymer-bound distannane preparation however no precautions against air oxidation were reported. Characterization by iodometry indicated high yields of distannane. In light of our NMR spectral findings, commercially available hexa-*n*-butyldistannoxane was treated with iodine[40]. The distannoxane consumed equimolar amounts of iodine as did hexa-*n*-butyldistannane. Clearly, characterization by iodometry is not a valid distannane quantitation method. These studies, including the identification of the products from distannoxane iodination, are continuing. Ideally the polymer-bound distannane preparation could be repeated with precautions regarding air exposure prior to NMR spectral analysis. Unfortunately, the solid state MAS NMR analyses became both cost and time prohibitive. These preparations will be repeated upon installation of a in-house solid state NMR spectrometer. Solid state ^{119}Sn NMR analyses cost, on average, $176 per sample and require 12 - 22 hours of spectrometer time. An in-house solid state spectrometer is slated for installation within 12 months.

2.2.5.3 Conclusions Regarding Structural Studies

The distannane preparations are not completely consistent with the stannol/stannoxane studies. The stannol/distannoxane ratio implies a dilution effect along the copolymer chain as more styrene is added. The hydrolysis of the chlorostannane copolymers supports the random distribution of tin species through-out the copolymer backbone. The relative amounts of distannoxane to stannol decreased with decreased loading of the hydrostannylated monomer **2.2**. The decrease in distannoxane was not exactly proportional to the

decrease in loading capacity, however changes were significant and consistent. Had the ratios not changed dramatically, then block co-polymerization of the functionalized monomers would have been suggested. Block copolymerization would essentially translate into pockets of chlorostannylated monomers, separated by amounts of non-functionalized polymer. The pockets of chlorostannylated monomers would be in close enough proximity to freely react with one another upon hydrolysis yielding large amounts of distannoxane species relative to stannols despite varied loading capacity.

The distannane species with the resulting single air oxidized product seem more consistent with a block co-polymerization of styrene and monomer **2.2** because there was no apparent dilution effect. The formation of a single species containing two polymer-bound tin sites linked by one oxygen, as a distannoxane, would require all tin sites to either be in close proximity or be flexible enough to allow movement into close proximity relative to one another. Hopefully, the continuing studies on distannane preparation will serve to clarify the actual polymer structure.

The composition of a copolymer produced by free radical polymerization can be postulated by using rate constant ratios for each possible propagation step as depicted in Figure 2.25. Growing chains ending with monomer 1 can react with monomer 1 or with monomer 2. The two rate constants describing these possibilities are k_{11} and k_{12}. The ratio of k_{11}/k_{12} is termed the r_1 value. Similarly, growing chains ending in monomer 2 can react with more monomer 2 by k_{22} or with monomer 1 by k_{21}. The ratio of k_{22}/k_{21} is termed r_2. Tabulations of r_1 and r_2 values are available for many combinations of monomer pairs[41].

Not surprisiningly, the r_1 and r_2 values for monomer **2.2** and divinylbenzene have not been determined. It is known that styrene and DVB, based on r_1 and r_2 values, yield a block copolymer with a highly crosslinked DVB core and flexible arms of polystyrene[48] . It is also known that styrene and 4-methylstyrene, based on $r_1 = 0.89$ and $r_2 = 0.99$[41], yield a random copolymer.

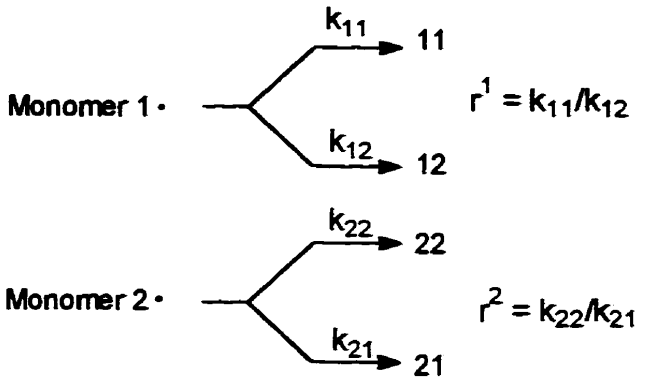

Figure 2.25: Relative rates for copolymerization

If it can be assumed that 4-methylstyrene and monomer **2.2** have similar selectivities, then styrene and monomer **2.2** should yield a random copolymer. Thus, copolymerization of styrene, monomer **2.2**, and DVB should yield a copolymer with a DVB core and flexible arms containing random monomer **2.2** and styrene.

If these analyses have validity, the high loading polymer **2.3A** appears to be comprised of a DVB core and flexible arms of highly functionalized polymer. The medium loading capacity copolymer **2.3B** would also be comprised of a DVB core but with a random distribution of chlorostannylated monomers and styrene monomers within the arms. This is a consequence of assuming similar, near integer, selectivity values for the chlorostannylated monomer **2.2** and styrene. Presumably the low loading copolymer **2.3C** would have a composition similar to the medium loading example. Copolymer **2.3C** should contain a DVB core and a random distribution of chlorostannylated monomer and styrene in the arms.

The minimally crosslinked arms extending from a highly crosslinked core might provide the necessary flexibility for distannane formation and subsequent air oxidation to distannoxane. There is an apparent difference between the amount of distannoxane formed from distannane oxidation versus that from

chlorostannane hydrolysis that is not readily explained.

2.2.6 Preparation of Other Polymer-Bound Functional Groups

2.2.6.1 Tin Hydrides

To further expand the spectrum of copolymer-bound organotin functional groups, tin hydrides and silylstannanes were targeted. Tin hydrides are a necessary intermediate for silylstannane preparation. A polymer-bound tin hydride **2.4** had been successfully prepared by Neumann[11] using di-*n*-butylaluminum hydride as the reducing agent. Di-*n*-butylaluminum hydride was not commercially available and its preparation was non-trivial[42]. As an alternative, lithium aluminum hydride (LAH) was used for the polymer-bound chlorostannane reduction. All preliminary studies were performed with the high loading capacity chlorostannane copolymer **2.3A**.

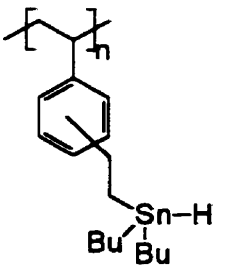

2.4

Polymer **2.3A** was reacted with excess LAH at room temperature in tetrahydrofuran (THF). FT-IR spectroscopy indicated a strong tin hydride stretch at 1805 cm^{-1}. The DRIFTS spectrum has been included in Figure 2.26 with the hydride stretch indicated. MAS solid state ^{119}Sn NMR spectroscopy indicated a mixture of four compounds; chlorostannane at +145 ppm, distannoxane/stannol at +100 ppm, trialkylstannane at -15 ppm, and tin hydride at -90 ppm. The chlorostannane was the predominant species in the mixture suggesting reduction was incomplete.

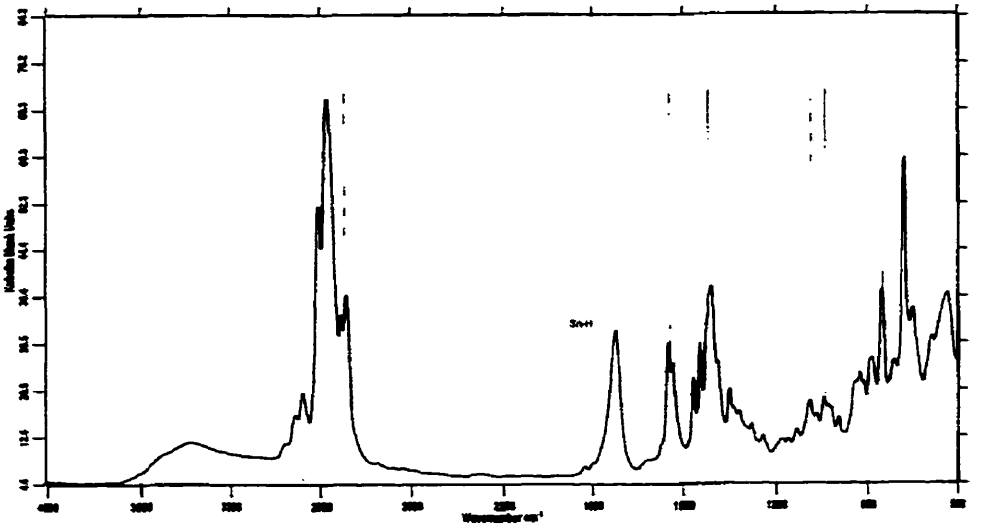

Figure 2.26: DRIFTS spectrum of polymer-bound tin hydride **2.4**

Copolymer **2.3A** was then reduced with excess LAH in refluxing THF. Once again, FT-IR spectroscopy indicated a strong tin hydride stretch at 1805 cm^{-1}. MAS solid state ^{119}Sn NMR spectroscopy indicated a mixture of three products; trialkylstannane at -17 ppm, distannoxane/stannol at +100 ppm, and tin hydride at -90 ppm with no chlorostannane species remaining. Tin hydride **2.4** was the major product. EDX analysis confirmed the absence of chlorine, suggesting reduction was complete. This same tin hydride product was analyzed on three occasions by solid state ^{119}Sn NMR spectroscopy. The ratio of tin hydride species to tin-oxygen species decreased dramatically over the 56 days it was studied. The integration ratio of Sn-H:Sn-O began as 2.23, and reduced to 0.73 and 0.31 on days 27 and 56 respectively. It was cost prohibitive to submit additional solid state ^{119}Sn NMR samples to further probe this oxidative phenomena. Presumably the tin hydride is air oxidized to stannol and/or distannoxane. This oxidation is known to occur by a radical chain mechanism in solution phase tin hydrides[10b]. Since more complete reduction of chlorostannane copolymer **2.3A** was observed under reflux, these reaction conditions were applied to the reduced loading copolymers.

Copolymer **2.3B** was reacted under reflux with excess LAH. The resultant product, **2.4B** was analyzed by FT-IR indicating a strong tin hydride stretch at approximately 1805 cm^{-1}. EDX analysis for elemental composition indicated no chlorine present. The copolymer was assumed to have been completely reduced but no solid state NMR spectra were obtained.

Applying these proven reaction conditions to copolymer **2.3C** resulted in no tin hydride as confirmed by FT-IR spectroscopy. Curiously, EDX analysis for elemental composition of this product indicated no chlorine. Apparently reduction had occurred but no tin hydride had survived on the polymer for analysis. This preparation was duplicated with similar results.

2.2.6.2 Silylstannanes

In solution, silylstannanes are successfully prepared by reaction of a stannyllithium with a silylchloride[30]. Repeating this established solution phase procedure, tri-n-butyltin hydride was deprotonated with lithium diisopropylamide (LDA) and quenched with trimethylsilylchloride. Analysis by solution phase ^{119}Sn NMR spectroscopy indicated trimethylsilyl(tri-*n*-butyl)-stannane as the major product at -120 ppm. Distannane, as a by-product in the spectrum at - 82 ppm, was present in approximately half the amount. A small amount of tin hydride remained at -88 ppm, indicating incomplete deprotonation by LDA.

Applying this method to the polymer-bound tin hydride, **2.4A** was reacted with LDA, prepared *in situ*, in an attempt to produce the copolymer-bound stannyllithium. The extent of deprotonation of **2.4A** was tested by quenching with CH_3OD, which should result in conversion of Sn-H to Sn-D. The resultant polymer was analyzed by FT-IR. A significant decrease in the relative size of the peak due to Sn-H at 1805 cm^{-1} was apparent in the spectrum as indicated in Figure 2.27. A new peak was observed at 1307 cm^{-1}, consistent with the isotopic shift for Sn-D.

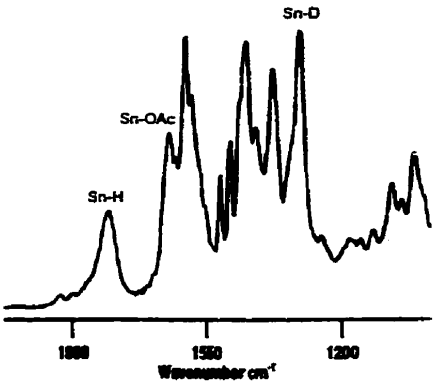

Figure 2.27: Expansion of DRIFTS spectrum of partially deuterated **2.4A**

After reacting copolymer **2.4A** with LDA, trimethylsilylchloride was added to quench the stannyllithium and form the silylstannane **2.17A** . This copolymer was washed with THF to remove any excess trimethylsilylchloride and then characterized. FT-IR analysis of the resultant polymer indicated only a small amount of tin hydride remained as evidenced by a significant decrease in the signal at 1805 cm^{-1}. However, the IR spectrum was of little further value since a peak due to Si-Sn was not expected in the normal IR region. More helpfully, EDX analysis indicated that silicon was present in approximately a 1:4 ratio compared to tin. This ratio is consistent with a 25% yield of copolymer-bound silylstannane. MAS solid state ^{119}Sn NMR spectroscopy indicated a mixture of four species in a ratio of 16:2:9:1 respectively. Chlorostannane was the major species with tin hydride the next most abundant. Trialkylstannane and silylstannane were present as minor species, with integration suggesting much less than 25% yield of silylstannane.

The tin hydride in the NMR spectrum was presumably from the incomplete deprotonation by LDA or quenching of the stannyllithium with a proton source. The alkylated tin species was carried over from the chlorostannane reduction that yielded product **2.4A**. Chlorostannane had to have been generated in the reaction as EDX analysis of the silylstannane

precursor **2.4A** had indicated no chlorine. As shown in Figure 2.28, the chlorostannane may have resulted from the reaction of stannol or distannoxane with trimethylsilylchloride. This would yield a copolymer-bound stannyl-siloxane and liberate chloride ion. The chloride ion could then attack the tin with trimethylsiloxy as a leaving group, resulting in the chlorostannane.

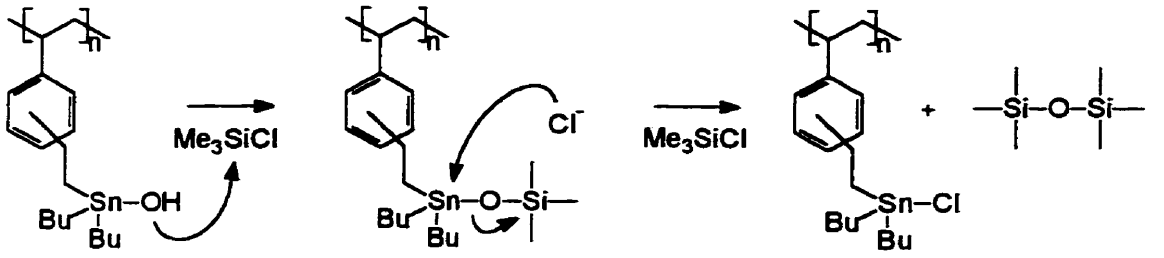

Figure 2.28: Proposed scheme for chlorostannane preparation

This possibility was not confirmed by reaction of distannoxane with trimethylsilylchloride. If correct, this method has the potential for simple regeneration of chlorostannane species from stannols and distannoxanes.

Various amounts of LDA were used in an attempt to improve silylstannane **2.17A** yields. The deprotonation was performed with 0.5, 1.0 and 2.0 equivalents of LDA relative to calculated maximum tin hydride **2.4A**. Unfortunately better yields were not realized, as indicated by EDX analysis for elemental composition. EDX analysis for the silylstannane **2.17A** preparations revealed a 1:4 ratio of silicon:tin for all three stoichiometric variations. These findings suggest the tin hydride must only be available as 25% of the maximum calculated yield. Thus, each stoichiometric experiment was essentially run with excess LDA amounts and yields were limited by the starting tin hydride availability. The limited success of this preparation is attributed to the purity of the copolymer-bound tin hydride **2.4A**.

Applying the silylstannane preparation, with equimolar LDA, to the medium loading capacity tin hydride **2.4B** resulted in a 1:10 silicon:tin ratio for

supposed silylstannane product **2.17B**, as determined by EDX analysis. No tin hydride was apparent after this preparation, as evidenced by the lack of a peak at 1805 cm^{-1} in the FT-IR spectrum. This may again be a comment on the purity of tin hydride available for deprotonation. No silylstannane preparation was attempted for the low loading copolymer since the tin hydride could not be formed in a detectable amount.

2.2.6.3 Improvements in the Silylstannane Preparation

Steps were taken to improve the yield of the polymer-bound tin hydride products **2.4**. Copolymer-bound distannoxane and stannol appeared to be a major byproduct with the lithium aluminum hydride (LAH) reduction. This may have resulted from a combination of tin hydride air oxidation and the hydrolysis of chlorostannane starting copolymer following incomplete reduction. After preparation of the tin hydride, the solid was washed with aqueous alcoholic sodium hydroxide to remove lithium and aluminum salts. If the tin hydride preparation was incomplete, the sodium hydroxide solution could hydrolyze any chlorostannane species still present.

The polymer-bound tin hydride **2.4B** preparation was repeated with LAH and the product washed with dilute aqueous acetic acid to remove the lithium and aluminum salts. FT-IR spectroscopic analysis indicated a pronounced tin hydride stretch at 1805 cm^{-1}. EDX analysis for elemental composition of this product indicated no chlorine, suggesting the complete reduction of the chlorostannane species **2.3B**. The hydride **2.4B** was then deprotonated with a slight excess of LDA (1.2 equivalents) and quenched with excess trimethylsilylchloride. FT-IR analysis of this supposed silylstannane **2.17B** indicated no tin hydride. Presumably LDA deprotonation was complete. EDX analysis for elemental composition indicated only a 1:20 ratio of silicon to tin. The silylstannane yield had not improved by eliminating the sodium hydroxide wash of the tin hydride **2.4B**. At this time, no solid state NMR spectra have

been obtained for the acid-washed tin hydride **2.4B** and the silylstannane **2.17B** prepared from it.

2.2.6.4 Tin Carboxylates

Attempts were made to prepare a copolymer-supported tin carboxylate of toluic acid **2.13** as a model for a possible solid phase carboxylic acid protecting group. The stannyltoluate **2.13** was prepared by reaction of the sodium salt of toluic acid and the chlorostannane polymer **2.3A** in refluxing benzene. Alternatively, the tin carboxylate **2.13** could be prepared with the hydrolysed polymer **2.12A** and toluic acid with azeotropic removal of water.

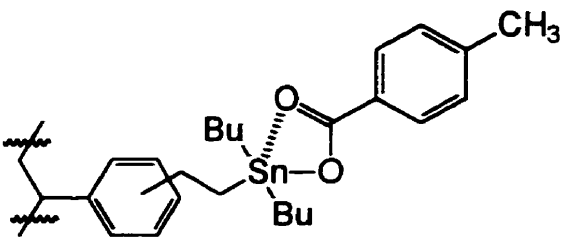

2.13

To assist in the characterization of this polymer-bound product, solution phase products were prepared. Tri-*n*-butylchlorostannane and the sodium salt of toluic acid were reacted in refluxing benzene. The resultant product was analyzed by FT-IR spectroscopy, showing a carbonyl stretch at 1638 cm^{-1} versus the starting material carboxylate salt at 1601 cm^{-1}. The observed carbonyl stretch was also different from toluic acid at 1684 cm^{-1}. Solution phase ^{119}Sn NMR spectroscopy for this product indicated a single tin signal at +108.5 ppm. This chemical shift is comparable to other tin carboxylates which appear from +96.3 ppm to +115.7 ppm in the literature, depending on the nature of the ester formed[43]. The polymer-bound stannyltoluate was characterized by FT-IR, indicating a carbonyl stretch at 1636 cm^{-1} which agrees with the solution phase product. MAS solid state ^{119}Sn NMR spectroscopy gave a single tin signal at +103 ppm. The tin carboxylate was generated quantitatively as evidenced by

the single tin species in the MAS solid state ^{119}Sn NMR spectrum.

The stability of the copolymer-bound tin carboxylate **2.13** was investigated with various reagents including trifluoroacetic acid, acetic acid, and methanol. The cleavage of stannyltoluate **2.13** was quantified by HPLC analysis. Cleavage was quantified as a function of reaction time with the reagent. The time course for tin carboxylate cleavage with trifluoroacetic acid, acetic acid, and methanol are presented in Figures 2.29, 2.30, and 2.31 respectively. Each cleavage study began with a methanol wash at room temperature as detailed in the Experimental (Section 2.3). The toluic acid cleaved with this initial wash was used as the zero time point for each curve.

Cleavage with 10% trifluoroacetic acid in dichloromethane represented the most efficient method for tin carboxylate cleavage. As illustrated in Figure 2.29, TFA caused 1.57 mmol of toluic acid to be cleaved per gram of polymer within 15 minutes of stirring. Although the reaction was allowed to proceed for 60 minutes, no further significant cleavage was seen beyond 15 minutes.

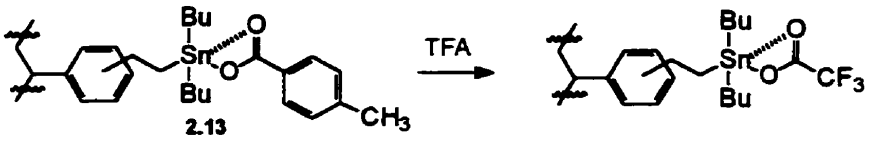

Stannyltoluate 2.13 Cleavage By TFA

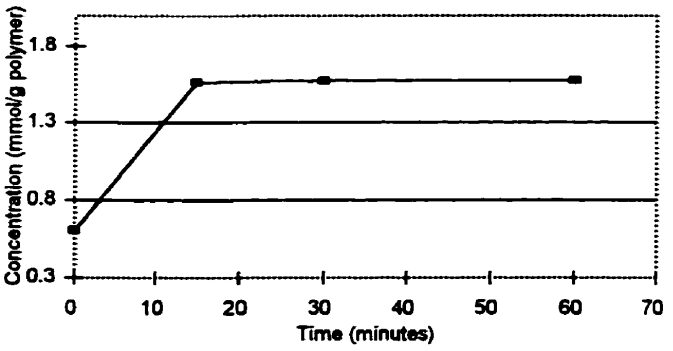

Figure 2.29:TFA / Dichloromethane cleavage of **2.13**

It seems that TFA causes complete cleavage of **2.13**. MAS solid state ^{119}Sn NMR spectroscopy indicated the stannytoluate signal at +103 ppm disappeared completely after TFA treatment. XPS analysis of the polymer following 60 minutes of reaction with trifluoracetic acid indicated that fluorine had become incorporated within the polymer. A new species was evident in the MAS solid state ^{119}Sn NMR spectrum at approximately +151 ppm. This may be attributed to the newly formed tin carboxylate of trifluoracetic acid.

Refluxing in a mixture of acetic acid and aqueous ethanol gave somewhat less rapid cleavage of polymer-bound stannyltoluate **2.13** than TFA/dichloromethane. As illustrated in Figure 2.30, acetic acid caused 1.25 mmol of toluic acid to be cleaved per gram of copolymer within 2 hours of reflux. After two hours, the cleavage of additional toluic acid was negligible. The curve shows a plateau from approximately 2 hours to 63 hours when the cleavage experiment was stopped.

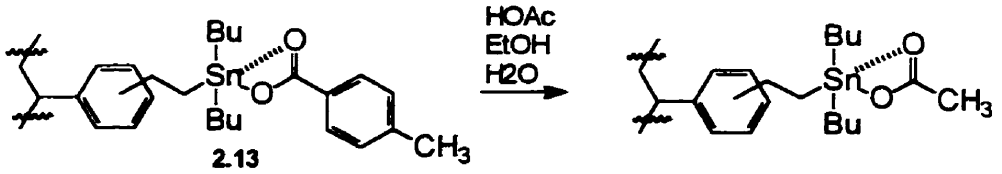

2.13

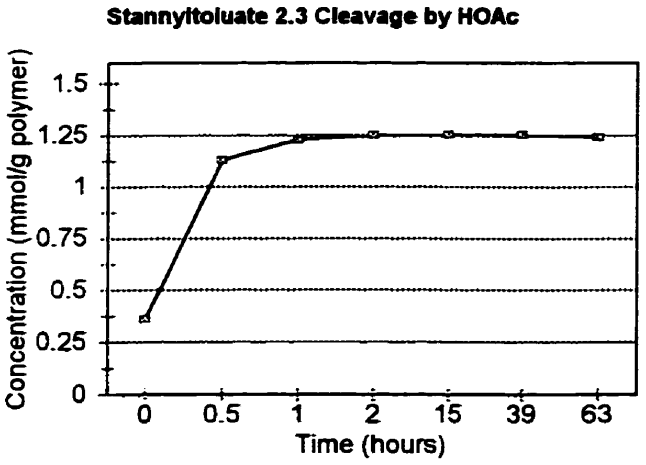

Figure 2.30: Acetic acid / aqueous ethanol cleavage of **2.13**

It appears that acetic acid in refluxing aqueous ethanol is unable to give complete cleavage of the tin carboxylate **2.13**. FT-IR analysis following the 63 hours of reflux indicates a tin carboxylate is still present at 1644 cm^{-1}. This ester could be attributed to either the original stannyltoluate **2.13**, a newly formed stannylacetate, or a combination of both. No MAS solid state ^{119}Sn NMR spectra were obtained for this product.

The methanol cleavage study for **2.13** emphasized the instability of polymer-bound stannyltoluate. As illustrated in Figure 2.31, copolymer **2.13** was stirred with methanol for a total of 120 minutes. By 30 minutes, 0.43 mmol of toluic acid had been cleaved per gram of solid support. Continuing the reaction to 120 minutes gave a small amount of additional cleavage. The cumulative amount after 120 minutes of cleavage was 0.49 mmol toluic acid per gram copolymer.

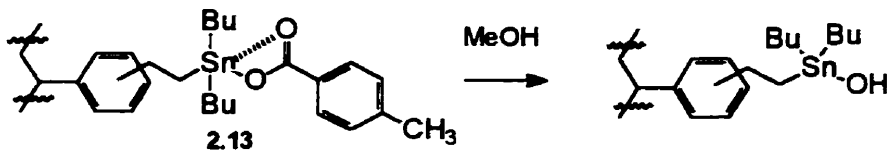

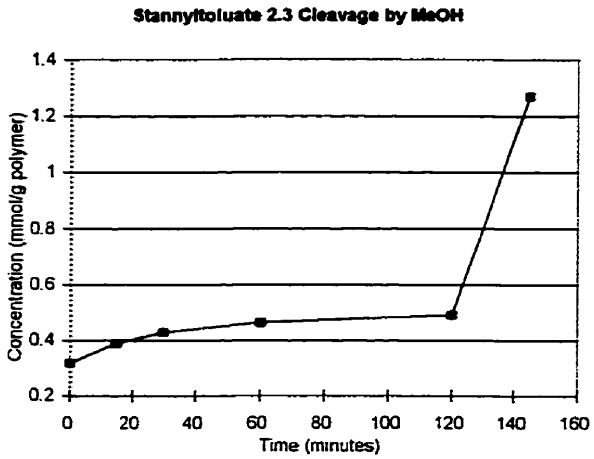

Figure 2.31: Methanol cleavage of **2.13**

The reaction appeared to be levelling off at less than complete toluic acid cleavage. To prove much more tin carboxylate **2.13** was available for cleavage, the polymer was stirred with10% TFA in dichloromethane at 120 minutes . After leaving the copolymer to stir with the TFA for 30 minutes, an additional 0.8 mmol of toluic acid had been cleaved from the solid support as indicated by the large jump in the experimental curve, Figure 2.31.

The amount of cleavage from each of the various reagents was substantial, ranging from about 40% to quantitative cleavage. The variability in cleavage amounts may be due in part to the swellability of the copolymer in each of these solvent systems. The polymer is highly swellable in dichloromethane and aqueous ethanol but swells less in 100% methanol. In addition, the relative amount of cleavage in TFA versus acetic acid is almost certainly a function of acid strength. TFA in dichloromethane would permeate the polymer as a neutral species. This neutral species, in combination with the great swelling ability of dichloromethane, would access all tin sites in the copolymer matrix. Acetic acid with a pK_a of approximately 5 is much weaker than trifluoroacetic acid, which gave quantitative cleavage .

2.2.7 Applications of Copolymer-Bound Functional Groups

This work targeted the preparation of polystyrene-bound distannoxanes/stannols **2.12**, tin carboxylates **2.13**, distannanes **2.6**, tin hydrides **2.4**, and silylstannanes **2.17**. Each of these functional groups have potential applications for solid phase organic chemistry (SPOC). The applications of distannanes, tin hydrides and silylstannanes were not investigated fully due to the difficulty associated with their preparation. We still desire a high yielding preparation method for these functional groups. The distannanes and silylstannanes are particularly attractive targets since they provide alternate synthetic routes to polymer-bound arylstannanes as discussed in Section 2.1. Tin hydrides are simply a necessary intermediate in the

silylstannane preparative route.

Ideally the chlorostannane copolymer could also be used as a solid phase protecting group for carboxylic acids. Solution phase trialkyltin groups have been applied as protecting groups for carboxylic groups in peptide synthesis[44]. Tethering the protecting group to a solid support was proposed to simplify purification. In solution phase, Greene has reported that tin carboxylates can be cleaved with water and alcohols[45].

A stannyltoluate **2.13** was prepared on the high loading capacity polymer **2.3A**. This tin carboxylate was to model a possible solid phase carboxylic acid protecting group. Our own cleavage studies indicated that along with water and alcohols, tin carboxylates can be extensively cleaved with acids. If alcohol can cause cleavage, presumably other weak nucleophiles can do similar damage. Cleavage with water, acids, alcohols, and other nucleophiles doesn't leave many reagents that a tin carboxylate can offer protection from. Unfortunately, the poor stability of the stannyltoluate **2.13** suggests that this solid phase protecting group would have little practical application in SPOC.

Stannols and distannoxanes are well documented as esterification and transesterification catalysts[34]. The SPOC application of these groups has been extensively studied. Polymer-bound tin oxides were applied as lactonization catalysts for ω-hydroxycarboxylic acids. This application is discussed in detail in Chapter three.

2.3 Experimental

Commercially available starting materials were used for the synthetic preparations which follow. Authentic (trimethylsilyl)tributylstannane was purchased from Gelest. Azo*bis*isobutyronitrile and technical grade styrene were purchased from Eastman Kodak. Authentic hexa-*n*-butyldistannane and all other preparative chemicals were purchased from Aldrich. BDH supplied all solvents as well as the phosphoric acid for HPLC eluents. EM Sciences supplied all silica for chromatographic separations.

Solution phase NMR spectra were recorded on either Varian Gemini XL-200 or XL-300 instruments. All solution phase ^{119}Sn NMR spectra were run with tetramethyltin as an internal reference. In-house MAS solid state NMR instrumentation was unavailable at the time of this research. The magic angle spinning (MAS) solid state spectra were run by technicians at a variety of NMR facilities including the University of Toronto (Bruker 200 and 300 MHz), University of Waterloo (Bruker 500 MHz), and Dow Chemical, Sarnia (Bruker 200 MHz). All solid state MAS ^{119}Sn NMR chemical shifts are reported in ppm relative to tetramethyltin or tetracyclopentyltin. Solid state NMR samples were all pre-swollen in $CHCl_3$ prior to analysis with the exception of the distannanes which were analyzed as non-swollen solids. All IR samples were analysed as neat powders on a Bruker ISS55 FT-IR using a diffuse reflectance infrared FT spectroscopy (DRIFTS) accessory manufactured by Spectratech. All IR data is given in Kubelka Munk units. EDX and XPS analyses were performed by a technician at Surface Science Western. EDX is used as a semi-quantitative measure of elemental composition. All numbers for atom % are subject to +/-10 % uncertainty.

HPLC analyses were done using a Waters 486 Tunable Absorbance Detector, Waters 600E System controller, and a Waters 746 Data Module. Injections were made with either a Rheodyne manual injector or a Waters 700 satellite WISP autoinjector. All eluents used with the HPLC were first filtered

through FP Vericel 0.45 µm membrane filters purchased from Gelman Sciences. Prior to injection, all samples were filtered through Gelman Sciences nylon Acrodisc 0.45 µm syringe tip filters. A Waters Bondapack C18 reverse phase column was used for analysis with a C18 guard column. Eluent composition, prepared with spectrophotometric grade solvents, varied depending on the analysis.

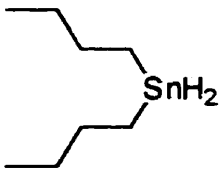

2.10

Preparation of Di-*n*-Butylstannane (**2.10**)

A three neck flask was charged with lithium aluminum hydride (15.3 g, 400 mmol) and diethyl ether (anhydrous, 700 mL). The flask was fit with a mechanical stirrer, dropping funnel and argon inlet. The dropping funnel was charged with di-*n*-butyldichlorostannane (122.5 g, 400 mmol) dissolved in diethyl ether (anhydrous, 300 mL). Under an argon atmosphere, the di-*n*-butyldichlorostannane was added to the reaction flask drop-wise over 50 minutes. The reaction flask was heated to reflux for 6 ½ hours then left to stir at room temperature overnight. Hydroquinone (1 g, 9.1 mmol) was added and the reaction was quenched by slow addition of water. Sodium potassium tartrate (20% aqueous, 500 mL) was used to coagulate the lithium salts and the organic layer was decanted. The organic phase was washed with water and brine, then dried over magnesium sulphate (anhydrous). The diethyl ether was removed and the product purified by vacuum distillation (40°C, 1.5 mm Hg) to yield 66.5 g (70%) of a pale yellow liquid. ^{1}H NMR spectroscopy suggested starting material contamination judging by the butyl group integration. However, the ^{119}Sn NMR spectrum refutes this conclusion. ^{1}H NMR (d_6-benzene) 4.75 (2H, Sn-H, J_{Sn-H}

1655 Hz), 1.6 - 0.8 (32H, Sn-*n*Bu). ^{119}Sn NMR (d_6-benzene) 0.0 (Me_4Sn reference), -202.1 (Sn-H_2).

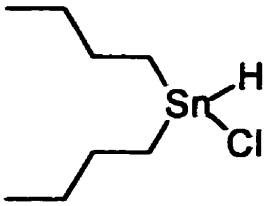

2.11

Preparation of Di-*n*-Butylchlorostannane (**2.11**)

This compound is typically prepared *in situ* and reacted immediately with divinylbenzene. For characterization purposes, it was generated and immediately analyzed. An NMR tube was charged with di-*n*-butyldichlorostannane (260 mg, 0.85 mmol), di-*n*-butylstannane **2.10** (200 mg, 0.85 mmol) and benzene (0.5 mL). Deuterated benzene (0.5 g) was added and the tube sonicated for 1 minute. ^{119}Sn NMR (d_6-benzene) +123.4 (Sn-Cl_2), +47.2 (Sn-HCl), -202.1 (Sn-H_2). The predominant peak was +47 ppm, peaks at +123.4 and -202.1 ppm were minor and of roughly the same intensity.

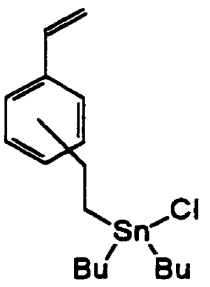

2.2

Preparation of 3- and -4-(2-dibutylchlorostannyl)ethyl)styrene (**2.2**)

Compound **2.2** was prepared by a method similar to Neumann[12]. Technical grade divinylbenzene (DVB) was first purified via silica column to

remove any free radical stabilizers. A polymer kettle was charged with DVB (36 g, 225 mmol), di-*n*-butyldichlorostannane (35 g, 115 mmol), **2.10** (27.5 g, 115 mmol) and azo*bis*isobutyronitrile) (AIBN, 1.25 g, 7.6 mmol). The reaction was left to stir at 1000 rpm for 17 hours under nitrogen, at 30°C. At reaction completion, an aliquot of the crude reaction mixture was removed for analysis. ^{1}H NMR (d_6-benzene) 7.5 - 7.1 (m, 4H, CH_{AR}), 6.75 (m, 1H, CH_{vinyl}), 5.8 (m, 1H, CH_{vinyl}), 5.25 (m, 1H, CH_{vinyl}), 3.0 (m, 2H, CH_2), 1.9 - 0.9 (m, 20H, Sn-CH_2 and *n*-Bu). Ethylvinylbenzene was also visible as an approximately 22% impurity. ^{13}C NMR (d_6-benzene) 136.7, 136.5 (CH, C_{vinyl} *m+p*), 128.9, 128.1, 128.0, 127.3, 126.5, 125.6, 124.3 (CH and C, C_{AR} *m+p+* ethylvinylbenzene), 114.1, 113.9 (CH, CH_{vinyl}), 113.1 (CH, CH_{vinyl}), 31.5 (CH, CH_2-Ph), 27.7 (CH, *n*Bu), 26.8 (CH, *n*Bu), 19.8, 19.6 (CH, CH_2-Sn), 17.7 (CH, *n*Bu), 13.6 (CH, *n*Bu). ^{119}Sn NMR (d_6-benzene) +143 (Sn-CH_2), -90 (Sn-H).

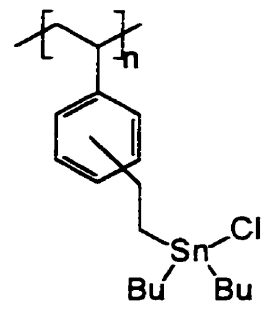

2.3

Preparation of Poly-3- and -4-(2-(dibutylchlorostannyl)ethyl)styrene-*co*-divinylbenzene (**2.3A**)

Compound **2.3A** was prepared in a method similar to Neumann[12]. Technical grade DVB was purified by a short silica column to remove free radical stabilizers. A polymer kettle containing monomer **2.2** (225 mmol), was charged with DVB (6.5 g, 40 mmol), octanol (70 mL), and methyl cellulose solution (0.25% aqueous, 250 mL). Additional AIBN (1.25 g, 7.6 mmol) was added and the mixture was refluxed at 1000 rpm under nitrogen. After 7 ½

hours, the reaction was cooled and decanted. The resulting solid was washed with water (approximately 500 mL), acetone (approximately 500 mL), and methanol (approximately 500 mL) and decanted from the polymer fines. After drying *in vacuo*, 58.7 g (65%) of a white granular solid was isolated. MAS solid state ^{13}C NMR (swollen in $CHCl_3$) 144, 128 (C+CH, C_{AR}), 42 (very broad, CH-Ph, CH_2-Ph, CH_2 backbone), 28.6 (CH, *n*Bu), 27.7 (CH, *n*Bu), 18.6 (CH, *n*Bu), 14.6 (CH, *n*Bu). MAS solid state ^{119}Sn NMR (swollen in $CHCl_3$) +148 (Sn-Cl). DRIFTS (cm^{-1}) 3060, 3022 (CH_{AR}), 2960, 2925, 2856 (CH_{ALIPH}), 1602, 1500 (C=C), 1451, 707. EDX analysis for elemental composition, Sn:Cl approximately 1:1 (2.32:2.10 atom %).

Preparation of Reduced Loading Capacity Copolymers (**2.3B**, **2.3C**)

Reduced loading capacity copolymers were prepared in a manner similar to polymer **2.3A**. Keeping the crosslinking amount constant at 20 mol%, the monomer **2.2** was reduced to one half (**2.3B**) and one tenth (**2.3C**) that of polymer **2.3A**. Styrene was purified through a silica column to remove free radical stabilizers before polymerization. Styrene was used to 'top up' the monomer content to 80 mol% according to the table below.

	Styrene (mol%)	DVB (mol%)	Monomer **2.2** (mol%)
2.3A	0	20	80
2.3B	40	20	40
2.3C	72	20	8

Swellability was determined by charging a 5mm NMR tube with 20 mm of packed, fine ground polymer. The tube was filled with solvent, sonicated 6 hours and left to sit. At 60 hours after sonication, the level of the polymer was measured and expressed as a percentage increase over the original level.

Characterization of **2.3B**: DRIFTS (cm^{-1}) 3060, 3026 (CH_{AR}), 2927, 2857

(CH_{ALIPH}), 1940 - 1800 (aromatic overtones), 1601, 1495 (C=C), 796, 705, 535. MAS solid state ^{119}Sn NMR (swollen in $CDCl_3$) +149.8 ppm. EDX analysis for elemental composition, Sn:Cl approximately 1:1 (0.94:0.84 atom %). Swellabilty: 300% ($CHCl_3$), 300% (EtOH), 180% (EtOH:H_2O (4:5)).

Characterization of **2.3C**: DRIFTS (cm^{-1}) 3060, 3026 (CH_{AR}), 2927, 2857 (CH_{ALIPH}), 1940 - 1800 (aromatic overtones), 1601, 1495 (C=C), 796, 705, 535. MAS solid state ^{119}Sn NMR (swollen in $CDCl_3$) +149.3 ppm. EDX analysis for elemental composition, Sn:Cl approximately 1:1 (0.37:0.32 atom %). Swellability: 140% ($CHCl_3$), 280% (EtOH), 500% (EtOH:H_2O (4:5)).

Preparation of Reduced Loading Capacity and Reduced Crosslinking Copolymer (**2.3D**)

Reduced loading capacity and reduced crosslinking polymer **2.3D** was prepared in a manner similar to polymer **2.3A**. DVB was reduced to 3 mol% and the remaining 97 mol% was comprised of styrene (87 mol%) and monomer **2.2** (10 mol%). DRIFTS (cm^{-1}) 3100, 3060, 3029 (CH_{AR}), 2949, 2925 (CH_{ALIPH}), 1940, 1871, 1802 (strong aromatic overtones), 1595, 1492, 1451 (C=C), 755, 700, 541. MAS solid state ^{119}Sn NMR (swollen in $CDCl_3$) +150.1 ppm. Swellability: 300% ($CHCl_3$), no swelling in EtOH or EtOH:H_2O (4:5). EDX analysis for elemental composition, Sn:Cl approximately 1:1 (0.33:0.31 atom %).

Mohr Titration to Determine Polymer Loading Capacity (**2.3A-D**)

Polymer loading was determined by quantitating the amount of chloride liberated upon hydrolysis for the preparation of **2.12A**. Free chloride can be quantitated by the Mohr method[35]. The filtrate from **2.12A** was diluted to a known volume (100 mL). Silver nitrate solution was standardized using sodium chloride with potassium chromate as the indicator. An aliquot (5 mL) of the reaction solution was neutralized to pH 7.0 and titrated with silver nitrate

solution (0.01102 M). The potassium chromate indicator gave a cloudy, orange-red endpoint. This titration was done in triplicate and the average titrant volume was used to determine the total chloride available as 1.53 mmol/g polymer. Theoretical calculated total chloride available is 2.35 mmol/g and so 68% of theoretical loading was realized. MAS Solid State ^{119}Sn NMR studies support the complete hydrolysis of all stannylchloride species available. This same procedure was repeated with the filtrates from **2.12B**, **2.12C**, and **2.12D**. Polymer **2.12B** gave a loading of 1.1 mmol/g, 46% of theoretical calculated loading. Polymer **2.12C** gave a loading of 0.24 mmol/g, 10% of theoretical calculated loading. Polymer **2.12D** gave variable results, the highest titration volume translated to 0.04 mmol/g loading. However, MAS solid state ^{119}Sn NMR confirmed that this polymer was not hydrolysed.

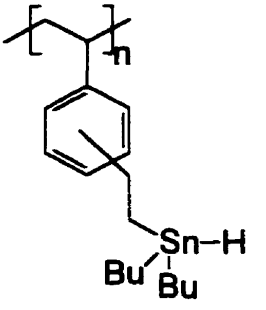

2.4

Preparation of a Tin Hydride: Poly-3- and -4-(2-(di-*n*-butylstannane)ethyl)-styrene-*co*-divinylbenzene (**2.4A**)

The polymer-bound tin hydride **2.4A** was prepared in a method similar to Kuivila[46]. A three neck flask, equipped with magnetic stir bar, was charged with lithium aluminum hydride (263.6 mg, 6.95 mmol) and fit with a dry addition arm, septum, and argon inlet. The dry addition arm had been previously charged with polymer **2.3A** (8.5257 g, 13.3 mmol). THF (60 mL, anhydrous) was added to the reaction flask and degassed at -78°C. The polymer **2.3A** was added and the contents were stirred at 0°C for 30 minutes then warmed to room

temperature and stirred an additional 16 hours under argon. After quenching with slow addition of water, the reaction was filtered and washed with water, sodium hydroxide (10% aqueous) and THF. The solid was dried *in vacuo* and analyzed. DRIFTS (cm^{-1}) 3060, 3022 (CH_{AR}), 2960, 2925, 2856 (CH_{ALIPH}), 1802 (Sn-H), 1602, 1500 (C=C), 1480, 1444, 872, 700. MAS solid state ^{119}Sn NMR (not swollen in $CHCl_3$) +145 (Sn-Cl), +120 to +80 (very broad, Sn-O species), -17 (Sn-Bu_3), -90 (Sn-H), approximately 6:6:3:2 relative intensity respectively. XPS analysis for elemental composition, Sn:Cl approximately 3:1 (1.46:0.58 atom %).

In an effort to improve yield, the reaction was repeated with reflux conditions for 6 ½ hours. The solid was then washed with water, sodium hydroxide (10% aqeuous) and THF. The solid was dried *in vacuo* and analyzed. DRIFTS (cm^{-1}) 3060, 3022 (CH_{AR}), 2960, 2925, 2856 (CH_{ALIPH}), 1802 (Sn-H), 1602, 1500 (C=C), 1480, 1444, 872, 700. MAS solid state ^{119}Sn NMR (swollen in $CHCl_3$) +110 to +80 (very broad, Sn-O species), -17 (Sn-Bu_3), -90 (Sn-H), approximately 3:1:6 relative intensity respectively. Over 56 days the ratio of Sn-H to Sn-O species decreased, presumably due to oxidation. The integration ratio of Sn-H:Sn-O was 2.23, 0.73, and 0.31 on days 1, 27 and 56 respectively. XPS analysis for elemental composition indicated no chlorine present.

The reaction was repeated as above, washing the polymer with water, acetic acid (5% aqueous), ethanol, and THF. The solid was dried *in vacuo* and analyzed. DRIFTS (cm^{-1}) 3060, 3022 (CH_{AR}), 292, 2890 (CH_{ALIPH}), 1809 (Sn-H), 1595, 1490 (C=C), 1451, 700. XPS analysis for elemental composition indicated no chlorine present. This method was applied to the reduced loading polymers **2.3B**, and **2.3C**, to yield the polymer-bound tin hydrides **2.4B**, and **2.4C** respectively.

Characterization of **2.4B**: DRIFTS (cm^{-1}) 3063, 3028 (CH_{AR}), 2922, 2856 (CH_{ALIPH}), 1940, 1872 (aromatic overtones), 1805 (Sn-H), 1597, 1490 (C=C),

14443, 754, 700. EDX analysis for elemental composition indicated no chlorine present.

Characterization of **2.4C**: DRIFTS (cm^{-1}) 3063, 3030 (CH_{AR}), 2929, 2856 (CH_{ALIPH}), 1945, 1872, 1798 (aromatic overtones), 1597, 1490 (C=C), 1450, 754, 700. EDX analysis for elemental composition indicated no chlorine present.

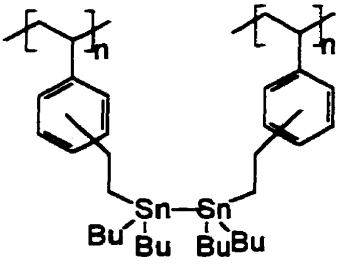

2.6

Preparation of a Distannane: Poly-2-(3- and -4-(styryl)ethyl)di-*n*-butyldistannane)-*co*-divinylbenzene (**2.6A**)

Lithium naphthalide was prepared by a method similar to Neumann[18]. A three neck flask was charged with lithium metal (30% suspension, 1.6254 g, 69.7 mmol). The flask was fit with an argon inlet, septum, and dry addition arm. The dry addtion arm had been previously charged with naphthalene (8.8671 g, 69.18 mmol). Addition of THF (100 mL, anhydrous) was following by degassing at -78°C. Naphthalene was added to the reaction and the contents were sonicated under argon. Within 15 minutes the reaction contents had turned dark green. After 2 hours of sonicating, three aliquots were removed and each titrated with standardized hydrochloric acid (0.1 M) using phenolphthalein indicator to a light red endpoint. The lithium napthalide concentration was determined to be 0.63 M.

A two neck flask, equipped with magnetic stir bar, was charged with polymer **2.3A** (2.0435 g, 3.19 mmol). The flask was fit with septum and argon

inlet. THF (50 mL, anhydrous) was added and the flask was degassed at -78°C. The reaction turned green immediately after adding lithium napthalide by syringe (6.6 mL, 4.15 mmol). Within 3 minutes, the colour had returned to off-white. The contents were left stirring under argon for 16 hours then filtered. After washing with isopropyl alcohol and diethylether, the solid was dried *in vacuo* at 70°C. DRIFTS (cm^{-1}) 3022 (CH_{AR}), 2925, 2856 (CH_{ALIPH}), 1595, 1506, 1478 (C=C), 1451, 789, 707. EDX analysis for elemental composition, Sn:Cl approximately 10:1 (2.77:0.28 atom %). MAS solid state ^{119}Sn NMR (not swollen in $CHCl_3$) +83.0 (Sn-O-Sn). The same procedure was used to prepared distannanes **2.6B** and **2.6C** from reduced loading polymers **2.3B** and **2.3C** respectively.

Characterization of **2.6B**: DRIFTS (cm^{-1}) 3035 (CH_{AR}), 2960, 2918, 2856 (CH_{ALIPH}) 1940, 1871, 1802 (aromatic overtones), 1602, 1492 (C=C), 1451, 789, 755, 700. EDX analysis for elemental composition indicated no chlorine present. MAS solid state ^{119}Sn NMR (not swollen in $CHCl_{3)}$ +83.0 ppm (Sn-O-Sn), -77.9, -99.8. Resolution was too poor to determine relative intensity but Sn-O-Sn was the major species in spectrum.

Characterization of **2.6C**: DRIFTS (cm^{-1}) 3056, 3029 (CH_{AR}), 2925, 2856 (CH_{ALIPH}), 1940, 1878, 1802 (aromatic overtones) 1602, 1492 (C=C), 1451, 755, 693. MAS solid state ^{119}Sn NMR (not swollen in $CHCl_3$) +83.5 (Sn-O-Sn). EDX analysis for elemental composition indicated no chlorine present.

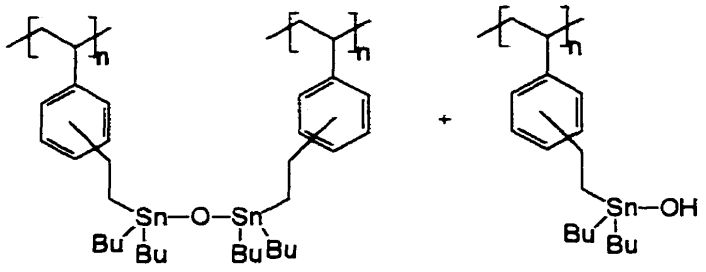

2.12 (mixture)

Preparation of a Tin Oxide:Poly-3- and -4-(2-(dibutylchlorostannol-distannoxane)ethyl)styrene-*co*-divinylbenzene (**2.12A**)

A flat bottom flask was charged with polymer **2.3A** (1.0628 g) and sodium hydroxide solution (50% in ethanol). The flask was left on a shaker for 16 hours then filtered through a sintered glass frit. The filter cake was washed with additional water and ethanol. All filtrate was collected and set aside for Mohr analysis. The solid was dried *in vacuo* overnight at 70°C and analysed. DRIFTS (cm^{-1}) 3026, 3010 (CH_{AR}), 2927, 2850 (CH_{ALIPH}), 1601, 1492 (C=C), 1440, 1360, 755, 703. MAS solid state ^{119}Sn NMR (swollen in $CHCl_3$) 103 (Sn-OH), 91 (Sn-O-Sn), approximately 1:3 relative intensity. The solid polymer **2.12A** was then subjected to 24 additional hours of hydrolysis in sodium hydroxide solution (50% in ethanol) at reflux temperature. MAS solid state ^{119}Sn NMR (swollen in $CHCl_3$) +101.1 (Sn-OH), +91.1 (Sn-O-Sn), approximately 1:3 relative intensity. All polymers (**2.3B**, **2.3C**, **2.3D**) were hydrolysed, with the exception of the additional 24 hours of reflux, in a similar manner.

Characterization of **2.12B**: DRIFTS (cm^{-1}) 3026, 3110 (CH_{AR}), 2927, 2850 (CH_{ALIPH}), 1594, 1490 (C=C), 789, 754, 705. MAS solid state ^{119}Sn NMR (swollen in $CHCl_3$) 100.8 (Sn-OH), 92.2 (Sn-O-Sn), approximately 1:2 relative intensity.

Characterization of **2.12C**: DRIFTS (cm^{-1}) 3060, 3026 (CH_{AR}), 2927, 2850 (CH_{ALIPH}), 1594, 1488 (C=C), 1453, 754, 705. MAS solid state ^{119}Sn NMR (swollen in $CHCl_3$) 100.6 (Sn-OH), 92.0 (Sn-O-Sn), approximately 2:1 relative intensity.

Characterization of **2.12D**: DRIFTS (cm^{-1}) 3060, 3029 (CH_{AR}), 2925, 2849 (CH_{ALIPH}), 1940, 1871, 1802 (aromatic overtones), 1595, 1492 (C=C), 1451, 1024, 755, 700. MAS solid state ^{119}Sn NMR (swollen in $CHCl_3$) +150.1 (Sn-Cl).

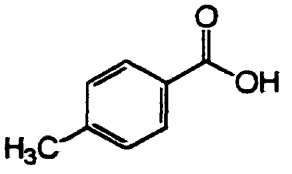

Preparing a Calibration Curve for Toluic Acid

Solutions of toluic acid were prepared in methanol with concentrations ranging from 1.13 mM to 11.3 mM. Duplicate injections of 5 µL each were used for quantitative HPLC analysis of the solutions. The raw data from the chromatograms is included in Table 2.6.

HPLC characterization: 30% CH_3CN, 70% H_2O (1 ml H_3PO_4 / 1 L), pH 3.0, 1 ml/min, UV detection, 220 nm, 0.05 AUFS, C18RP column, retention time = 16.5 minutes.

Table 2.6: HPLC results for calibration curve of toluic acid

Concentration (x) (mM)	Peak Area #1 ($x10^4$)	Peak Area #2 ($x10^4$)	Average Peak Area (y) ($x10^4$)
0	0	0	0
1.13	271.82	270.98	271.40
2.26	584.19	565.14	574.67
5.6	1349.05	1360.46	1354.74
11.3	2735.56	2901.04	2818.30

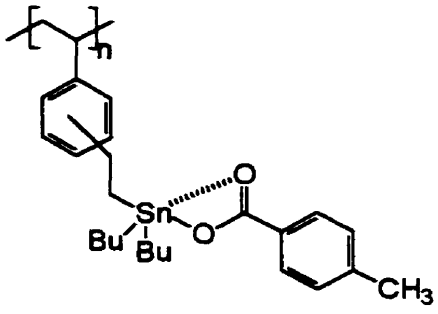

2.13

Preparation of a Tin Carboxylate: Poly-3- and -4-(2-(di-*n*-butyl(*p*-toluicstannylate)ethyl)styrene-*co*-divinylbenzene (**2.13**)

The polymer-bound *p*-toluic tin ester was prepared by the method of Frankel[44]. A single neck flask, equipped with magnetic stir bar, was charged with polymer **2.3A** (760.8 mg, 1.29 mmol), the sodium salt of toluic acid (202.7 mg, 1.28 mmol) and benzene (15 mL). The flask was fit with a condenser and drying tube then left to reflux. After 16 hours, the polymer was filtered through a sintered glass frit, rinsed with fresh benzene and dried *in vacuo*. The solid polymer was then analysed. DRIFTS (cm^{-1}) 3019 (CH_{AR}), 2963, 2927, 2857 (CH_{ALIPH}), 1639 (C=O), 1601, 1540 (C=C), 1350, 750, 700. Solid State MAS ^{119}Sn NMR (swollen in $CHCl_3$) 104.0 (Sn-O-C=O).

To distinguish toluic acid chemically bound as the ester from toluic acid physically trapped within the polymer, the polymer **2.13** was soxhlet extracted in refluxing benzene for 24 hours. The solvent was then concentrated and redissolved in methanol for HPLC analysis. Comparison to a standard curve for toluic acid indicated 0.54% of the original toluic acid liberated during soxhlet extraction. In addition, a sintered glass filter was charged with **2.13** and chloroform (10 ml). Toluic acid is known to be soluble in chloroform at room temperature. The polymer was left to soak in the chloroform for 10 minutes then filtered. The filtrate was evaporated to dryness then redissolved in methanol (5 ml) and analyzed by HPLC. Comparison to a standard curve for toluic acid indicated 1.3% of the original toluic acid liberated.

Determining the Stability of the Polymer-Bound Tin Carboxylate (**2.13**)

The methanol used in these experiments was of spectrophotometric grade. Karl Fisher analysis, in duplicate, indicated 0.012% water contamination. The filtrate injections were compared to a standard HPLC curve for toluic acid. Injection volumes varied from 5 - 10 µL. Each injection was done in duplicate and an average peak area was used to calculate the amount of toluic acid present in the original filtrate solution.

Experiment 1: Methanol Cleavage of **2.13**

A sintered glass filter was charged with **2.13** (315.7 mg) and the contents washed with methanol (10 mL). The filtrate was diluted with methanol (50 mL) and analyzed by HPLC. The filter cake was dried *in vacuo* and transferred to a single neck flask fitted with a magnetic stir bar. The flask was charged with methanol (7 mL) and left to stir. After 15 minutes the reaction was filtered through a sintered glass frit. The filtrate was analyzed by HPLC. The filter cake was transferred to a single neck flask fitted with a magnetic stir bar. The flask was charged with methanol (7 mL) and left to stir. After 15 minutes the reaction was filtered through a glass frit. The filtrate was analyzed by HPLC. This process was repeated for 30 minutes and 1 hour respectively. All filtrates were analyzed by HPLC and this data is presented in Table 2.7.

Table 2:7: Toluic Acid released from methanol cleavage of 2.13 vs time

Cumulative Time	µmol/g	Cumulative µmol/g polymer
0 minutes	319	319
15	71.2	390.2
30	38.3	428.5
60	35.9	464.4
120	28.1	492.5

Experiment 2: Trifluoroacetic Acid Cleavage of **2.13**

A sintered glass filter was charged with **2.13** (302.8 mg) and the contents of the filter were washed with methanol (10 mL). The filtrate was diluted with methanol (50 mL) and analyzed by HPLC. The filter cake was dried *in vacuo* and a portion transferred to a single neck flask (259.9 mg). The flask was charged with trifluoroacetic acid solution (10% in dichloromethane). The reaction was left to stir for 15 minutes at room temperature and filtered through a sintered glass frit. The filtrate was evaporated to dryness, redissolved in methanol (25 mL), and analyzed by HPLC. The filter cake was transferred back to a single neck flask and stirred in trifluoroacetic acid solution (10% in dichloromethane). After 15 minutes, the reaction was filtered through a sintered glass frit. The filtrate was evaporated to dryness, redissolved in methanol (5 mL), and analyzed by HPLC. This process was repeated with a 30 minute stir period. All filtrates were analyzed by HPLC and compared to a toluic acid calibration curve to yield a time course for trifluroacetic acid cleavage. This data is presented in Table 2.8. The remaining solid support was analyzed by MAS solid state ^{119}Sn NMR (swollen in $CHCl_3$) +151 ppm.

Table 2.8: Toluic acid released from TFA cleavage of 2.13 vs time

Cumulative Time	µmol/g	Cumulative µmol/g
0 minutes	605.7	605.65
15	960	1565.7
30	10	1575.7
60	3.6	1579.3

Experiment 3: Acetic Acid Cleavage of **2.13**

A sintered glass filter was charged with **2.13** (300.8 mg) and the contents of the filter were washed with methanol (10 mL). The filtrate was diluted with

methanol (50 mL) and analyzed by HPLC. The filter cake was dried *in vacuo* and a portion transferred to a single neck flask (241.5 mg). The flask was charged with acetic acid solution (0.38 M in 95% ethanol) and refluxed 30 minutes. The reaction contents were immediately filtered through a sintered glass frit. The filtrate was evaporated to dryness and redissolved in methanol (25 mL) for HPLC analysis. The filter cake was transferred to a single neck flask. The flask was charged with acetic acid solution (0.38 M in 95% ethanol) and refluxed 30 minutes. The reaction contents were immediately filtered through a sintered glass frit. The filtrate was evaporated to dryness and redissolved in methanol (5 mL) for HPLC analysis. The process was repeated with 60 minutes, 15 hours, 24 hours, and an additional 24 hours of reflux respectively. Each filtrate was evaporated to dryness and redissolved in methanol (5 mL) for HPLC analysis. All filtrates were analyzed by HPLC and compared to a toluic acid calibration curve to yield a time course for acetic acid cleavage. This data is presented in Table 2.9. The polymer was analyzed by DRIFTS spectroscopy after cleavage. The spectrum indicated a stretch at approximately 1640 cm^{-1}.

Table 2.9: Toluic acid released with acetic acid cleavage of 2.13 vs time

Cumulative Time	µmol/g	Cumulative µmol/g
0 hours	362.5	362.5
0.5	770	1132.5
1	100	1232.5
2	18.4	1250.9
15	3.6	1254.5
39	2.0	1256.5
63	0.8	1257.3

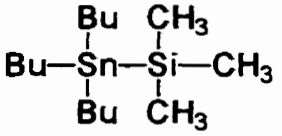

2.15

Preparation of (Trimethylsilyl)tributylstannane (**2.15**)

The silylstannane **2.15** was prepared according to the method of Chenard[47] for NMR spectral characterization. The crude reaction mixture was characterized with no further purification. ^{1}H NMR (d_6-benzene) 1.65 (m, 3H, Bu), 1.5 - 1.3 (m, 5H, Bu), 1.05 - 0.8 (m, 8H, Bu), 0.3 (s, 3H). ^{13}C NMR (d_6-benzene) 30.6 (CH, Bu), 28.0 (CH, Bu), 14.0 (CH, Bu), 8.2 (CH, Bu), 1.6 (CH, CH_3). ^{119}Sn NMR (d_6-benzene) -13.7 (SnR_4), -84.9 (Sn-Sn), -89.7 (Sn-H), -122.2 (Sn-Si), approximately 2:2:1:14 relative intensity.

Determining the Stability of (Trimethylsilyl)tributylstannane (**2.15**)

Authentic silylstannane **2.15** was tested for both air and moisture stability over a period of 30 days. A sample of **2.15** was prepared and characterized by NMR spectroscopy. ^{1}H NMR (d_6-benzene) 1.65 (m, 2H, Bu), 1.4 (m, 2H, Bu), 1.0 (m, 5H, Bu), 0.3 (s, 3H). ^{13}C NMR (d_6-benzene) 30.8 (CH, Bu), 28.1 (CH, Bu), 14.0 (CH, Bu), 8.5 (CH, Bu), 1.6 (CH, CH_3). ^{119}Sn NMR (d_6-benzene) -122.2 (Sn-Si). Twenty-one days later, the same sample was re-characterized by NMR spectroscopy. No changes were evident in the ^{1}H, ^{13}C, or ^{119}Sn NMR spectra. A sample of neat **2.15** was exposed to air for 7 days then characterized by NMR spectroscopy. No changes were evident in the ^{1}H, ^{13}C, or ^{119}Sn NMR spectra. A sample of **2.15** was treated with water, extracted into deuterated benzene, then dried over sodium sulfate (anhydrous). The sample was then characterized by NMR spectroscopy. No changes were evident in the ^{1}H, ^{13}C, or ^{119}Sn NMR spectra.

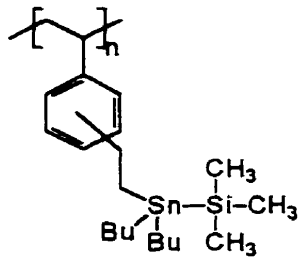

2.17

Preparation of a Silylstannane: Poly-3- and -4-(2-(di-*n*-butyl(trimethylsilyl)stannane)ethyl)styrene-*co*-divinylbenzene (**2.17A**)

A three neck flask, equipped with magnetic stir bar, was fit with septum, argon inlet and dry addition arm. The addition arm had been previously charged with tin hydride **2.4A** (605.3, 1.0 mmol). THF (anhydrous, 60 mL) was added by syringe and then degassed at -78°C. The flask was then charged with diisopropylamine (160 µL, 1.14 mmol) and n-BuLi (0.96 M in heptanes, 1.2 mL, 1.15 mmol). This solution was left to stir for 1 hour at 0°C under argon. The polymer **2.4A** was added and the reaction was left to stir at room temperature under argon to give a pale yellow suspension. After 1 ½ hours, trimethylsilylchloride (0.5 mL, 3.95 mmol) was added and the reaction immediately turned to a white suspension. The reaction was left to stir at room temperature under argon for 16 hours. The reaction was quenched by addition of water then filtered through a sintered glass frit. The solid was washed with additional water, water/ethanol (1:1), and ethanol then dried *in vacuo* before analysis. DRIFTS indicated minimal tin hydride **2.4A** starting material. DRIFTS (cm^{-1}) 3060, 3010 (CH^{AR}), 2980, 2920 (CH_{ALIPH}), 1620, 1480 (C=C), 1350, 790, 700. EDX analysis for elemental composition Sn:Si:Cl approximately 4:1:1 (2.10: 0.62:0.43 atom %). MAS solid state ^{119}Sn NMR (swollen in $CHCl_3$) +145 (Sn-Cl), -15 (R_3Sn), -90 (Sn-H), -120 (Sn-Si) with relative intensity 16:2;9:1 respectively.

To improve the Sn:Si ratio from EDX analysis, the reaction was repeated with an excess of lithium diisopropylamide. The procedure was otherwise similar to that above. DRIFTS (cm^{-1}) 3060, 3010 (CH^{AR}), 2980, 2920 (CH_{ALIPH}), 1620, 1480 (C=C), 1350, 790, 700. EDX analysis for elemental composition Sn:Si:Cl approximately 4:1:2 (2.05:1.22:0.56 atom %).

The silylstannane preparation was applied to the reduced loading polymer **2.4B** using an equimolar amount of lithium diisopropylamide. DRIFTS (cm^{-1}) 3060, 3010 (CH_{AR}), 2900, 2840 (CH_{ALIPH}), 1600, 1490 (C=C), 1450, 750, 700. EDX analysis for elemental composition Sn:Si:Cl approximately 14:11:1 (2.08:1.61:0.14). Polymer **2.4C**, the reduced loading tin hydride, was not conclusively made. Consequently, the silylstannane **2.17C** preparation was not attempted.

2.4 References

1. Merrifield, R.B. *J. Am. Chem. Soc.* **1963**, *85*, 2149.
2. Balkenhohl, F.; von dem Bussche-Hunnefeld, C.; Lansky, A.; Zechel, C. *Angew. Chem. Int. End. Engl.* **1996**, *35*, 2288.
3. Hermkens, P.H.H.; Ottenheijm, H.J.C.; Rees, D. *Tetrahedron* **1996**, *52*, 4527.
4. Laszlo, P. Preparative Chemistry Using Supported Reagents **1987**, Academic Press, San Diego.
5. (a) Leznoff, C.C. *Acct. Chem. Res.* **1978**, *11*, 327. (b) Frechet, J.M.J. *Tetrahedron* **1981**, *37*, 663. (c) Crowley, J.I.; Rapoport, H. *Acc. Chem. Res.* **1976**, *9*, 135.
6. Czarnik,A.W.; DeWitt, S.H. A Practical Guide to Combinatorial Chemistry **1997**, American Chemical Society, Washington.
7. Bunin, B.A.; Ellman, J.A. *J. Am. Chem. Soc.* **1992**, *114*, 10997.
8. Terrett, N.K. Combinatorial Chemistry **1998**, Oxford University Press, Oxford.
9. Novabiochem The Combinatorial Chemistry Catalog **1998**, CN Biosciences, Switzerland.
10. (a) Van Der Kerk, G.J.M. Organotin Compounds: New Chemistry and Applications Zuckerman, J.J. (Ed), *Adv. Chem. Ser.* **1976**, 157. (b) Davies, A.G. Organotin Chemistry **1997**, VCH, Weinheim. (c) Smith, P.J. Chemistry of Tin **1998**, Blackie, London. (d) Pereyre, M.; Quintard, J.P.; Rahm, A. Tin in Organic Synthesis **1986**, Butterworths, London.
11. Neumann, W.P.; Peterseim, M. *React. Polym.* **1993**, *20*, 189.
12. Gerigk, U.; Gerlach, M.; Neumann, W.P.; Vieler, R.; Weintritt, V. *Synthesis* **1990**, 448.
13. Gerlach, M.; Jordens, F.; Kuhn, H.; Neumann, W.P.; Peterseim, M. *J. Org. Chem.* **1991**, *56*, 5971.

14. Neumann, W.P.; Peterseim, M. *Synlett* **1992**, 801.
15. Bokelman, C.; Neumann, W.P.; Peterseim, M. *J. Chem. Soc. Perkin I* **1992**, 3165.
16. Dygutsch, D.P.; Neumann, W.P.; Peterseim, M. *Synlett* **1994**, 363.
17. Harendza, M.; LeBmann, K.; Neumann, W.P. *Synlett* **1993**, 283.
18. Junggebauer, J.; Neumann, W.P. *Tetrahedron* **1997**, *53*, 1301.
19. Kuhn, H.; Neumann, W.P. *Synlett* **1994**, 123.
20. Weinshenker, N.M.; Crosby, G.A.; Wong, J.Y. *J. Org. Chem.* **1975**, *40*, 1967.
21. Schumann, H.; Pachaly, B. *Angew. Chem. Int. Ed. Engl.* **1981**, *20*, 1043.
22. Culbert, P. Bioreductive Alkylating Agents as Probes for Tissue Hypoxia Ph.D. Thesis **1992**, University of Western Ontario, London.
23. Windrell, H.S.; Horst, W.D.; Braun, L.; Oldendorf, W.H.; Hattner, R.; Parker, H. *J. Nucl. Med.* **1980**, *21*, 947.
24. Hunter, D.H.; Marinescu, A.M.; Loc'h, C.; Maziere, B. *J. Labelled Cmpd. Radiopharm.* **1995**, *37*, 144.
25. Hunter, D.H.; Zhu, X.Z. *J. Labelled Cmpd. Radiopharm* **1999**, in press.
26. Pollock, C. Protodestannylation of Polymer-Supported Arylstannanes, M.Sc. Thesis **1997**, University of Western Ontario, London.
27. Janabi, M. Synthesis and Characterization of Polymer-Bound Aryl Compounds, 4th Year Honours Research Thesis **1998**, University of Western Ontario, London.
28. Manning, B. Polymer-Bound Benzaldehyde for the Preparation of Radiopharmaceuticals and Pharmaceuticals, 4th Year Honours Research Thesis **1999**, University of Western Ontario, London.
29. Marzinzik, A.L.; Felder, E.R. *J. Org. Chem.* **1998**, *63*, 723.
30. Wiberg, E.; Stecher, O.; Andrascheck, H.J.; Kreuzbichler, I.; Staude, E. *Angew. Chem. Int. Engl. Ed.* **1963**, *2*, 507.
31. Mori, M.; Kaneta, N.; Shibasaki, M. *J. Org. Chem.* **1991**, *56*, 3486.

32. Lipshutz, B.H.; Reuter, D.C.; Ellsworth, E.L. *J. Org. Chem.* **1989**, *54*, 4975.

33. Kosugi, M.; Shimizu, K.; Ohtani, A.; Migita, T. *Chem. Lett.* **1981**, 829.

34. Mascaretti, O.A.; Furlan, R.L.E. *Aldrichimica Acta* **1997**, *30*, 55.

35. Day Jr, R.A.; Underwood, A.L. Quantitative Analysis 2nd Edition **1967**, Prentice Hall, Eaglewood Cliffs.

36. Dumartin, G.; Kharboutli, J.; Delmond, B.; Pereyre, M. *Organometallics* **1996**, *15*, 19.

37. Smith, J.; White, R.F.M.; Smith, L. *J. Organomet. Chem.* **1972**, *40*, 341.

38. Alexandrov, Y.A.; Tarunin, B.I. *J. Organomet. Chem.* **1982**, *238*, 125.

39. Salomon, M.F.; Salomon, R.G. *J. Am. Chem. Soc.* **1979**, *101*, 4290.

40. Khan, M.A.; Hunter, D.H.; Janabi, M. **1998**, unpublished data.

41. Brandrup, J.; Immergut, E.H. Polymer Handbook 3rd Edition **1989**, John Wiley and Sons, Chichester.

42. Von, H.J. *Chemiker Ztg. Chem. Apparatur* **1962**, *86*, 563.

43. Klein, J.; Borsdorf, R. *J. Prakt. Chem.* **1993**, *335*, 465.

44. Frankel, M.; Gertner, D.; Wagner, D.; Zilka, A. *J. Org. Chem.* **1965**, *30*, 1596.

45. Greene, T. Protective Groups in Organic Synthesis **1981**, John Wiley and Sons, New York.

46. Kuivila, H.G.; Beumel Jr., O.F. *J. Am. Chem. Soc.* **1961**, *83*, 1246.

47. Chenard, B.L.; Van Zyl, C.M.; *J. Org. Chem.* **1986**, *51*, 3561.

48. Sherington, D.C. Polymer Supported Reactions in Organic Synthesis Hodge, P.; Sherington, D.C (Ed) **1980**, John Wiley and Sons, Chichester.

Chapter 3 - Lactonization via Polymer-Bound Organotin Oxides

3.1 Introduction

3.1.1 Applications of Lactones

Medium and large sized lactones figure prominently in the skeletons of numerous natural products. Many lactone-based compounds possess potent antibacterial properties. Lactone-based antibiotics are commonly used for respiratory tract and skin infections. They are also indispensable when conventional β-lactam type antibiotics, like penicillin, produce allergic reactions.

Lactone-based antibiotics can be divided into two types. The macrolides contain large lactone rings of 12 members or more. These include the familiar erythromycin and clarithromycin antibiotics. The other family encompasses the medium ring-size lactones of 8 - 11 members. A common antibiotic of this type is cephalosporin, derived from cephalosporide D with an eight-membered lactone skeleton. Macrolides are more commonly used than medium-sized lactone antibacterials.

The majority of lactone-based products are isolated from natural sources or prepared from naturally occurring bacterial metabolites. In general, naturally occurring lactone-based antibiotics demonstrate poor pharmokinetic properties due to variable absorption rates[1]. Synthesis of novel, non-naturally occurring lactone-based compounds may address the erratic intestinal absorption problems. In addition, pharmaceutical companies are interested in expanding the antibacterial spectrum of lactone-based compounds. This will clearly require some synthetic tinkering.

3.1.2 ω-Hydroxycarboxylic Acid Lactonizations

Judging from various reviews, much energy has focussed on the total synthesis of macrolides and medium-sized lactones[2]. The experiences gained

from these lengthy syntheses can be applied to novel lactone-based antibacterial development. Novel lactone-based antibiotics will require intensive lab synthesis.

Tylosin [3a]

3.1

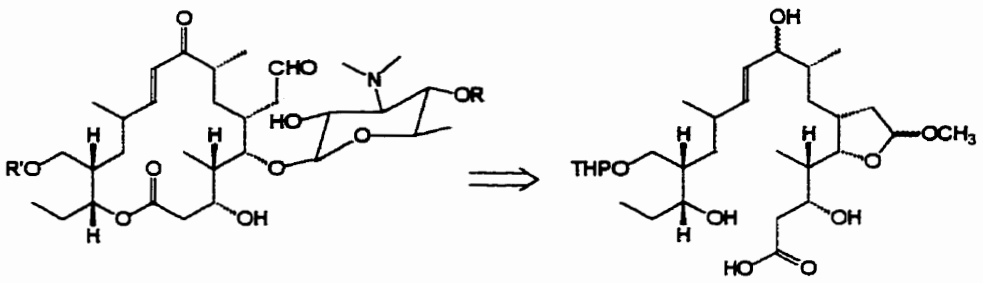

Tylosin
R = mycarosyl, R' = mycinosyl

Seco-Acid Precursor

Erythromycin [3b]

3.2

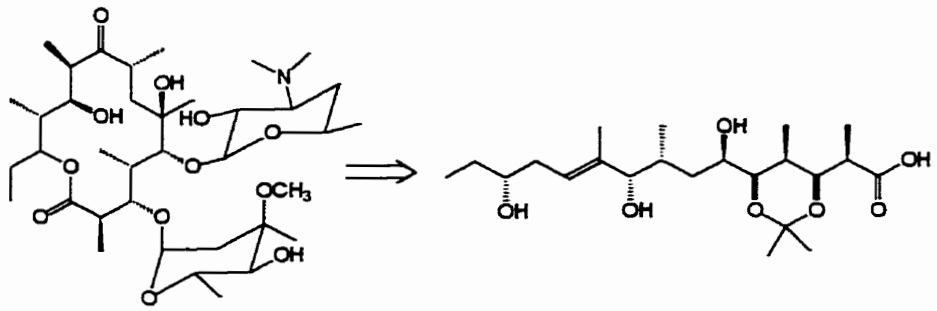

Erythronolide A

Seco-Acid Precursor

Methymycin [3c]

3.3

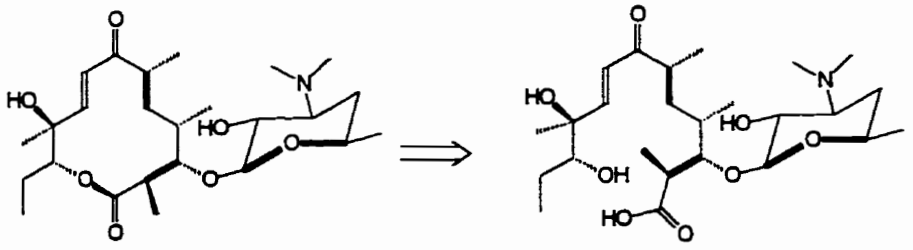

Methymycin

Seco-Acid Precursor

Figure 3.1: Antibiotics prepared from seco-acid precursors

Many existing macrolide syntheses, from common organic precursors, require the cyclization of long-chain hydroxycarboxylic acids, also called seco-acids. Lactonization of seco-acids is one of the most direct ways to prepare a macrocyclic skeleton. Many macrolide antibiotic total syntheses have included macrolactonizations of seco-acids. A few representative seco-acids and the antibiotics ultimately resulting from them are included in Figure 3.1.

Tylosin, the first entry, is used for prophylaxis in veterinary medicine. The seco-acid precursor yields a tylonide hemiacetal which is readily converted to the antibacterial. Erythromycin, the second entry, is a common antibiotic. The seco-acid yields erythronolide B, an aglycone of erythromycin. The third entry, Methymycin, is a 12 membered lactone that displays broad spectrum antibacterial activity.

3.1.2.1 Existing Methods for ω-Hydroxycarboxylic Acid Lactonizations

Table 3.1 represents a partial compilation of the methods available for seco-acid lactonizations. This summary was compiled from the recent literature and includes data for both medium and large ring lactones synthesized from the corresponding hydroxycarboxylic acids. Conversion of the seco-acid to a hydroxy-ester is necessary for entries 3 and 9 prior to lactonization. Oligomeric byproduct yields have been included in parenthesis. Oligomeric byproduct yields were not available for entries 7 and 9.

A survey of the literature reveals a multitude of methods for seco-acid lactonization of 12 member or larger rings. Many of these methods result in large amounts of oligomeric byproducts which can compromise lactone yields. The preparation of medium ring-size lactones is underepresented in the literature. Many lactonization methods result in enormous amounts of oligomeric byproducts for these ring sizes. Entries 5 and 10 represent two of the few methods that can generate medium lactones in respectable yields. The synthetic difficulty for medium lactone preparation has been attributed to high

ring strain. Ring strain, as it relates to cyclization, will be discussed in Section 3.1.4.

Table 3.1: Comparison of ω-hydroxyacid lactonization methods					
Reagent		% Lactone (Oligomers) for Ring-Size			
		9	11	13	16
1	Methylchloropiperidnium Iodide[4a]	13 (34)	--	69 (14)	84 (3)
2	$Me_2NCH(OCH_2$-*t*-$Bu)_2$[4a]	0 (14)	--	--	--
3	$TiCl_4$ - $AgClO_4$ /(*p*-$CF_3C_6H_4CO)_2O$[4a]	0 (40)	70 (23)	75 (7)	89 (4)
4	$TiCl_2(OTf)_2$/TMSCl(*p*-$CF_3C_6H_4CO)_2O$[4a]	--	--	83 (10)	88 (10)
5	$Sc(OTf)_3$ / (*p*-$NO_2C_6HCO)_2O$[4a]	52 (3)	77 (2)	91 (3)	92 (<1)
6	Dipyridyl Disulfide[4a]	8 (41)	--	66 (7)	80 (5)
7	$BF_3 \cdot ET_2O$[4a]	--	--	41	77
8	Cs_2CO_3 / DMF[4b]	--	23 (55)	62 (30)	83 (17)
9	Hydrous Zirconium Oxide[4c]	36	--	8	52
10	1,2-*bis*-dimethylsilylbenzene/ $Me_2Si(OTf)_2$[4d]	87 (8)	83 (10)	87(10)	--

Many existing lactonization methods give low lactone yields and high oligomeric byproduct yields. In addition, harsh reaction conditions, including acidic and basic reagents, can destroy highly functionalized seco-acids. A need exists for mild, efficient macrolide preparations employing neutral reaction conditions.

3.1.2.2 Existing Organotin Reagents for ω-Hydroxycarboxylic Acid Lactonizations

Organotin compounds have been applied to intermolecular esterification of carboxylic acids[5]. Otera and coworkers have shown that stannoxane reagents catalyze esterification reactions in high yield[6]. Not surprisingly, organotin oxides have since been shown to catalyze the lactonization of ω-hydroxycarboxylic acids. In general, organotin oxides are mild, nearly neutral reagents for seco-acid lactonization. However, the use of organotin catalysts with known toxicity can further complicate applicability and purification. A summary of organotin oxide mediated lactonization methods is included in Table 3.2. Conversion of the seco-acid to an ester is necessary for entries 3 and 4 prior to lactonization.

Table 3.2: Comparison of ω-hydroxyacid lactonization methods mediated by organotin oxide

Reagent		% Lactone (Oligomer) for Ring Size			
		9	11	13	17
1	Bu_2SnO[7a]	0 (20)	0 (36)	22	60 (15)
2	Bu_2SnO (Cl)[7b]	--	--	0	81
3	Bu_3SnH[7c]	--	0 (65)	42 (19)	81 (14)
4	Bu_3SnOMe[7c]	--	0 (82)	45 (40)	70 (0)

Entries 1, 3, and 4 have included oligomeric byproduct yields, as indicated in parenthesis. Collectively, these methods are unsuccessful for medium lactone preparation. Yields for larger lactones of 13 and 17 members are moderate for all organotin oxide methods, however yields of oligomeric byproducts are substantial for entries 1, 3, and 4.

Although organotin mediation represents a mild way to generate lactones, several disadvantages need to be addressed. Namely, efficient

removal of the catalyst, significant loss of yield to oligomerization for all ring-sizes, and the absence of medium ring-size lactone products.

3.1.3 Organotin Compounds as Lactonization Catalysts

It has been proposed that tin oxides can serve a dual role in the lactonization mechanism. Tin can increase the nucleophilicity of any oxygen atoms bound to it[8] but it can also act a Lewis acid catalyst, polarizing the carboxylic acid group towards nucleophilic attack. In this manner, the tin oxides can doubly activate the seco-acids towards reaction.

Both Steliou[9] and White[7c] have proposed similar mechanisms for organotin catalysis. Both mechanisms begin with preferential stannylation on the hydroxy group of the seco-acid. Steliou based the hydroxystannylation on studies of Davies[10] with dialkylcarbonates and bis(trialkyltin) oxides. White based the hydroxystannylation on studies by Pommier[11] with trialkystannoxides and halogenated alcohols. The mechanism proposed by Steliou is included in Figure 3.2.

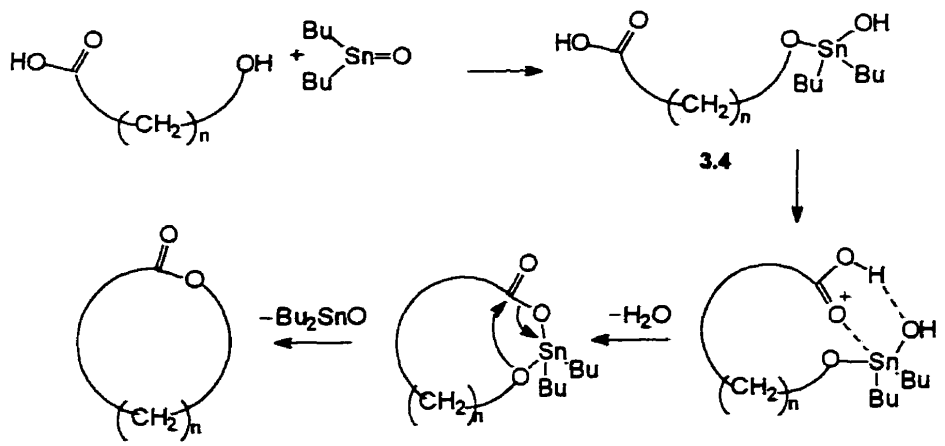

Figure 3.2: Steliou's[9] mechanism for dibutyltin oxide catalysis

The seco-acid reacts with di-*n*-butyltin oxide to yield the alkoxytin carboxylic acid **3.4**. The free carboxylic acid can then wrap around to the same

tin atom of the alkoxide. Once within proximity, the carboxylic acid can bond to the tin, thus increasing its coordination number to five. With the original functionalities in close proximity, intramolecular attack of the tin alkoxide oxygen occurs on the carbonyl carbon. This attack yields a lactone and the free di-*n*-butyltin oxide. This attack proceeds by double activation where the alkoxide oxygen is rendered more nucleophilic due to covalent bonding to tin. Additionally, the carbonyl carbon becomes more electrophilic via coordination to tin.

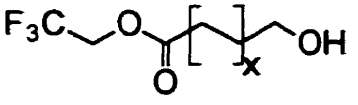

3.13

White's proposed mechanism, while similar, requires the seco-acid conversion to a hydroxytrifluorocarboxylate **3.13**. This hydroxytrifluoro-ethylcarboxylate is preferentially stannylated at the hydroxy group, rendering it more nucleophilic. As a trifluorocarboxylate ester, the seco acid is already activated towards nucleophilic attack and coordination of the carboxylate group to the tin may be unnecessary for cyclization to occur. No extensive mechanistic studies went into either of these proposed mechanisms however the 'double activation' proposal appears reasonable in light of the electropositive nature of tin relative to oxygen.

Oligomeric byproducts result when two separate seco-acids become activated and are in high enough concentration to react with one another. The activated carboxylate may not be attacked by its own tin alkoxide but rather that of another seco-acid giving intermolecular reaction as illustrated in Figure 3.3. In this case, double activation of the both chains is not necessary. However, at least one chain would need to be activated at the hydroxy end and the other at the carboxylic acid end for intermolecular reaction.

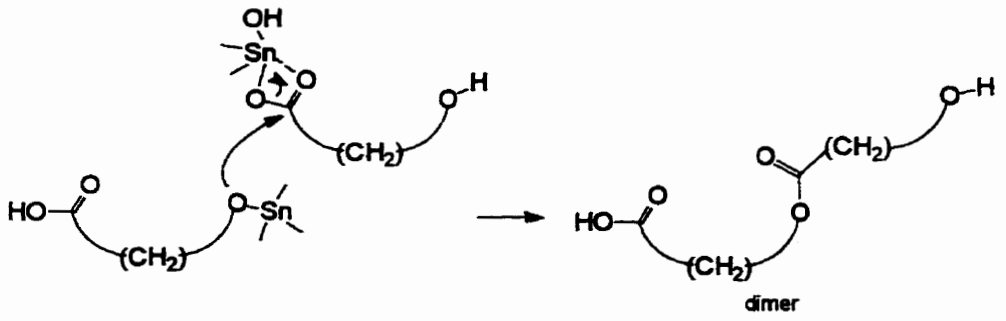

Figure 3.3: Intermolecular reaction of seco-acids with organotin mediation

3.1.4 Cyclization of Bifunctional Molecules

Lactone-based antibiotics, synthesized in the lab, often rely on intramolecular cyclization of seco-acids to form the macrocyclic skeleton. Seco-acids, with hydroxy and carboxylic acid functionalities are bifunctional molecules. Bifunctional molecules can react in an intramolecular or intermolecular manner, as represented schematically in Figure 3.4.

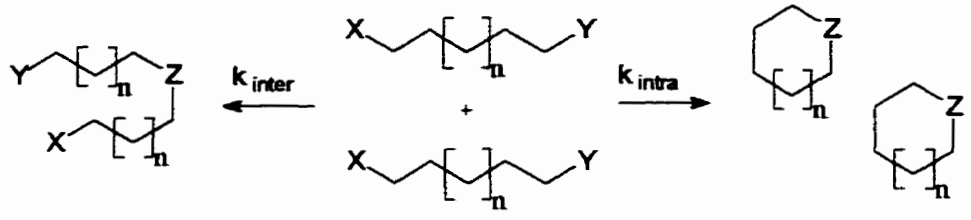

Figure 3.4: Reactions of bifunctional molecules

Intramolecular cyclization would result in a cyclic product. Alternatively, intermolecular reaction of several bifunctional molecules leads to oligomeric and polymeric products. Both intramolecular and intermolecular reactions compete when a bifunctional molecule is present. Generalizations, regarding the competitive outcome of these two processes, have been offered. These generalizations are predominantly based on the ring-sizes being targeted.

Intramolecular cyclization rates are a function of both activation energy and the statistical probability of each end of the bifunctional molecule coming together to react. Intuitively, the statistical probability of two ends coming into proximity should decrease with increasing ring-size. This factor is often coined the 'hunting factor' - an entropic comment on each end 'hunting out' the other to react. Alternatively, activation energy can be a reflection of the ring strain associated with intramolecular cyclization. Ring strain results from the combination of torsional strain, bond angle deformation within the cyclic structure, and through-space trannsannular repulsion[12]. In medium ring-sizes, torsional and trannsannular strain is very large so as to become prohibitive for 8 - 11 member ring formation. When the activation energy for cyclization becomes too great, intermolecular reactions are favoured.

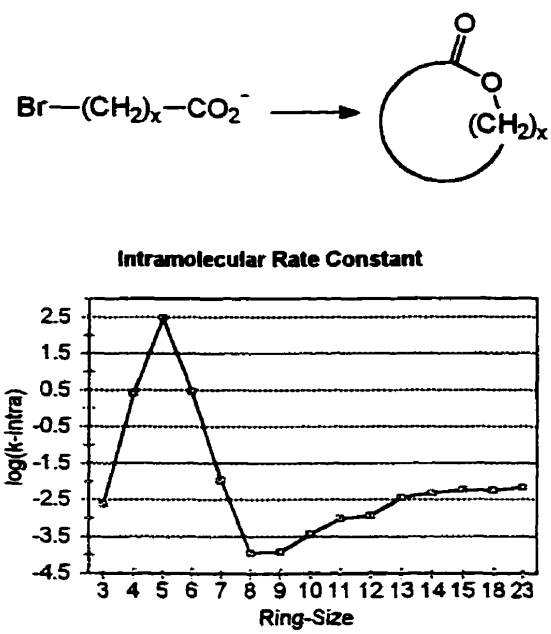

Figure 3.5: Intramolecular rate constant (s^{-1}) as a function of ring-size

Figure 3.5 illustrates the reactivity profile for the base-catalyzed lactonization of ω-bromocarboxylates as a function of ring size[13]. An enormous

range of reactivity is observed as ring size changes from 5 to 22 members. The profile indicates that 5 - 7 membered rings can be prepared fairly efficiently. Ring sizes of 8 - 12 members are disfavoured with rate constants as low at 10^{-4} sec^{-1}. The larger ring strain associated with medium ring-size lactones results in reduced intramolecular cyclization rate constants. A plateau effect occurs in the large ring-size range of 13 - 23 members. The rate constant in this range does not appear sensitive to ring-size. Rings of the 13 - 23 member size are thought to be low in ring strain energy.

Intermolecular reactions are bimolecular processes whereas cyclizations are unimolecular. As such, concentration can be altered to favour intramolecular versus intermolecular reaction. Specifically, dilute solutions favour intramolecular cyclization. The working concentration when intramolecular and intermolecular reaction rates are equal is termed the effective molarity (EM). Working above the EM favours oligomerization while concentrations below the EM favour cyclic products[14].

The EM profile for the lactonization of ω-bromocarboxylates based on ring-size is shown in Figure 3.6[12]. The rate constant for intermolecular reaction does not change significantly with increasing chain length. As a result, the EM profile has the same relative shape as the reactivity profile in Figure 3.5. The EM profile allows for comparisons of ring closure efficiency amongst a wide range of cyclization methods.

Most bifunctional cyclization reactions are performed several magnitudes of concentration below the EM. These dilute conditions ensure intramolecular cyclization predominates over intermolecular reaction. This method of bifunctional molecule cyclization is often referred to as infinite dilution. Using the EM curve in Figure 3.6, applying the infinite dilution technique to medium ring-size lactonizations would translate into concentrations at the micromolar level. This may be considered an impractical working concentration since such large volumes of solvent would be required to perform the cyclization at

moderate scale.

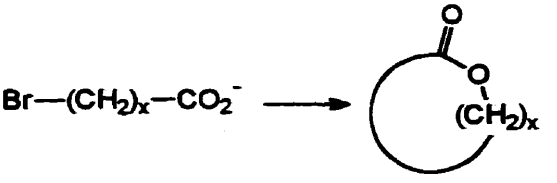

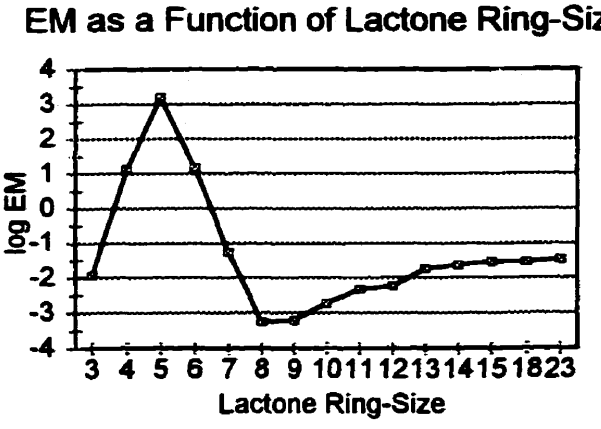

Figure 3.6: EM profile for ω-bromocarboxylic acid lactonizations

3.1.4.1 Methods Favouring Intramolecular Cyclization

A lactonization catalyst that only increases the intramolecular cyclization rate would have widespread application. Size-selective catalysis, whereby a solid catalyst has pore sizes that can only accommodate starting material and monomeric cyclization products, has been applied to seco-acid lactonization[15] with some success. Zeolite-catalyzed macrolactonization of 15-hydroxypentanoic acid occurred in 51% yield using reaction conditions ten times more concentrated than the EM. Size exclusionary 'in pore' acid catalysis had a favourable effect on the intramolecular cyclization rate, or alternatively a detrimental effect on intermolecular reaction rate.

Size exclusion catalysis is not a feasible route for tin reagents as no organotin catalysts of controlled pore size have been developed. Another

proposed method to favour intramolecular cyclization would use spatially exclusive catalysis. Specifically, each catalytic site would be spatially isolated from adjacent catalytic sites. This would eliminate two activated seco-acids coming into close enough proximity to react and should favour intramolecular cyclization as the reaction route, thus increasing k_{intra} over k_{inter}.

Tethering an organotin reagent, as a pendant functionality, to a solid phase support would combine several advantages. Namely, organotin reagents have been reported as mild lactonization catalysts. The solid phase tether would allow control of loading capacity, such that catalytic sites could be spatially discrete. The isolated catalytic species could lead to increased lactonization yields and reduced oligomeric byproducts. A secondary benefit, although significant, would be the simple purification a solid phase catalyst would afford. The purification benefits of solid phase organic chemistry (SPOC) have been discussed in Chapter 2.

3.1.5 Preparation of Lactones via Solid Phase Organotin Oxides

Our laboratory has extensive experience with both the preparation and application of a polystyrene-based chlorostannane copolymer **3.5**. It has been shown that hydrolysis of this copolymer with basic aqueous ethanol leads to a mixture of copolymer-bound stannol **3.6** and distannoxane **3.7** and it is possible to significantly alter the distannoxane/stannol ratio.

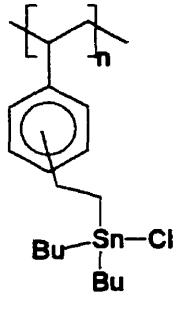

3.5

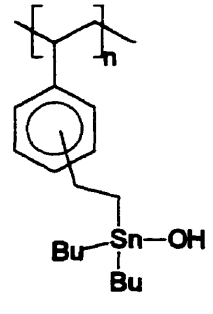

3.6

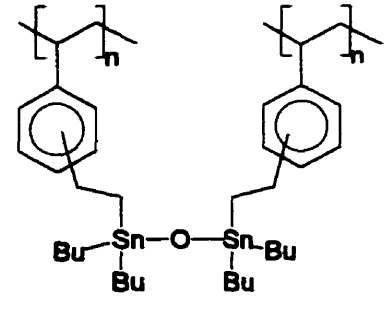

3.7

The solid phase distannoxane species is similar to the solution phase hexa-*n*-butyldistannoxane reagent used by both White[7c] and Steliou[9] in preliminary seco-acid lactonization studies. Neither Steliou or White included lactonization yields with their preliminary investigations of distannoxane reagent for seco-acid lactonization.

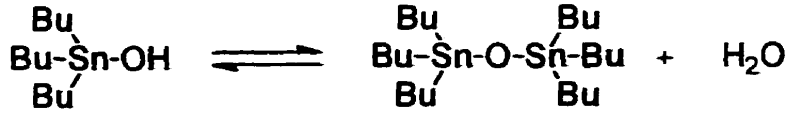

Figure 3.7: Solution phase stannol/distannoxane equilibrium

It is known that tri-*n*-butylstannol and hexa-*n*-butyldistannoxane are in equilibrium[16] as indicated in Figure 3.7. It was unclear what role each component would play in the lactonization catalysis. The relative amounts of polymer-bound stannol **3.6** and distannoxane **3.7** can be altered with copolymer loading capacity. Presumably, increased stannol amounts, evidenced by MAS solid state ^{119}Sn NMR spectroscopy, suggests sufficient spatial separation as to make distannoxane formation between sites less plentiful in the reduced copolymer loading cases.

No catalyst, tethered to a solid support strictly for the purpose of seco-acid lactonization, has been reported in the literature. However, various condensations of carboxylic acids using solid phase catalysis[17] have been documented and seco-acid lactonization should be a reasonable extension of this chemistry.

3.1.5.1 Proposed Project

We wished to determine if these copolymer-bound tin oxides **3.6/3.7** could act as lactonization catalysts. If they did catalyze the lactonization of ω-hydroxycarboxylic acids, it was possible that intramolecular reaction might be

favoured. Intermolecular reaction, as explained in the previous section, occurs when two seco-acids are activated in close proximity. If the tin active sites could be spatially separated within the copolymer matrix, the likelihood of two seco-acids being activated in close proximity would be reduced. The polymeric support would, in effect, dilute the tin catalyst.

If oligomeric byproducts could be reduced, higher lactone yields could be realized than for existing organotin reagents. In addition, previously unattainable lactones of 8 - 11 members may be observed. As with most SPOC applications, using the organotin oxide as a solid phase reagent would also reduce the inherent toxicity of solution phase tin reagents and make them safer to use. The solid phase would allow for removal of all tin contamination by filtration, leading to simple purification.

To this end, lactones of 17, 13, 11 and 8 members were targeted to represent both medium and large ring-size products. The ω-hydroxycarboxylic acids corresponding to these lactone sizes were either commercially available or accessible from commercially available precursors.

3.2 Results and Discussion

3.2.1 Summary

Employing conditions similar to Steliou[7a], lactonizations of ω-hydroxycarboxylic acids were attempted using solid phase distannoxane/stannol catalysis near the effective molarity (0.03M). The lactonizations had variable success based on the ring-size targeted. The solid phase distannoxane/stannol catalyst was successful for the preparation of large ring-size lactones. Hexadecanolide, a 17 membered lactone, was prepared in 55% yield with 27% oligomeric byproducts. Dodecanolide, a 13 membered lactone, was prepared in 10% yield with 78% oligomeric byproducts. This preparation gave lactone yields roughly comparable to existing tin-mediated methods[4a]. The solid phase catalyst failed to improve lactone yields or reduce oligomeric byproducts.

Medium ring-size lactones proved more difficult to synthesize. Heptanolide and decanolide, 8 and 11 membered lactones respectively, were not prepared by this solid phase catalyst approach. The attempted lactonization of 10-hydroxydecanoic acid did result in substantial amounts of oligomeric byproducts (49%). The lactonization of 7-hydroxyheptanoic acid resulted in smaller amounts of oligomeric byproducts (10%). These observations are in agreement with existing tin mediated lactonization methods. A successful method for medium ring-size lactone preparation, via tin mediation, has not been reported in the literature.

The use of a solid phase catalyst did lead to one important benefit. Purification was straightforward, requiring filtration and trituration to yield lactone products almost exclusively. In addition, competition studies with both solution and solid phase reagents provided information regarding a possible mechanism for tin catalyzed lactonizations of hydroxycarboxylic acids. Insight regarding the distannoxane/stannol solid phase has been gained.

3.2.2 Lactonization via Polymer-Bound Stannol/Distannoxane

Initially, a direct comparison of solution and solid phase distannoxane/stannol lactonization catalysis was desired. As a result, the reaction conditions used by Steliou[7a] were applied to our studies. Specifically, the distannoxane/stannol copolymer was present as a 10 mol % catalyst relative to the hydroxycarboxylic acid. The reactions were run at 0.03 M hydroxycarboxylic acid in refluxing mesitylene for 19 hours. For the lactonization of 16-hydroxyhexadecanoic acid and 12-hydroxydodecanoic acid, a concentration of 0.03 M is very close to the anticipated effective molarity[14], whereas 0.03M is approximately one hundred times above the effective molarity for 8 and 11 membered lactones. With these working concentrations, we wished to determine if the distannoxane/stannol polymer could catalyze lactonizations and produce reasonable lactone yields.

Following 19 hours of mesitylene reflux, the reaction was filtered to remove the organotin solid phase. After rinsing with fresh mesitylene and chloroform, the organotin catalyst was characterized by FT-IR spectroscopy, MAS solid state ^{119}Sn NMR spectroscopy, and wet chemical methods. The rinse solvents were combined with the original mesitylene filtrate and evaporated to dryness, yielding an oily residue. Trituration of the residue with methanol extracted a soluble product, leaving insoluble byproducts behind. The solid remaining after trituration was characterized by FT-IR spectroscopy, solution phase ^{1}H NMR spectroscopy, mass spectroscopy (MS), freezing point depression, and quantified by gravimetry. The methanol soluble material proved to be lactones and were characterized by HPLC. Refractive index (RI) detection was necessary, rather than the more typical UV detection, since both 16-hydroxyhexadecanoic acid and hexadecanolide contained weak chromophores.

When lactonization of 16-hydroxyhexadecanoic acid using the solid phase catalyst **3.6/3.7** failed to show dramatic improvement over solution phase

preparations, optimization of reaction conditions was addressed. All optimization was performed with 16-hydroxyhexadecanoic acid. Ultimately, the reaction conditions determined from these optimization studies were applied to heptanolide, decanolide and dodecanolide preparations.

3.2.2.1 Effect of Varying Catalyst Proportions

A chlorostannane copolymer **3.5** of 1.6 mmol/g loading was hydrolyzed with basic aqueous ethanol to yield a mixture of copolymer-bound stannol **3.6** and distannoxane **3.7**. The distannoxane/stannol ratio was approximately 3:1 as determined from the relative peak sizes in the MAS solid state ^{119}Sn NMR spectrum of this compound. This copolymer represents the highest distannoxane proportion available for this system through hydrolysis of the chlorostannane species. The amount of organotin catalyst, relative to 16-hydroxyhexadecanoic acid, was varied at 5, 10, 50, 100, and 200%. Reaction solution concentrations were held constant at 0.03M in refluxing mesitylene over 19 hours.

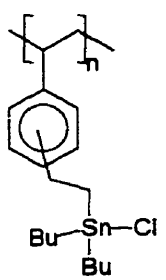

3.5

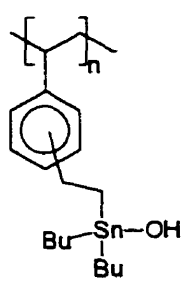

3.6

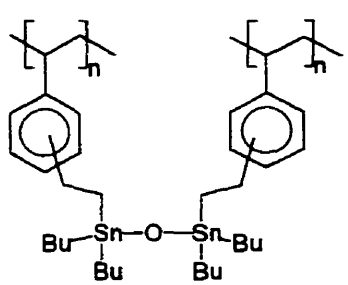

3.7

The resultant yields of lactone and insoluble byproducts are presented in Table 3.4. Varying the proportion of catalyst greatly effected the product yield. Yields were maximal at 10% catalyst (entry 2) and decreased from there with both higher catalyst amounts (entries 3,4,5) and lower catalyst amounts (entry 1). The change in yield with catalyst will be discussed in terms of a reaction

mechanism in Section 3.2.5.

Table 3.4: Effect of catalyst stoichiometry on hexadecanolide yield			
1.7 mmol/g Polymer	Organotin Sites/ Hydroxyacid	Lactone Yield (%)	Byproducts (%)
Control	no catalyst	0	0
1	5% catalyst	0	6
2	10% catalyst	55	27
3	50% catalyst	29	27
4	equimolar	18	25
5	2 x excess	7	1

Unreacted 16-hydroxyhexadecanoic acid amounts have not been included in Table 3.4. Entries 2, 3, and 4 gave good mass balances accounting for 75 - 90% of starting material. Entries 1 and 5 gave very poor mass balances of about 50%. Non-quantitative analysis of the condenser and Dean Stark trap used in the lactonizations indicated substantial amounts of 16-hydroxy-hexadecanoic acid. In addition, at the extreme temperature of refluxing mesitylene, some loss mass may be attributable to volatilized starting material or lactone.

Analysis of the copolymer-bound organotin catalyst **3.6/3.7** after lactonization indicated that unreacted 16-hydroxyhexadecanoic acid had also become physically trapped within the polymer. Following lactonization, the polymers were washed with 10% trifluoroacetic acid (TFA) and dichloromethane. As explained in Chapter 2, these are known conditions to cleave any tin carboxylates or tin alkoxides within the polymer matrix. The dichloromethane also swells the polymer considerably, allowing trapped starting material to be extracted. HPLC analysis of the wash solution indicated 19 -

22% of the initial 16-hydroxyhexadecanoic acid starting material in the 100 and 200% experiments. Unfortunately, TFA washing does not discriminate between starting material physically trapped within the polymer from starting material chemically bound to the polymer as tin carboxylate or tin alkoxide. However, it does serve alleviate mass balance concerns.

FT-IR spectral analysis of the polymer following lactonization, prior to TFA washing, indicated a small absorbance in the 1640 cm^{-1} range that is indicative of a tin carboxylate. A concomitant absorbance for tin alkoxides at approximately 1070 cm^{-1} was not observed. However, tin alkoxides are hydrolytically unstable and may hydrolyze prior to analysis[16]. FT-IR spectroscopic analysis of the polymer following TFA washing indicated strong carbonyl stretches at 1700 and 1635 cm^{-1}. These two signals are presumably from the trifluoroacetic acid becoming both trapped and chemically bound to the polymer.

3.2.2.2 Effect of Catalyst Loading

Significant amounts of solid by-products resulted from the copolymer-bound distannoxane/stannol **3.7/3.6** mediated lactonization of 16-hydroxyhexadecanoic acid, when the amount of catalyst was varied. Since intermolecular reaction requires two seco-acids to become activated near each other, increasing the distance between adjacent catalytic sites on the copolymer was proposed in an attempt to favour intramolecular versus intermolecular reaction. Distannoxane formation within the copolymer requires two tin species in close proximity. Alternatively, each tin species must be flexible enough to move into close proximity. Reduced amounts of distannoxane may be indicative of more space between tin sites such that adjacent tins are not in close enough proximity to form distannoxanes. If adjacent tins are spatially discrete than perhaps intermolecular reaction may be reduced.

This study was done with three different loading capacity copolymers,

distinguishable by the distannoxane/stannol ratio observed in the MAS solid state ^{119}Sn NMR spectra for each. Each copolymer was used as a 10% catalyst, as well as an equimolar reagent, relative to 16-hydroxyhexadecanoic acid. As with all other reactions done thus far, concentration, temperature and reaction time were kept constant. The resultant yields for hexadecanolide and solid byproducts are summarized in Table 3.5.

Table 3.5: Effect of catalyst loading on hexadecanolide yield

Polymer Loading		Distannoxane/ Stannol	Polymer/ Hydroxyacid	Lactone (%)	Byproducts (%)
1	High	3.0	10% catalyst	55	27
2	High	3.0	equimolar	18	25
3	Medium	2.0	10% catalyst	35	41
4	Medium	2.0	equimolar	20	11
5	Low	0.5	10% catalyst	21	20
6	Low	0.5	equimolar	11	11

The highest lactone yield was observed for entry 1. This preparation used the highest loading copolymer as a 10% catalyst. Yields were generally better when the organotin oxide was used catalytically (entries 1, 3, 5) as opposed to equimolar amounts (entries 2, 4, 6). No obvious pattern, based on polymer loading capacity, was observed for the yield of oligomeric byproducts. Significant amounts of oligomeric byproducts were formed for all reactions within this study, with amounts slightly higher when the copolymer was used as a 10% catalyst rather than equimolar reagent. This observation is in agreement with the previous stoichiometric study of Section 3.2.2.1.

From Chapter 2, it was concluded that reduced polymer loading leads to reduced distannoxane amounts on the polymer. This study has shown that reduced polymer loading also leads to reduced lactonization yields. Attempts to

separate adjacent tin sites by reducing copolymer loading capacity did not lead to decreased intermolecular byproducts as anticipated.

3.2.2.3 Effect of Reaction Temperature

A number of 16-hydroxyhexadecanoic acid lactonizations gave poor mass balance. While some of the hydroxycarboxylic acid had become trapped/bound within the copolymer, significant amounts of starting material were evident on the condensor walls and in the Dean Stark reservoirs used in these reactions. This observation indicates that some 16-hydroxyhexadecanoic acid or hexadecanolide was vapourizing from the reaction solution.

Mesitylene refluxes at 162 - 164°C. Xylenes, which reflux at 137 - 144°C, were used as alternative solvent for the lactonization of 16-hydroxyhexadecanoic acid. Reaction solution concentration, reaction time and stoichiometry were kept constant. Performing the reaction at lower temperature gave a reduced yield of lactone (10%), with more solid byproducts (47%) as well as substantial amounts of unreacted 16-hydroxyhexadecanoic acid. The reaction was also attempted in chloroform, a significantly lower boiling solvent at 61°C. No hexadecanolide or oligomeric byproducts were observed in this reaction. The best overall conversion of starting material to products, both intra and intermolecular, occurred with mesitylene. Apparently the high temperature of refluxing mesitylene is necessary for respectable conversion yields.

3.2.2.4 Optimized Lactonization Conditions

The reaction conditions best suited for solid phase distannoxane/stannol **3.7/3.6** catalyzed lactonization of 16-hydroxyhexadecanoic acid were determined. The 1.6 mmol/g loaded chlorostannane copolymer **3.5**, upon hydrolysis, is best used as a 10% catalyst relative to seco-acid with a 19 hour mesitylene reflux, giving the highest lactone yields. As stated in Section 3.2.2,

workup leads to three components, organotin catalyst, methanol soluble products, and methanol insoluble products. The methanol soluble products were characterized by HPLC. All yields were determined by HPLC analysis using a calibration curve of the authentic lactone. Starting materials were quantified by comparison to a calibration curve of the original seco-acids. A typical chromatogram for a lactone quantification is included in Figure 3.8.

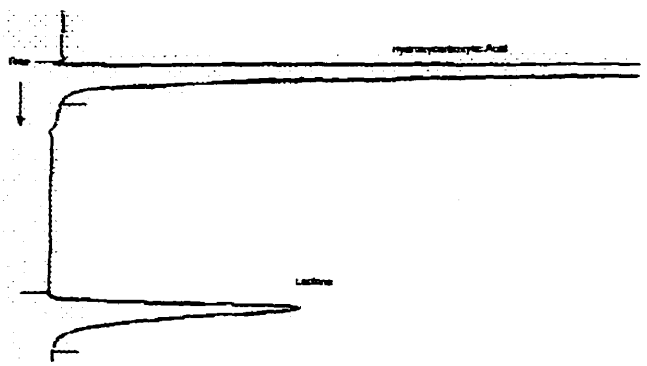

Figure 3.8: Typical Chromatogram of Lactonization Filtrate

The copolymer proved reuseable although yields were compromised, with hexadecanolide being prepared in only 38% yield with the recycled catalyst compared to 55% with new catalyst. In addition, 52% of the 16-hydroxyhexadecanoic acid was incorporated into solid byproducts after recycling the copolymer-bound organotin oxide catalyst. As a result, new distannoxane/stannol copolymer **3.7/3.6** was used for each lactonization preparation.

3.2.3 Preparative Results

The optimized reaction conditions just mentioned for hexadecanolide were applied to the preparation of heptanolide, decanolide and dodecanolide. The results are shown in Table 3.6. All lactone yields were determined by HPLC analysis with comparison to standard calibration curves of authentic

lactone samples. Authentic lactones were prepared by Baeyer Villiger oxidation of the corresponding cyclic ketones. All solid byproduct yields were determined by gravimetry. The yields from these smaller ring-size lactones were much poorer than for hexadecanolide.

Table 3.6: Preparative results for all lactones attempted		
Ring Size	Lactone (%)	Solid Byproducts(%)
17	55	27
13	10	78
11	0	49
8	0	17

As anticipated, large ring-size lactones could be prepared using solid phase distannoxane/stannol **3.7/3.6** catalysis. These lactones, hexadecanolide and dodecanolide , have been previously prepared by solution phase tin catalysis as summarized in Table 3.7. These existing methods are compared to the copolymer-bound distannoxane/stannol system.

Table 3.7: Lactone yield comparison to existing tin oxide methods				
Ring-Size	Reagent			
	Polymer **3.6/3.7**	Bu_2SnO[7a]	Bu_3OMe[7c]	$Bu_2SnO(Cl)$[7b]
8	0	--	--	--
11	0	0	0	--
13	10	22	42	0
17	55	60	81	81

The polymer-bound catalyst did not lead to improved lactone yield nor did it reduce the amount of solid byproducts relative to existing solution phase

methods. However, catalysis by solid phase distannoxane/stannol **3.7/3.6** did simplify purification. All traces of the catalyst were removed by filtration.

The large ring-size lactones exhibit lower ring strain than medium ring-size lactones and as a result, are easier to prepare. This observation was confirmed with the attempted synthesis of decanolide and heptanolide. Neither of these medium ring-size lactones were prepared by solid phase distannoxane /stannol catalysis. However, solid byproducts were observed in both cases. Lactones, in the 8 -11 member ring-size, have no reported preparation by solution phase tin catalysis in the literature. Very few preparations exist in the literature for even non-tin catalyzed medium ring-size lactonizations. In fact, only scandium triflate[4a] catalysis has allowed for preparation of the entire series of medium ring-size lactones from hydroxycarboxylic acids in greater than 50% yield.

The difficulty associated with medium ring-size lactone preparation was anticipated. As discussed in Section 3.1.4, it is known that intramolecular cyclization rates are a function of activation energy and a 'hunting factor'. Strain effects, measured as the enthalpy of activation (kcal/mol), indicate the highest ring strain over the 8 through 12 membered ring sizes. Judging from our poor lactone yields, the solid phase distannoxane/stannol catalyst was unable to lower the activation energy enough to make medium ring-size lactone formation viable in this particular study.

3.2.4. Characterization of Solid Byproducts

The solids isolated from hexadecanolide and dodecanolide preparations were analyzed by FT-IR, NMR, MS, and freezing point depression. Mixed melting points with the seco-acids confirmed the solids were not starting material. Melting points were typically broad, usually encompassing a 4 - 10°C range, which suggests a mixture of compounds. ^{1}H NMR spectra were similar to the authentic lactones in terms of chemical shift. FT-IR spectra suggested

ester or lactone type products as judged by the carbonyl stretch at 1730 cm^{-1} rather than seco-acid starting material at 1684 cm^{-1} . The typical O-H stretching of 3300-2500 cm^{-1} for carboxylic acids was not observed. Mass spectroscopy (MS) proved ambiguous and contradictory. Exact mass determination was attempted but secondary ions generated in the spectrometer could not be distinguished from original species.

Using the solid isolated from the 12-hydroxydodecanoic acid lactonization as an example, electron impact (EI) LRMS indicated ions at 199, 397, 594, 792, and 988 m/z. Peaks were also visible at 181, 379, 576, and 774 m/z. This series of ions is consistent with monomeric through pentameric polylactone products of the general formula $(C_{12}H_{22}O_2)_n$, and dehydrated lactones of the general formula $(C_{12}H_{22}O_2)_n - H_2O$. A representative low resolution EI-MS spectrum is included in Figure 3.9. The peaks representing the monomeric thru pentameric series are indicated on the spectrum.

In an attempt to minimize fragmentation, chemical ionization (CI) MS with isobutane as the carrier gas indicated peaks at 199, 397, 595, 793 and 989 m/z. These peaks represent the same species of formula $(C_{12}H_{22}O_2)_n$ +1 from the EI-MS, some in a dehydrated state (-18 m/z). Generally, M+1 ions generated by CI-MS are not as high energy as when generated by electron impact[18]. However, CI-MS can also cause recombination of fragment ions within the spectrometer and this leads to the ambiguity of whether some of the higher mass species were actually from recombination. Despite these uncertainties, the mass spectroscopic data suggests that the solid byproducts are mixtures of polylactones, not polyesters. Relative peak intensities could not be used from the spectra since each polylactone product would have a different volatility in the inlet of the mass spectrometer.

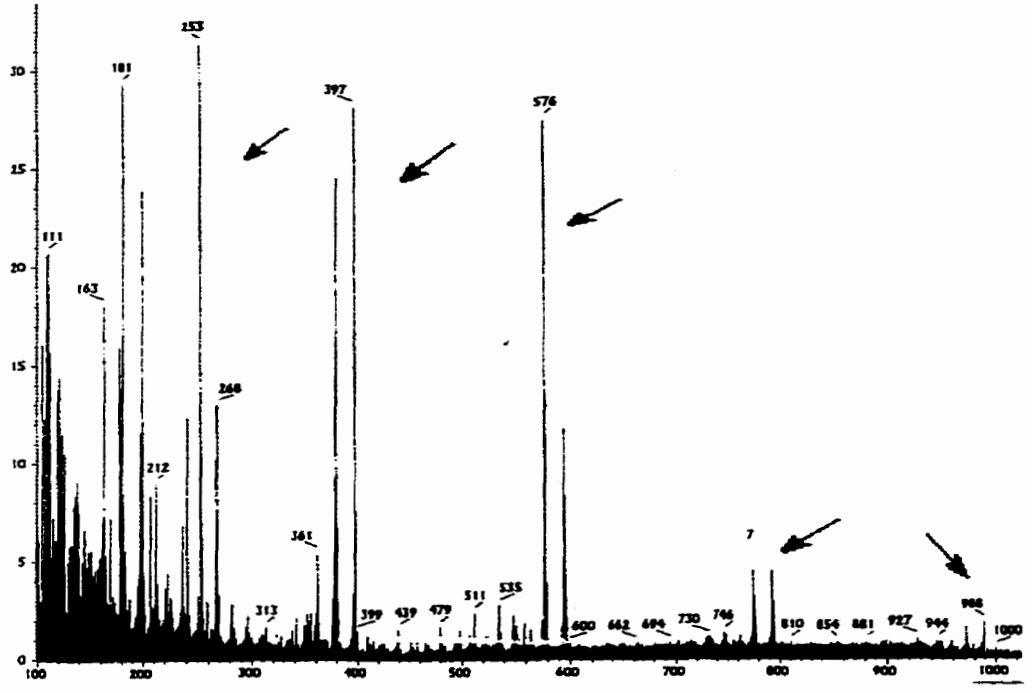

Figure 3.9: LR-MS (EI) of solid byproduct isolated from 12-hydroxydodecanoic acid lactonization

The same sort of MS dilemma, except with monomeric through tetrameric polylactones, was observed for the lactonization of 16-hydroxyhexadecanoic acid. An alternate method was needed to determine the oligomeric byproduct molecular weights.

3.2.4.1 Camphor Freezing Point Depression

At this point, mass determination reverted to the colligative property technique of freezing point depression. It has been demonstrated that the decrease in freezing point (ΔT) for a substrate is proportional to the molality of an impurity.

$$\Delta T \propto K \cdot m \quad \text{where m = moles solute / kg solvent}$$

Camphor was chosen for this study because our solid byproducts were soluble in molten camphor and camphor has a very large coefficient of freezing point depression. The freezing point of 1 kg of camphor is depressed by 40°C in the presence of 1 mole of impurity[19].

The validity of this approach was confirmed by determining the molecular weight of authentic dodecanolide. A standard curve using known molalities of cyclododecanone as an impurity was first constructed. Comparing this standard curve to that obtained for dodecanolide, the lactone molecular weight was determined to be 189 g/mol. This compares favourably to the actual molecular weight of 198 g/mol. This method was then used with the solid isolated from the 12-hydroxydodecanoic acid lactonization. Comparing the same cyclododecanone standard curve with that constructed from various amounts of solid / kg camphor gave a number average molecular weight of 910 g/mol which is approximately 4.5 lactone units per polylactone for the solid product.

Alternatively, a standard curve was prepared from commercially available hexadecanolide. Comparing the curve constructed from various amounts of solid / kg camphor for the compound isolated from the 16-hydroxyhexadecanoic acid lactonization, the number average molecular weight was determined at 586 g/mol which is approximately 2 units per polylactone.

All experimental evidence points to these solids being cyclic lactones not linear polyesters. No free carboxylic acid or alcohol functionalities were visible in the FT-IR spectrum. The polylactones were sufficiently small that a free carboxylic acid or alcohol should not be diluted by other ester functionalities within the molecule. Had the number average molecular weights for the solid byproducts been larger, a acid and alcohol may no longer be visible in the FT-IR spectrum. The ^{1}H NMR chemical shifts of the hydroxycarboxylic acids, particularly the methylenes adjacent to the acid and alcohol functionalities, are substantially different from the solid oligomeric byproducts isolated. These hydroxycarboxylic acid chemical shifts would be expected in the linear polyester

case. The EI and CI-MS data also supports polylactone versus polyester products.

The lactonization of 12-hydroxydodecanoic acid resulted in polylactones of 4 ½ average unit size. A polylactone of just 4 units represents a ring of 52 members. This is an enormous polylactone, but ring strain would presumably be low and the reactivity profile in Figure 3.5 indicates little change in the intramolecular rate constant after a ring becomes larger than 13 members. For the 16-hydroxyhexadecanoic acid lactonization, the solid was determined to be, on average, a 2 unit polylactone. Two units represent a ring of 34 members. The solids isolated from the lactonizations of 7-hydroxyheptanoic acid and 10-hydroxydecanoic acid were not analysed in this manner.

3.2.5 Mechanistic Aspects

As mentioned in Section 3.1.3, previous solution phase studies with di-*n*-butyltin oxide catalyzed lactonizations were based on the premise that stannylation of a seco-acid would preferentially occur at the hydroxy functionality. This would lead to initial formation of a ω-alkoxystannylcarboxylic acid **3.4**. The mechanistic scheme is shown again in Figure 3.10.

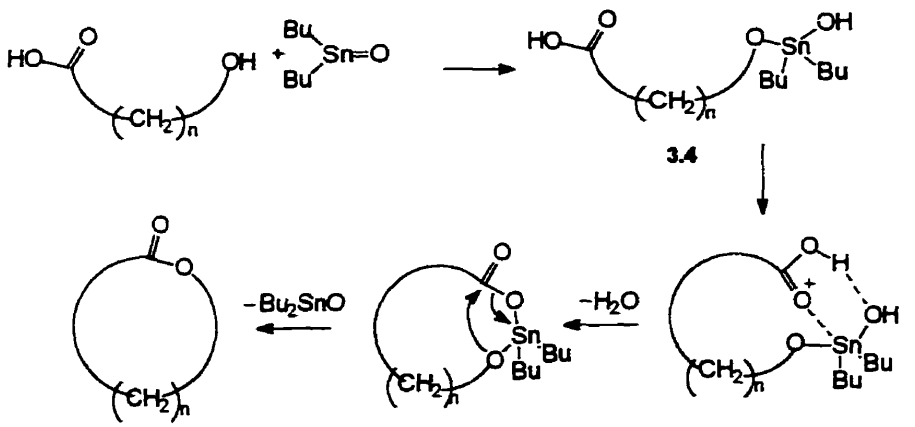

Figure 3.10: Stelliou's [9] proposed lactonization mechanism

This mechanistic proposal of Steliou[9] has the free carboxylic acid coordinating to the same tin atom following extrusion of water. The tin doubly activates both ends of the bifunctional seco-acid. An intramolecular rearrangement ensues to yield the lactone product, extruding the original tin catalyst.

The preferential hydroxystannylation was based on Davies' preparation of organotin alkoxides[10]. Our own interpretation of Davies' original 1971 study does not support the notion of preferential hydroxystannylation. However, the stannylation sequence should make little difference as long as the seco-acid is doubly activated at both carboxylic acid and alcohol functionalities prior to cyclization.

3.2.5.1 Preferential Stannylation

In the process of optimizing lactonization yields, some reactions were performed to better understand the mechanism by which the polymer behaved. Our experimental findings contradict the preferential hydroxystannylation of seco-acids.

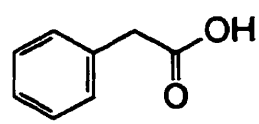

3.14

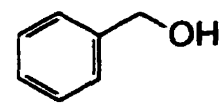

3.15

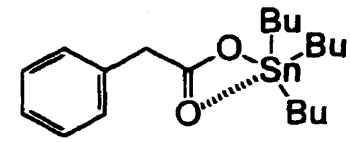

3.16

In Section 2.2.6.4, a distannoxane/stannol copolymer formed a tin carboxylate quantitatively from the sodium salt of toluic acid. This quantitative conversion was apparent in the MAS solid state ^{119}Sn NMR spectrum. In this study, reacting equimolar amounts of phenylacetic acid **3.14** and benzyl alcohol **3.15** with hexa-*n*-butyldistannoxane leads to the conclusion that a tin carboxylate, presumably stannylphenylacetate **3.16**, forms preferentially to the tin alkoxide of benzyl alcohol. This conclusion was made from the solution

phase ^{119}Sn NMR spectrum. Three species were visible in the spectrum, tin carboxylate, stannol, and distannoxane. A tin alkoxide, based on chemical shifts of similar compounds, would lead to a species near +80 ppm[20]. Our competition study involved the direct analysis of a reaction aliquot without work-up. As a result, the hydrolytic instability of tin alkoxides should have been circumvented. A tin alkoxide, if present in the reaction aliquot, should have been detected. The phenylacetic acid and hexa-*n*-butyldistannoxane were present in an equimolar ratio, therefore the tin carboxylate did not form in 100% as evidenced by the remaining distannoxane/stannol in the NMR spectrum.

An analogous reaction on the solid phase stannol/distannoxane copolymer with benzyl alcohol **3.15** and phenylacetic acid **3.16** in a 2:1:1 ratio, was performed. DRIFTS analysis indicated the presence of a tin carboxylate at 1644 cm^{-1}. A tin alkoxide of benzyl alcohol would be expected at approximately 1070 cm^{-1} [10]. No stretch other than 1062 cm^{-1}, attributable to the polymer itself, was observed in this region.

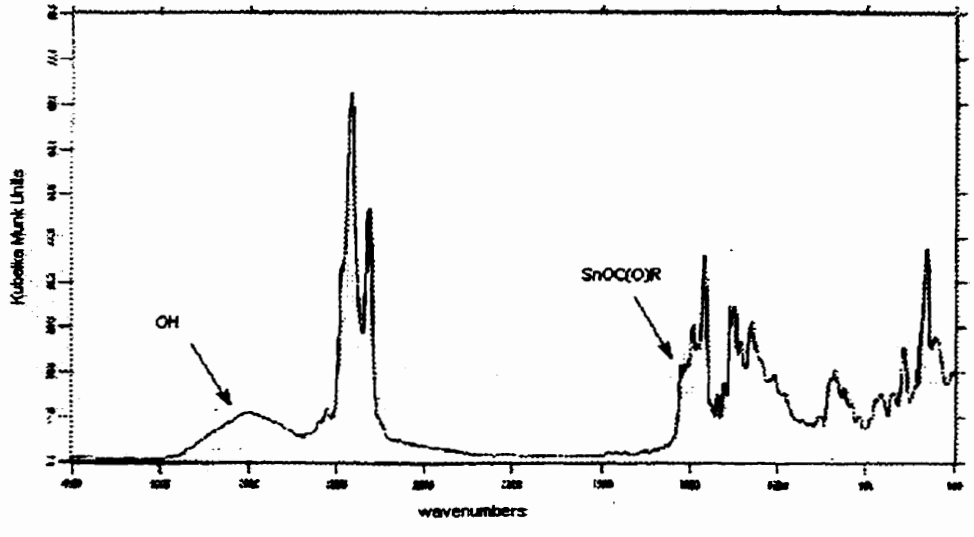

Figure 3.11: DRIFTS spectrum from reaction of **3.6/3.7** and 16-hydroxyhexadecanoic acid

Finally, an equimolar reaction of the distannoxane/stannol copolymer

and 16-hydroxyhexadecanoic acid in refluxing benzene for 1 hour indicated free alcohol at 3320 cm^{-1} and tin carboxylate at 1637 cm^{-1} in the DRIFTS spectrum as indicated in Figure 3.11. These observations again supported the preferential stannylation of carboxylic acids versus alcohols. This is not to say that tin alkoxides cannot form on the polymer, but our experimental evidence indicated preferential tin carboxylate formation.

3.2.5.2 Summary of Experimental Observations

It has not proven simple to generate a mechanistic picture which rationalizes all of the experimental findings for copolymer-bound tin oxide catalysis of seco-acid lactonizations. These diverse observations have been summarized.

The copolymer-bound distannoxanes/stannol **3.7/3.6** preferentially stannnylate the carboxylic acid functionality of a seco-acid. This was determined by both solution and solid phase competition studies. However, double activation of the seco-acid does require tin alkoxide formation. Presumably, under the high temperature and anhydrous conditions of these seco-acid lactonizations, a tin alkoxide could form.

We have observed a sharp dependence on lactone yield as a function of copolymer-bound catalyst/hydroxyacid ratio. Maximum yields were observed when the catalyst was present in 10% relative to the seco-acid. Overall conversions dropped essentially to zero when the catalyst was reduced to 5% relative to seco-acid.

Similarly, the 200% catalyst relative to seco-acid, gave minimal yields of lactone and oligomeric byproducts. This is contrary to the trend where more catalyst leads to faster reaction and more product. Both the 100% and 50% catalyst relative to seco-acid gave moderate yields for lactones and oligomeric byproducts, falling between the 200 and 10% results respectively. There must be opposing factors which affect yield as the catalyst amount is increased.

Reduced loading capacity copolymers gave lower yields of lactones. When the catalyst was present in 10% relative to seco-acids, conversion yields were moderate for all three variable loading copolymers, ranging from 83 - 41% conversion. MAS solid state ^{119}Sn NMR studies of the hydrolysed chlorostannane polymers **3.5** have indicated that reduced loading capacity leads to reduced distannoxane **3.7** species relative to stannol **3.6**. Since reduced loading gives reduced lactone yields, distannoxane may be the catalytic species responsible for lactone formation. These observations are summarized in Table 3.8 when the organotin catalyst was present at 10% relative to seco-acid.

Table 3.8: Distannoxane/stannol ratio as a function of conversion yields

Polymer Loading	Ratio **3.7/3.6**	mmol **3.7**/ mmol **3.6** (calc'd)	Lactone Yield (%)	Oligomer Yield (%)	Conversion Yield (%)
1.6	3	0.6 / 0.4	55	27	83
1.1	2	0.37 / 0.37	35	41	76
0.24	0.5	0.04 / 0.16	21	20	41

Finally, the solid byproducts isolated from the lactonization of 12-hydroxydodecanoic acid and 16-hydroxyhexadecanoic acid are cyclic polylactones, not linear polyesters.

3.2.5.3 Mechanistic Speculation

A mechanistic scheme has been generated based upon two assumptions: esterification of seco-acids occurs by double activation, and distannoxanes are the catalytic species for lactone formation. While there is no unambiguous evidence for either of these assumptions, there are indicators that they are not unreasonable. If the distannoxane species is necessary for lactone formation, it could be postulated that double activation occurs with one

tin for each functionality of the seco-acid. Double activation with a polymer-bound distannoxane would leave each 'activated' end of the seco-acid in close proximity for intramolecular reaction to the lactone, as indicated in path A of Figure 3.12.

Reduced amounts of distannoxane gave reduced amounts of lactone as indicated in Table 3.8. However, distannoxane cannot be the sole catalytic species since the medium loading polymer gave comparable conversion yields of seco-acid. Conversion was roughly similar with distannoxane/stannol ratios of 3.0 and 2.0, giving 83 and 76% conversion respectively. These observations support that double activation is necessary for both intra and intermolecular reaction but double activation via a distannoxane species is necessary for conversion to lactone products. The low loading copolymer had only one tenth the tin atoms of the high loading copolymer and a distannoxane/stannol ratio of 0.5. By the time the stannol amount had become two times the distannoxane in this low loading copolymer, the conversion yield had dropped by half.

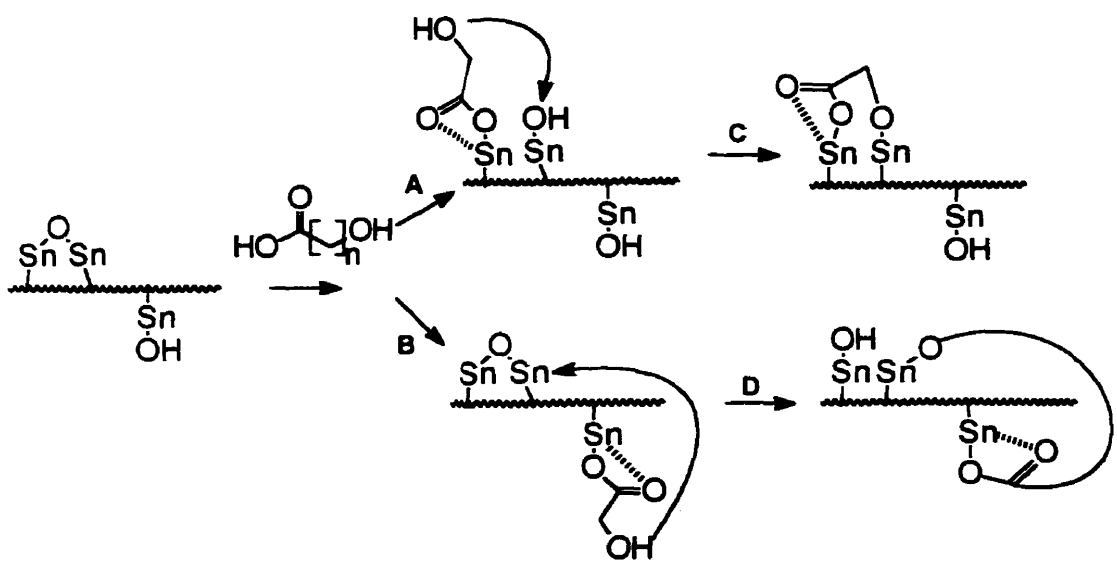

Figure 3.12: Schematic of double activation possibilities

Figure 3.12 illustrates a copolymer that contains both stannol and

distannoxane sites. A seco-acid can react in one of two ways with the solid support as indicated by path A and B. The distannoxane doubly activates a seco-acid, in close enough proximity that intramolecular reaction is possible as indicated in path C. The stannol species can only bind a seco-acid at one functionality , as a tin alkoxide or a tin carboxylate. In path B, if the stannol binds a seco-acid at the carboxy end but the hydroxy end cannot come into proximity with another tin site, double activation does not occur and no reaction would be observed. If the non-activated end of the seco-acid can reach another tin site, as indicated by path D, than this seco-acid becomes doubly activated. This double activation has the two tin sites spatially removed and intermolecular reaction would result only if a second seco-acid were attached nearby, as indicated in the next schematic, Figure 3.13.

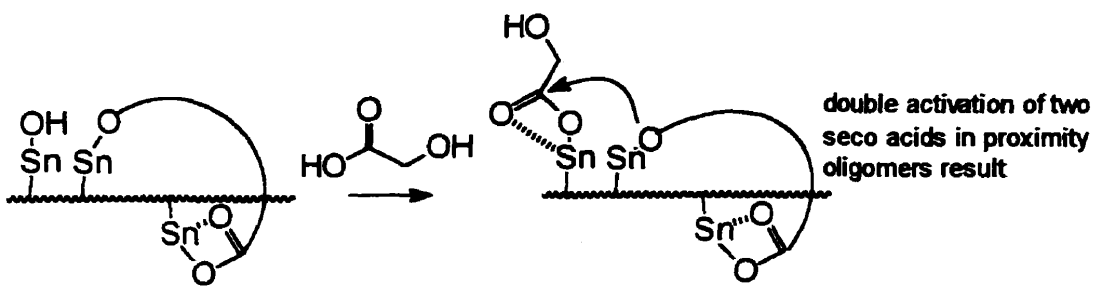

Figure 3.13: Intermolecular reaction from initial stannol-single activation

In the high loading copolymer with a distannoxane/stannol ratio of 3.0, distannoxane sites are abundant allowing for double activation. The double activation of the seco-acid occurs in close proximity and lactonization is the favoured route. Even if some seco-acid should bind to stannol, enough tin sites are available for the other end of the seco-acid to become activated, leading to oligomeric byproducts. This could be represented as a combination of path C and D in Figure 3.12, occurring simultaneously on the high loading capacity copolymer. To test this mechanistic hypothesis, the 100% distannoxane copolymer resulting from the air oxidation of distannane **2.6** should be applied

to seco-acid lactonization in future. This distannane-distannoxane has been discussed in Chapter 2.

In the medium loading copolymer, with a distannoxane/stannol ratio of 2.0, double activation of a seco-acid in close proximity would be reduced because the amount of distannoxane is reduced. More seco-acid would be singly activated by binding to stannol. Because loading is moderate, the bound seco-acid can reach another tin site to activate its second functionality as indicated in Figure 3.12 (path D) and oligomers result.

For the low loading copolymer, with a distannoxane/stannol ratio of 0.5, most seco-acid will bind to stannol to give single activation. On average, each tin site is separated by ten monomeric styrene units. As a result, the copolymer is dilute and these singly activated seco-acids will not reach a second tin site to activate their remaining functionality. With reduced amounts of double activation, intermolecular reaction is reduced and conversion yields decrease.

Both ends of the stoichiometric spectrum gave poor conversion yields for 16-hydroxyhexadecanoic acid lactonization. At 5% catalyst relative to seco-acid, all the tin sites on the copolymer could be occupied as tin carboxylates including both tin sites from distannoxane which would normally lead to lactonization. In addition, free seco-acid would be in solution. It is possible that higher conversion with this catalytically small amount simply requires more time. At 200% catalyst, there are sufficient sites that no seco-acid should be free in solution. If all seco-acid is bound on the copolymer, with free tin sites between, the statistical probability of double activation in the correct proximity for any reaction, be in inter or intramolecular, should be reduced as shown schematically in Figure 3.14. Although not as severe, a similar scheme would be expected for the 100% reaction. Most of the seco-acid should be bound to the copolymer, possibly in a spatial orientation that prevents an activated hydroxy group from coming into the proximity of an activated carboxylate.

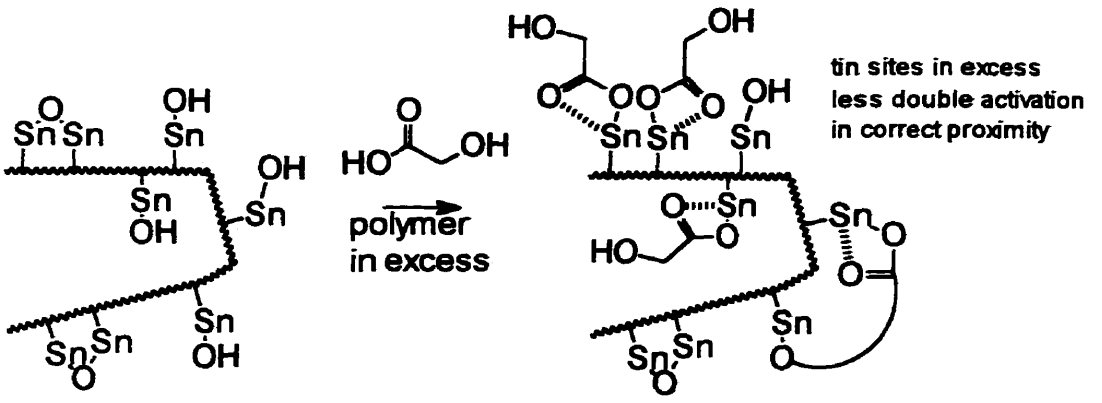

Figure 3.14: Excess copolymer relative to seco-acid preventing proper orientation of activated species

By combining the individual schematics for each mechanistic feature, a potential overall reaction route is given in Figure 3.15. A seco-acid can react with a polymer-bound distannoxane to give a tin carboxylate (path A). A second tin, from the original distannoxane, is in close proximity such that the hydroxy end of the seco-acid reacts with it to become doubly activated (path C). The doubly activated seco-acid has both head and tail in close proximity and an intramolecular reaction ensues to give lactone products. Alternatively, a seco-acid reacts with a polymer-bound stannol (path B and E). After forming a tin carboxylate, if the hydroxy end of the seco-acid cannot reach another tin site than no double activation occurs (path F). If the seco-acid cannot be doubly activated there is no reaction. If the seco-acid hydroxy end can reach a second tin site (path D) than double activation is realized and an intermolecular reaction results, yielding oligomers which eventually lead to the experimentally observed polylactones.

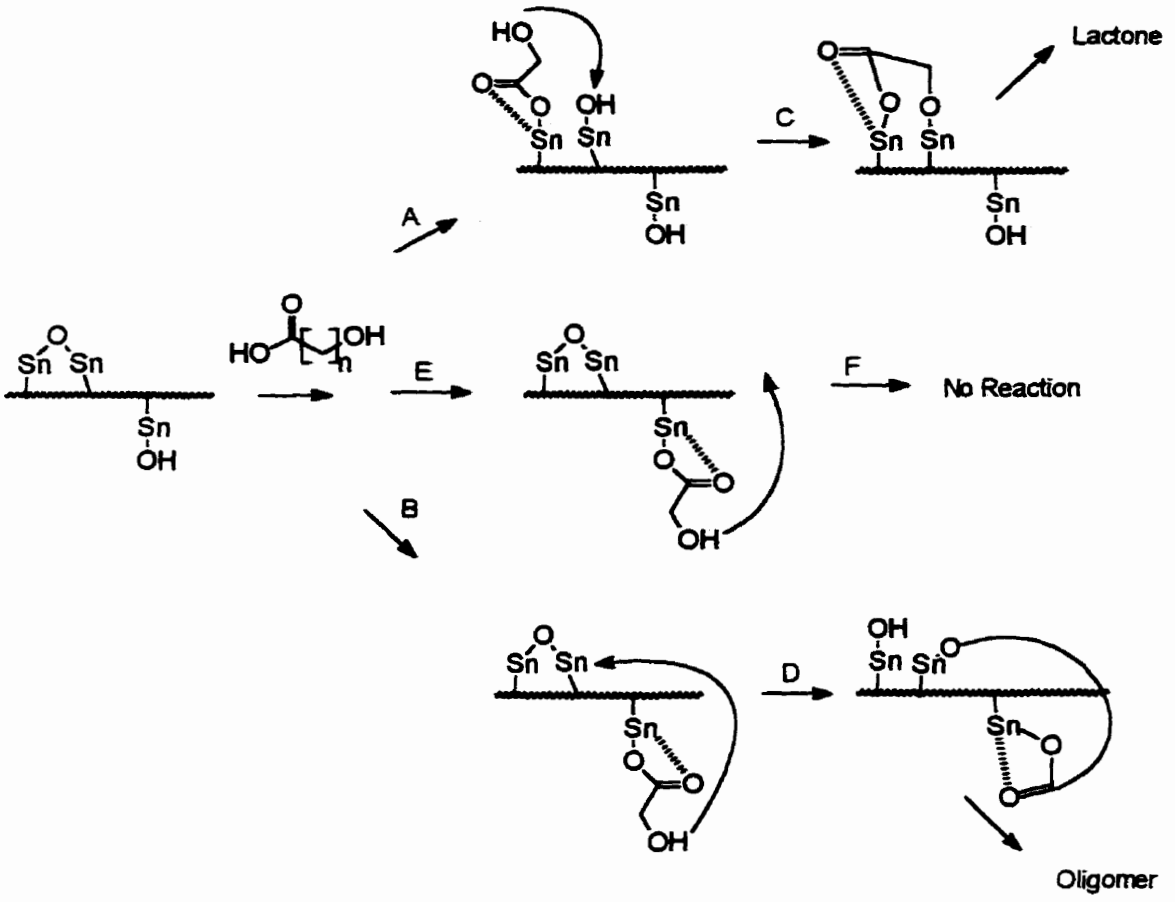

Figure 3.15: Route to lactonization by solid phase organotin catalysis

3.2.6 Conclusions

Tethering a distannoxane/stannol reagent to a polystyrene-based copolymer did give lactones of hydroxycarboxylic acids. Compared with solution phase, purification was greatly simplified by the use of a solid phase catalyst. However, no improvement in lactone yields as observed by the use of a supported organotin catalyst. No reduction in oligomeric byproducts was observed. The tethering of the catalyst to a solid phase polymer did not lead to the medium-ring size lactones previously unattainable via tin catalysis although reactions were run approximately one hundred times above the anticipated EM. The polymer does not discriminate intermolecular from intramolecular reaction.

Contrary to expectations, reduced loading capacity and hence isolated catalytic sites did not lead to improved lactone yields. It appears that stannol species yield oligomeric products and distannoxane species yield lactone products. Each of the organotin oxide copolymers in this study contained both distannoxane and stannol species, a limitation of the chlorostannane copolymer hydrolysis route to these catalysts.

It appears that diluting the tin active sites within the copolymer matrix slows reaction. This may be a consequence of the necessity of double activation for reaction to occur. Our system requires two tin species to effect the double activation. At the same time, if these two tin sites are not in close proximity, oligomers seem to predominate.

3.3 Experimental

Commercially available starting materials were used for the synthetic preparations which follow. Authentic hexadecanolide was purchased from Lancaster. All hydroxycarboxylic acids except for 7-hydroxyheptanoic acid were purchased from Aldrich. The 7-hydroxyheptanoic acid was prepared by hydrolysis of the authentic lactone. The cycloketone precursors to authentic lactones and m-choroperbenzoic acid were also purchased from Aldrich. All silica and alumina for chromatographic separations was from EM Science. BDH provided all the other reagents and solvents including HPLC eluents, potassium dihydrogen orthophosphate, phosphoric acid, and sodium borohydride.

NMR spectra were recorded on either Varian Gemini XL-200 or XL-300 instruments. All IR samples were analysed as neat powders on a Bruker ISS55 FT-IR using a diffuse reflectance infrared FT spectroscopy (DRIFTS) accessory manufactured by Spectratech. All IR data is given in Kubelka Munk units.

HPLC analyses were done using a Hewlett Packard 1047A Refractive Index Detector, SSI 300 LC Pump, Varian 905320 Pulse Damper, and Waters 746 Data Module. All solvents used with the HPLC were first filtered through FP Vericel 0.45 μm membrane filters purchased from Gelman Sciences. Prior to injection, all samples were filtered through Gelman Sciences nylon Acrodisc 0.45 μm syringe tip filters. All HPLC samples were injected manually, using a Rheodyne injector, onto a Waters Bondapack C18 10 μm reverse phase column. Eluent composition, prepared with HPLC grade solvents, varied depending on the sample being analysed.

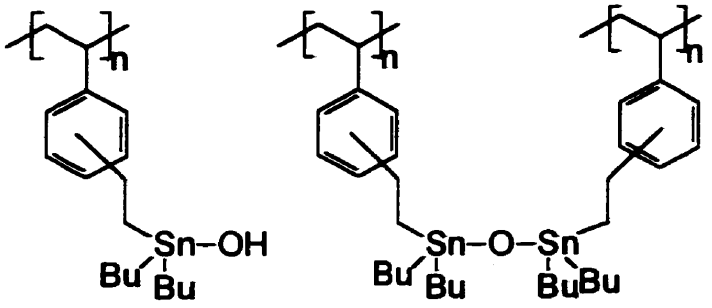

3.6 **3.7**

Preparation of a Tin Oxide (**3.6/3.7**):Poly-3- and -4-(2-(dibutylchlorostannol/distannoxane)ethyl)styrene-co-divinylbenzene

Copolymer **3.5** and copolymers **3.6/3.7** were initially prepared in Chapter 2 as compounds **2.3** and **2.12** respectively. The preparation of the hydrolysed copolymers is given again here since these polymers were used repeatedly.

High loading: A flat bottom flask was charged with polymer **3.5** (1.0628 g) and sodium hydroxide solution (50% in ethanol). The flask was left on a shaker for 16 hours then filtered through a sintered glass frit. The filter cake was washed with additional water and ethanol. All filtrate was collected and set aside for Mohr analysis. The solid was dried *in vacuo* overnight at 70°C and analysed. DRIFTS (cm^{-1}) 3026, 3010 (CH_{AR}), 2927, 2850 (CH_{ALIPH}), 1601, 1492 (C=C), 1440, 1360, 755, 703. MAS solid state ^{119}Sn NMR (swollen in $CHCl_3$) 103 (Sn-OH), 91 (Sn-O-Sn), approximately 1:3 relative intensity. Solid State MAS ^{119}Sn NMR (swollen in $CHCl_3$) +101.1 (Sn-OH), +91.1 (Sn-O-Sn), approximately 1:3 relative intensity. All copolymers (medium and low) were hydrolysed in a similar manner.

Characterization of medium loading copolymer **3.6/3.7**: DRIFTS (cm^{-1}) 3026, 3110 (CH_{AR}), 2927, 2850 (CH_{ALIPH}), 1594, 1490 (C=C), 789, 754, 705. MAS solid state ^{119}Sn NMR (swollen in $CHCl_3$) 100.8 (Sn-OH), 92.2 (Sn-O-Sn), approximately 1:2 relative intensity.

Characterization of low loading copolymer **3.6/3.7**: DRIFTS (cm^{-1}) 3060,

3026 (CH_{AR}), 2927, 2850 (CH_{ALIPH}), 1594, 1488 (C=C), 1453, 754, 705. MAS solid state ^{119}Sn NMR (swollen in $CHCl_3$) 100.6 (Sn-OH), 92.0 (Sn-O-Sn), approximately 2:1 relative intensity.

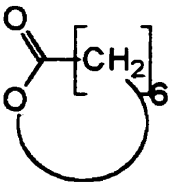

3.8

Preparation of Heptanolide - Authentic Sample (**3.8**)

Heptanolide was prepared via Baeyer-Villiger oxidation in a method similar to Meyer[21]. A single neck flask, equipped with magnetic stirbar, was charged with m-chloroperbenzoic acid (technical grade, 60% presumed, 19.52 g, 64.5 mmol), cycloheptanone (5 ml, 42.4 mmol) and dichloromethane (150 mL). The reaction was wrapped in aluminum foil and left to stir for 3 days at room temperature. TLC analysis on day 3 in 25% ethyl acetate/hexanes showed significant amounts of starting material. As a result, the flask was charged with more m-chloroperbenzoic acid (3.05 g, 10.1 mmol) and left to stir for an additional 24 hours. The reaction solution was filtered on day 4 to remove m-chlorobenzoic acid, as confirmed by ^1H NMR spectroscopy. The filtrate was washed with aqueous sodium hydroxide (0.1 N), extracted into ethyl acetate, and dried over anhydrous magnesium sulfate. Purification by silica column with an eluent beginning at 33% ethyl acetate/hexanes and ramping to 100% ethyl acetate yielded 1.95 g (65%) of a pale amber oil. ^1H NMR ($CDCl_3$) 4.27 (m, 2H, CH_2), 2.45 (m, 2H, CH_2), 1.75 (m, 2H, CH_2), 1.6 - 1.25 (m, 6H, CH_2). ^{13}C NMR ($CDCl_3$) 176.4 (C, C=O), 67.6 (CH, CH_2O), 30.9, 30.5, 28.0, 25.4, 23.5 (CH, CH_2). HRMS for $C_7O_2H_{12}$, calculated 128.0837, observed 128.0838. HPLC characterization in 35% methanol, 65% KH_2PO_4 (10 mM), pH

6.0, flow rate 1.0 mL/min, 32 x 10^{-5} RIU/FS, 40°C, retention time = 8.9 minutes.

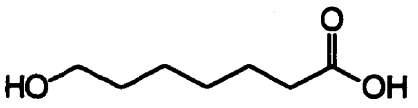

3.9

Preparation of 7-Hydroxyheptanoic Acid (**3.9**)

The hydrolysis of heptanolide **3.8** was performed in a similar manner to Yamamoto[4a]. A single neck flask, equipped with magnetic stir bar, was charged with heptanolide **3.8** (167.5 mg, 1.31 mmol) and methanol (10 mL). A saturated solution of aqueous KOH (1 mL) was added and the reaction was left to stir 24 hours at room temperature. The solution was evaporated to near dryness, redissolved in aqueous HCl (1.0 N) then extracted into ethyl acetate and dried over sodium sulfate. Subsequent purification by silica flash chromatography beginning with 33% ethyl acetate/hexanes and ramping to 100% ethyl acetate removed all starting material, leaving the product on the column. The silica was extracted with THF to yield 34.6 mg (18%) of product. ^{1}H NMR ($CDCl_3$) 7.0 (bs, 2H, OH), (m, 2H, CH_2), 2.35 (m, 2H, CH_2), 1.6 (m, 4H, CH_2), 1.35 (m, 4H, CH_2). HPLC characterization in 35% methanol, 65% KH_2PO_4 (10 mM), pH 6.0, flow rate 1.0 mL/min, 32 x 10^{-5} RIU/FS, 40°C, retention time =19.0 minutes.

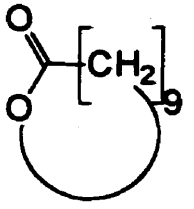

3.10

Preparation of Decanolide - Authentic Sample (**3.10**)

Decanolide preparation was attempted in a similar manner to heptanolide **3.8** in negligible yield. As a result, m-chloroperbenzoic acid was purified according to the method of Fieser[22] with phosphate buffer. This purification removed any m-chlorobenzoic acid contamination. The reaction proceeded over 5 days and was worked up as for **3.8**. A ^{1}H NMR spectrum of the crude mixture indicated only 50% reaction. As a result, the reaction was continued with additional m-chloroperbenzoic acid (purified) for another 7 days. After the combined 12 days the reaction was worked up to yield 389 mg (47%) of a yellow oil. The purification of this compound differed from **3.8**. The oil was dissolved in methanol (40 mL) and treated with $NaBH_4$ (101.1 mg, 2.8 mmol) for 45 minutes. The reaction was quenched with water and the methanol was removed *in vacuo*. The subsequent aqueous solution was extracted with dichloromethane and dried over anhydrous magnesium sulfate. The resulting oil was applied to an alumina column and eluted with 25% ethyl acetate/hexanes ramping tc 100% ethyl acetate to yield 114.0 mg (11%) of a pale yellow oil. ^{1}H NMR (CDCl3) 4.2 (m, 2H, CH_2), 2.35 (m, 2H, CH_2), 1.7 (m, 4H, CH_2), 1.6 - 1.2 (m, 10H, CH_2). MS for $C_{10}O_2H_{18}$, calculated 170.1307, observed 170.1306. HPLC characterization in 50% methanol, 50% KH_2PO_4 (10 mM), pH 6.0, flow rate1.0 mL/min, 32 x 10^{-5} RIU/FS, 40°C, retention time = 31.4 minutes.

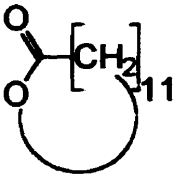

3.11

Preparation of Dodecanolide - Authentic Sample (**3.11**)

Dodecanolide was prepared in a similar manner to decanolide **3.10** with the exception that technical grade m-chloroperbenzoic acid (60% approximately) was used directly without purification. The reaction proceeded over 6 days with additional m-chloroperbenzoic acid added on days 4 and 5. Work-up and subsequent treatment with $NaBH_4$ followed by alumina column chromatography yielded 3.58 g (71%) of a pale yellow oil. ^1H NMR ($CDCl_3$) 4.15 (m, 2H, CH_2), 2.35 (m, 2H, CH_2), 1.65 (m, 4H, CH_2), 1.5 - 1.25 (m, 14H, CH_2).MS for $C_{12}O_2H_{22}$, calculated 198.1619, observed 198.1614. HPLC characterization in 65% methanol, 35% KH_2PO_4 (10 mM), pH 6.0, flow rate1 mL/min, 32 x 10^{-5} RIU/FS, 40°C, retention time = 44.9 minutes.

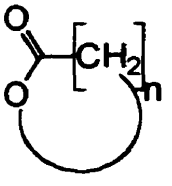

n = 6 **3.8**
n = 9 **3.10**
n = 11 **3.11**
n=15 **3.12**

General Preparation: Lactonization of ω-Hydroxycarboxylic Acids using Organotin Oxide Copolymer **3.6/3.7** as Catalyst (**3.8**, **3.10**, **3.11**, **3.12**)

Lactonization reaction conditions, using the organostannane copolymer **3.6/3.7** as catalyst, were optimized for 16-hydroxyhexadecanoic acid. All subsequent lactonizations of various ring sizes were then attempted in a similar manner. The preparation of hexadecanolide is provided as an example of the optimized reaction conditions.

A single neck flask, equipped with a magnetic stir bar, was charged with 16-hydroxyhexadecanoic acid (345.6 mg, 1.27 mmol), organostannane copolymer **3.6/3.7** (1.7 mmol/g, 87.7 mg, 0.13 mmol), and mesitylene (45 mL). The flask was fitted with a Dean Stark trap and condensor and left to reflux for 19 hours. The reaction solution was filtered, washing the solid with fresh mesitylene and chloroform, and the filtrate concentrated *in vacuo*. Trituration of the resultant residue in methanol, followed by centrifugation gave a solution of lactone product which was diluted to a known volume. The solid remaining after trituration was identified as oligomeric polylactones and their characterization is detailed elsewhere in this section. The solution of lactone product was then injected onto an HPLC. HPLC conditions: 85% methanol, 15% H_2O (1 mL H_3PO_4/ 1 L), pH 3.0, flow rate 1 mL/min, 32 x 10^{-5} RIU/FS, 40°C. The resulting peak area was compared to HPLC calibration curves constructed for both authentic hexadecanolide (retention time = 16.5 minutes) and 16-hydroxyhexadecanoic acid (retention time = 7.6 minutes). HPLC indicated a lactonization yield of 55% with less than 1% 16-hydroxyhexadecanoic acid starting material left unreacted. Gravimetric analysis of the solid left after trituration indicated a 27% yield of polylactone by-products.

Characterization of Solid Byproducts from Lactonization of 16-Hydroxyhexadecanoic Acid

The solid remaining after trituration was dried *in vacuo* and analysed by ^{1}H NMR ($CDCl_3$) 4.1 (m, 2H, CH_2), 2.3 (m, 2H, CH_2), 1.6 (m, 4H, CH_2), 1.4 - 1.2 (m, 22H, CH_2). DRIFTS 2942, 2857 (aliphatic CH), 1728 (ester C=O). LR-MS indicated peaks at 255, 490, 744, and 998 which coincides with monomer through tetrameric polylactones.

Camphor freezing point depression was used as an independent means of determining average molecular weight. Authentic hexadecanolide was used to prepare a standard calibration curve. A known amount of camphor and

hexadecanolide were melt mixed in a test tube with the aid of a small stir bar. A thermometer was inserted into the melt through a close-fitting stopper. A disposal needle pierced the stopper to act as a pressure vent. The temperature was recorded at the onset of crystallization with various concentrations of hexadecanolide. Each sample was analysed in duplicate.

Standard Curve - Hexadecanolide and Camphor Freezing Points		
mmol/g camphor	freezing point #1	freezing point #2
control	178.0	177.0
0.633	148.5	148.0
0.177	168.0	167.5
0.101	171.5	172.0

The data was analysed by linear regression using least squares method to yield: $y = -42.40x + 176.62$ ($r^2 = 0.9859$).

The same procedure was used with the solid isolated after trituration and the slopes of each line were compared to determine the average molecular weight of the polylactone products at 585.89 +/- 15.9 g/mol. This is approximately 2 monomer units (254 g/mol) per polylactone.

Solid Isolated from Trituration After Lactonization - Camphor freezing Point Depression		
mg compound/g camphor	freezing point #1	freezing point #2
41.46	173.0	172.5
131.42	167.5	167.5

Characterization of Solid Byproducts from Lactonization of 12-Hydroxydodecanoic Acid

The solid remaining after trituration was dried *in vacuo* and analyzed by ^{1}H NMR ($CDCl_3$) 4.15 (m, 2H, CH_2), 2.35 (m, 2H, CH_2), 1.65 (m, 4H, CH_2), 1.5 - 1.25 (m, 14H, CH_2). LR-MS by CI indicated peaks at 199, 397, 595, 793, and 989 which coincides with monomeric through pentameric lactone products. Camphor freezing point depression was used to determine molecular weight in a similar manner to the hexadecanoic polylactone products. Cyclododecanone was used to prepare a standard curve. Dodecanolide, the authentic lactone prepared by an independent method was also analyzed by this technique to confirm the method's accuracy.

Standard Curve - Cyclododecanone and Camphor Freezing Points		
mmol/g camphor	freezing point #1	freezing point #2
control	177.0	176.5
0.57	153.5	153.0
0.42	158.5	159.0
0.29	164.5	163.0
0.14	169.5	169.5
0.09	172.5	172.0

The data was analysed by linear regression using least squares method to yield: $y = -40.67x + 175.87$ ($r^2 = 0.9928$).

The same procedure was used with authentic dodecanolide and the slopes of each line were compared to determine the average molecular weight of the compound at 189.07 +/- 5.1 g/mol.

Authentic Dodecanolide and Camphor Freezing Point Depression		
mg/g camphor	freezing point #1	freezing point #2
104.17	153.15	154.0
70.81	161.0	160.5
21.82	170.5	170.0

Applying the same method to the solid isolated after trituration from the lactonization of 12-hydroxydodecanoic acid and comparing the slope to the standard curve obtained for cyclododecanone, gave an average molecular weight of 911 +/- 1.9 g/mol. This corresponds to approximately four and a half monomeric units (198 g/mol) per polylactone.

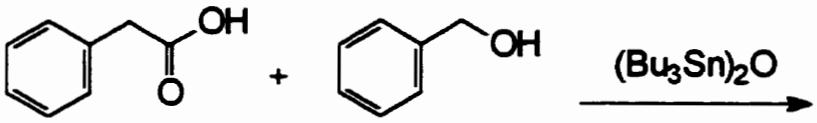

3.14 **3.15**

Competition Studies: Reaction of Hexa-*n*-Butyldistannoxane with Benzyl Alcohol and Phenylacetic Acid

A single neck flask, equipped with magnetic stir bar, was charged with benzyl alcohol **3.15** (80.4 mg, 0.74 mmol), phenylacetic acid **3.14** (103.1 mg, 0.76 mmol), and benzene (25 mL). Hexa-*n*-butyldistannoxane (451.0 mg, 0.76 mmol) was added. The flask was fitted with a Dean Stark trap and condensor with argon inlet, then left to reflux. After 16 hours, a reaction aliquot was removed and analyzed by ^{119}Sn NMR spectroscopy. ^{119}Sn NMR (benzene-d_6) 89.2 (brs, Sn-O-Sn), 102 (brs, Sn-OH), 104.5 (Sn-O-C(O)R)).

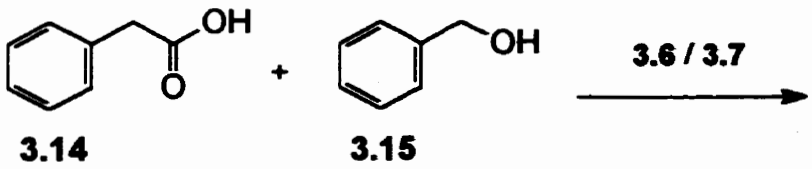

3.14 **3.15**

Competition Studies: Reaction of Organostannane Polymer **3.6, 3.7** with Benzyl Alcohol and Phenylacetic Acid

A single neck flask, equipped with magnetic stir bar, was charged with organostannol/stannoxane copolymer **3.6/3.7** (1.67 mmol/g, 298.3 mg, 0.50 mmol), benzyl alcohol **3.15**, (23 µL, .22 mmol), phenylacetic acid **3.14** (30.4 mg, .22 mmol), and benzene (15 mL). The flask was fitted with a Dean Stark trap and condensor with drying tube and left to reflux 2 hours. The polymer was filtered under an inert atmosphere and rinsed with fresh benzene. DRIFTS analysis was performed attempting to keep air exposure at a minimum. DRIFTS 3088, 3020 (CH_{AR}), 2958, 2917, 2862 (CH_{ALIPH}), 1649 (Sn-O-C(O)R), 1620, 1580 (C=C), 1066, 792, 703. There were no atypical absorptions in the 1200 - 900 cm^{-1} region.

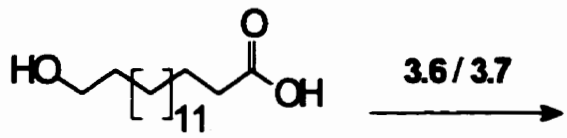

Competition Studies: Reaction of Organostannol/stannoxane Polymer with Equimolar 16-Hydroxyhexadecanoic Acid

A single neck flask, equipped with magnetic stir bar, was charged with 16-hydroxyhexadecanoic acid (59.4 mg, 0.22 mmol), organostannol/stannoxane polymer (1.8 mmol/g, 123.3 mg, 0.22 mmol) and benzene (15 mL). The flask was fitted with a dean stark trap and condensor with drying tube and left to

reflux. After 1 hour an aliquot was removed and filtered under an inert atmosphere, rinsing with fresh benzene. An additional aliquot was removed at 4 hours. DRIFTS analysis was performed attempting to keep air exposure at a minimum for both samples. DRIFTS 1 hour aliquot: 3320 (alcohol), 3020 (CH_{AR}), 2929, 2856 (CH_{ALIPH}), 1637 (Sn-O-C(O)-R), 1604, 1557 (C=C), 1062, 794, 707. The 4 hour aliquot gave essentially the same DRIFTS spectrum. No absorbances were observed in the 1800 - 1650 cm^{-1} or 1200 - 900 cm^{-1} regions for either aliquot.

3.4 References

1. Bryskier, A.J.; Butzler, J.P.; Neu, H.C.; Tulkens, P.M. Macrolides - Chemistry, Pharmacology and Clinical Uses **1993**, Arnette-Blackwell, Paris.
2. (a) Paterson, I.; Mansuri, M.M. *Tetrahedron* **1985**, *41*, 3569. (b) Rousseau, G. *Tetrahedron* **1995**, *51*, 2777. (c) Ogliaruso, M.A.; Wolfe, J.F. Synthesis of Lactones and Lactams **1993**, John Wiley and Sons, New York.
3. (a) Masamune, S.; Hayase, Y.; Chan, W.K.; Sobczak, R.L. *J. Am. Chem. Soc.* **1976**, *98*, 7874. (b) Corey, E.J.; Nicolau, K.C.; Melvin Jr.; L.S. *J. Am. Chem. Soc.* **1975**, *97*, 654. (c) Masamune, S.; Kim, C.U.; Wilson, K.E.; Spessard, G.O.; Georghiou, P.E.; Bates, G.S. *J. Am. Chem. Soc.* **1975**, *97*, 3512.
4. (a) Ishihara, K.; Kubota, M.; Kurihara, H.; Yamamoto, H. *J. Org. Chem.* **1996**, *61*, 4560 and references cited therein. (b) Kriuzinga, W.H.; Kellog, R.M. *J. Am. Chem. Soc.* **1981**, *103*, 5183. (c) Kuno, H.; Shibagaki, M.; Takahashi, K.; Honda, I.; Matsushita, H. *Chem. Lett.* **1992**, 571. (d) Mukaiyama, T.; Izumi, J.; Shiina, I. *Chem. Lett.* **1997**, 187.
5. Mascaretti, O.A.; Furlan, R.L.E. *Aldrichimica Acta* **1997**, *30*, 55.
6. Otera, J.; Yano, T.; Kawabata, A.; Nozaki, H. *Tetrahedron Lett.* **1986**, *27*, 2383.
7. (a) Steliou, K.; Poupart, M.A. *J. Am. Chem. Soc.* **1983**, *105*, 7130. (b) Otera, J.; Yano, T.; Himeno, Y.; Nozaki, H. *Tetrahedron Lett.* **1986**, *27*, 4501. (c) White, J.D.; Green, N.J.; Fleming, F.F. *Tetrahedron Lett,* **1993**, *34*, 3515.
8. Pommier, J.C.; Pereyre, M. Advances in Chemistry Series Zuckerman, J.J. (Ed), **1976**, Vol 157, American Chemical Society, Washington.
9. Steliou, K.; Szcygielska-Nowosielska, A.; Favre, A.; Poupart, M.A.;

Hanessian, S. *J. Am. Chem. Soc.* **1980**, *102*, 7578.

10. Davies, A.G.; Kleinschmidt, D.C.; Palan, P.R.; Vasishtha, S.C. *J. Chem. Soc. (C)* **1971**, 3972.
11. Pommier, J.C.; Delmont, B.; Valade, J. *Tetrahedron Lett.* **1967**, *52*, 5289.
12. Illuminati,G.; Mandolini, L. *Acc. Chem. Res.* **1981**, *14*, 95.
13. Kirby, A. Advances in Physical Organic Chemistry Volume 17, Gold; Bethel (Ed) **1980**, Academic Press, London and references cited therein.
14. Galli, C.; Mandolini, L. *J. Chem. Soc. Chem. Commun.* **1982**, 251.
15. Ookoshi, T.; Onaka, M. *Tetrahedron Lett.* **1998**, *39*, 293.
16. Davies, A.G. Organotin Chemistry **1997**, VCH, Weinheim.
17. Hodge, P. Polymer Supported Reactions in Organic Synthesis Sherington, D.C.; Hodge, P. (Ed) **1980**, Wiley and Sons, Chichester.
18. Silverstein, R.M.; Bassler, G.C.; Morrill, T.C. Spectrophotometric Identification of Organic Compounds 5th Ed **1991**, John Wiley and Sons, New York.
19. Atkins, P.W. Physical Chemistry 4th Ed **1990**, Freeman and Company, New York.
20. Smith, P.J.; White, R.F.M.; Smith, L. *J. Organomet. Chem.* **1972**, 40, 341.
21. Meyer, W.L.; Patterson, W.T.; Reed, S.A.; Leister, M.C.; Schneider, H.J.; Schmidt, G.; Evans, F.E.; Levine, R.A. *J. Org. Chem.* **1992**, *57*, 291.
22. Fieser, L.F.; Fieser, M. Reagents for Organic Synthesis **1967**, Wiley, New York.

Appendices

Appendix A

Lisinopril Spectral Characterization

As discussed in Section 1.2.3.4, a ^1H NMR spectroscopic diagnostic for successful amide bond formation with Lisinopril was required. An amide of Lisinopril and m-iodobenzoic acid was prepared and attempts were made to characterized it by ^1H NMR spectroscopy. This characterization proved very difficult and we found it necessary to return to Lisinopril, characterizing the starting material by both ^1H and ^{13}C NMR spectroscopy. A brief explanation of the step by step characterization of Lisinopril, along with some representative spectra, is included below.

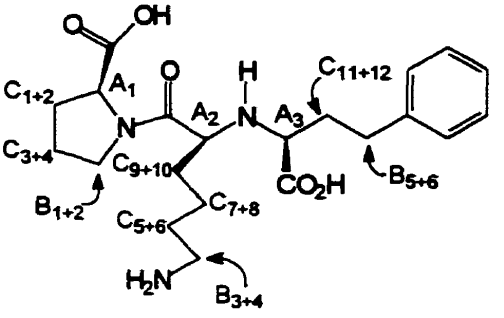

1.1

1) Lisinopril was divided into four types of protons, A through C and aromatics. These divisions were based on anticipated chemical shifts as calculated from chemical shift tables[1].

2) Beginning with the proton spectrum, the aromatic protons of Lisinopril are quite distinct. The aromatic signal at 7.1 - 7.4 ppm is attributed to five protons. With this information, each signal could be assigned a relative integration as indicated at the base of each peak in Figure A.1.

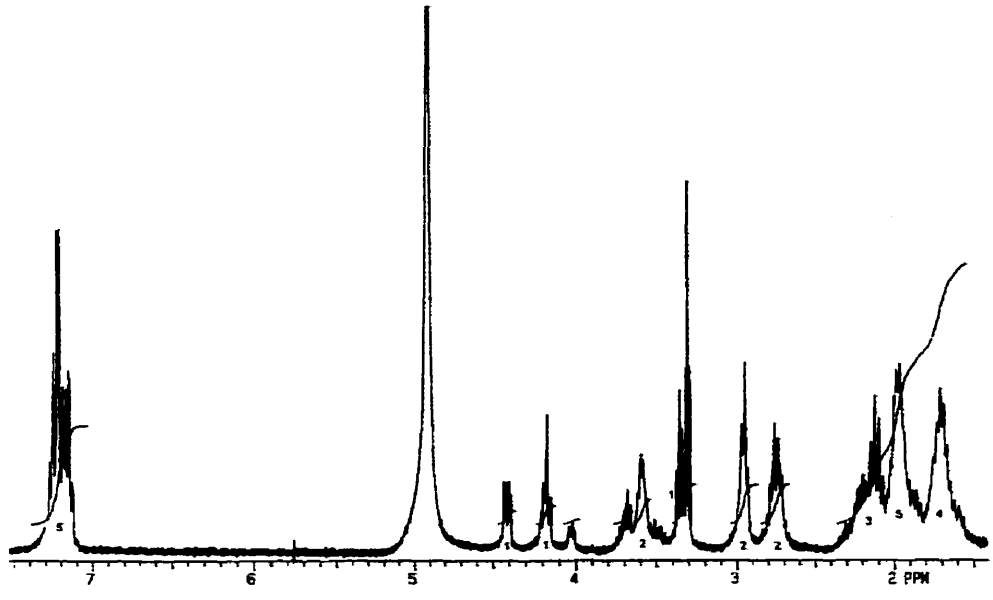

Figure A.1: ^{1}H NMR spectrum of Lisinopril

3) From the DEPT (fully edited, not included), 2 methine signals were apparent at 63 and 59 ppm. By HETCOR, the carbon at 63 ppm correlated to two proton signals. The only non-aromatic methine protons were of 'A' type. In addition, the proton signals for each of the three correlations from the HETCOR integrated for one proton. The 'A' protons had been located in the ^{1}H NMR spectrum as indicated in Figure A.2.

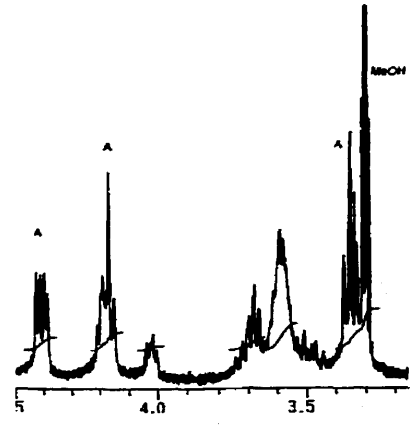

Figure A.2: Expansion of ^{1}H NMR spectrum of Lisinopril

4) A methylene signal, as determined from the DEPT spectrum, correlated to two proton signals in the HETCOR as indicated on the partial spectrum in Figure A.3. From the integration values determined in Figure A.1, one of these correlations integrates for one proton. From this information, each proton on this methylene carbon must be distinct. In addition, the chemical shift of this methylene suggested it was a 'C' type.

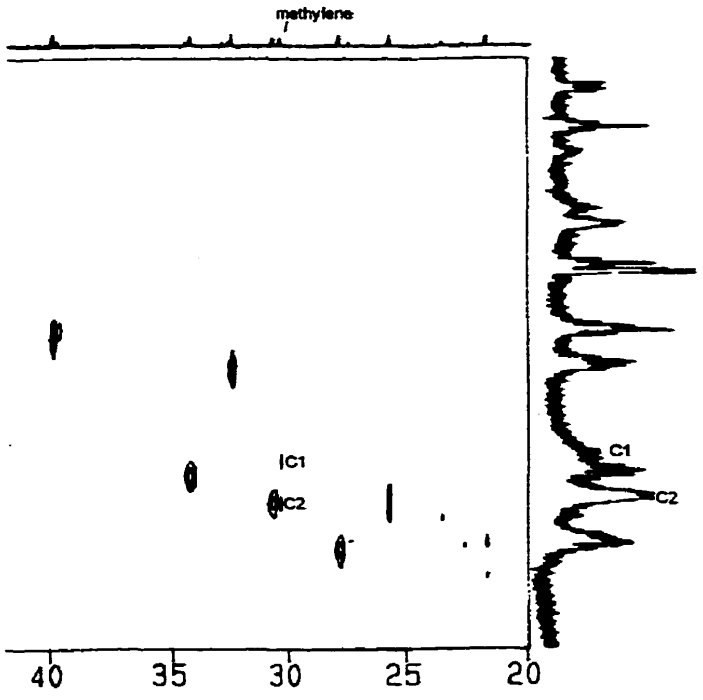

Figure A.3: Partial HETCOR spectrum for lisinopril

5) From the COSY, this split proton 'C' signal correlated to an 'A' type at 4.4 ppm, as indicated in the COSY spectrum of Figure A.4. Presumably, the only distinct geminal protons should be located on the proline ring of Lisinopril, one above the plane of the ring and one below. These protons had been assigned as C_{1+2}, adjacent to A_1 on the proline ring.

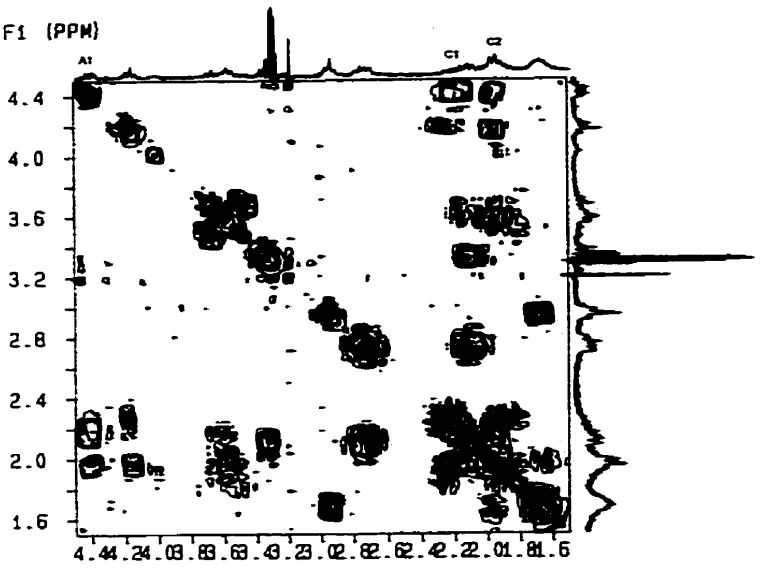

Figure A.4: COSY spectrum of Lisinopril

6) Protons C_{1+2} correlated back into the C_2 proton signal in the COSY. This C_2 signal integrated for 5 protons. Thus C_{3+4} had been assigned as well. Completing the proline ring, C_{3+4} showed a correlation in the COSY to a signal appropriate for a 'B' type as indicated in Figure A.5. This signal integrates for two protons and was assigned as B_{1+2}. Thus the first definite assignments had been made.

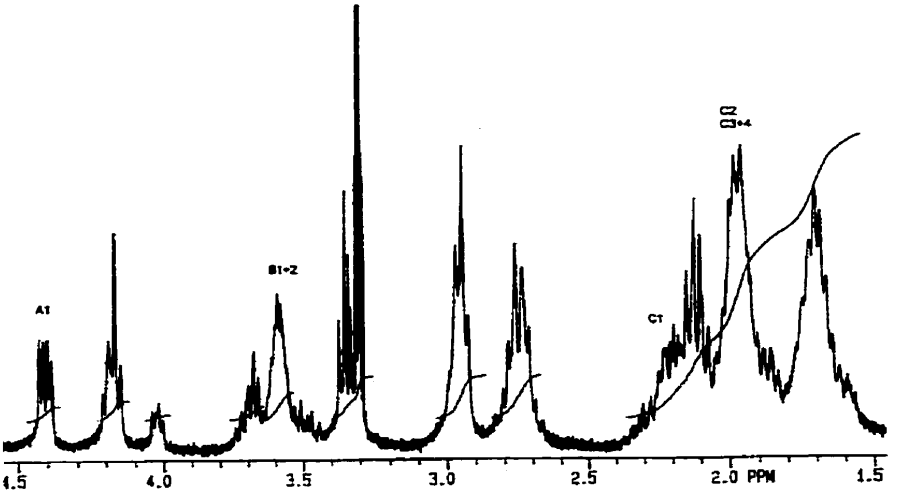

Figure A.5: Expansion of ^{1}H NMR spectrum of Lisinopril

7) Returning to the alkyl expansion from the ^{1}H NMR spectrum, DEPT had indicated that all of these signals were methylenes. One signal at 2.2 ppm integrated for two protons, as indicated on Figure A.6. The other alkyl integrations are also included at the base of each signal in this expansion.

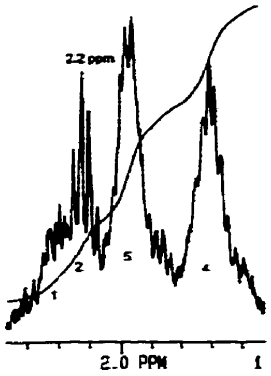

Figure A.6: Expansion of ^{1}H NMR spectrum of Lisinopril

8) The COSY had indicated that this peak at 2.2 ppm correlated to two signals. Since no other carbons had indicated nonequivalent geminal protons in the HETCOR and no single 'C' type is wedged between two 'B' type methylenes within Lisinopril, then the signal correlates to both an 'A' type and a 'B' type as indicated in the COSY of Figure A.7.

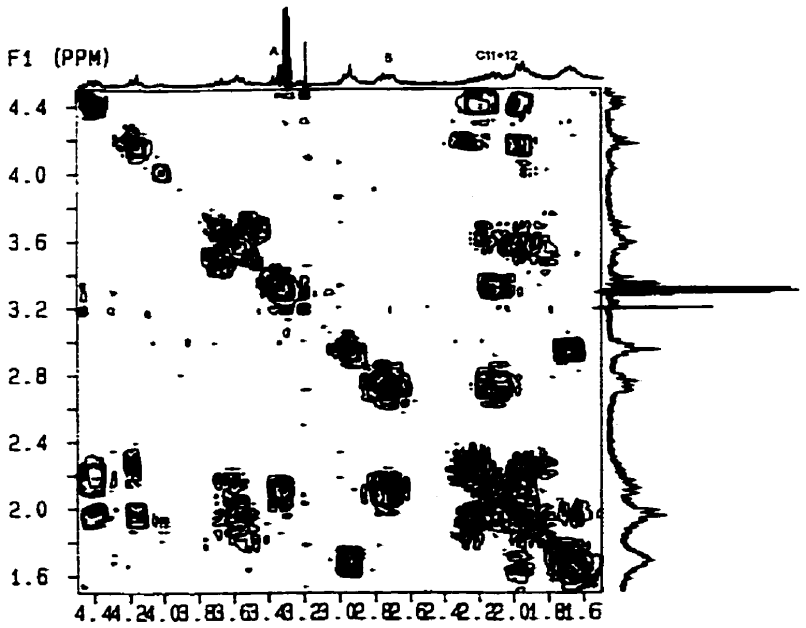

Figure A.7: COSY spectrum of Lisinopril

9) Only one 'C' type methylene, C_{11+12}, is wedged between an 'A' and 'B', identification of the aromatic linker arm had thus been completed as indicated in Figure A.8.

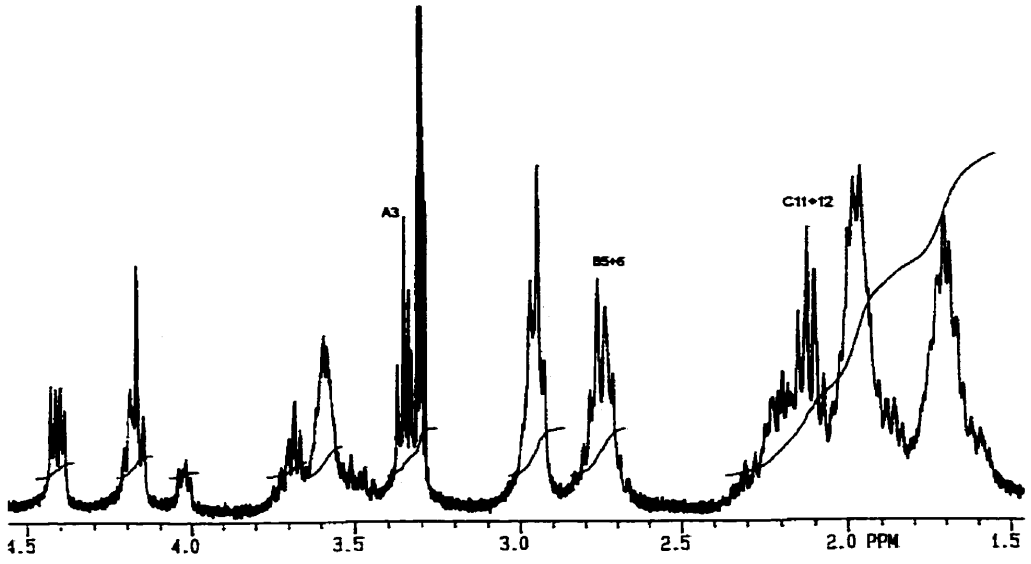

Figure A.8: ^{1}H NMR spectrum of Lisinopril

10) The only unassigned signals that remained were attributed to the lysyl side chain of Lisinopril. By elimination, 4.2 ppm is the only 'A' type remaining and was assigned A_3. Similarly, B_{3+4} were assigned to 2.95 ppm in the ^{1}H NMR spectrum. In the COSY, the A_3 and B_{3+4} signals both correlate to a 'C' type signal. This signal integrated for four protons so A_3 must correlate to a 'C' type methylene that is coincident with a 'C' type methylene correlating to B_{3+4}.

11) This combined 'C' type signal is assigned C_{5+6} and C_{9+10}, from the COSY. These four protons correlate to only one other signal at 1.7 ppm. This signal integrated for 5 protons originally. Subtracting the previously assigned C_2 and C_{3+4}, this leaves two protons, thus C_{7+8} have been assigned.

The ^{1}H NMR spectrum, with complete assignments is shown in Figure A.9. The

lysyl side chain assignments were confirmed from a TOCSY of a Lisinopril derivative. These assignments, particularly that of protons B_{3+4}, provided a spectral diagnosis for amide formation.

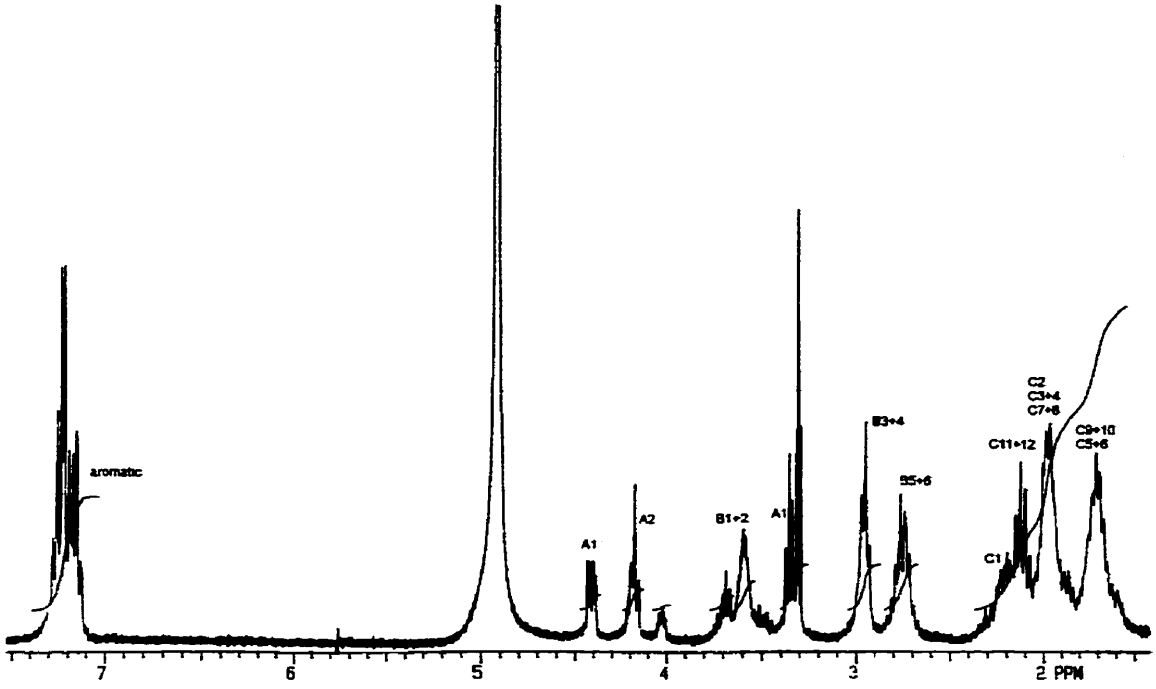

Figure A.9: Fully assigned ^1H NMR spectrum of Lisinopril

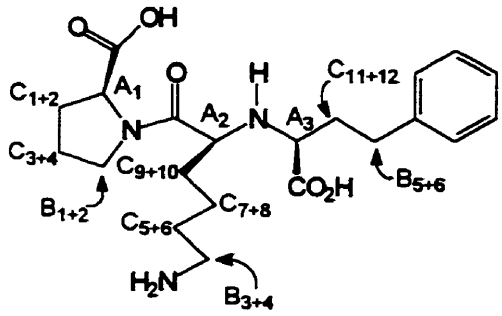

1.1

References:

1. Silverstein, R.M.; Bassler, G.C.; Morrill, T.C Spectrophotometric Identification of Organic Compounds 5 th Edition, **1991**, John Wiley and Sons, New York.

Appendix B

Crystal Structure Determination Summary

The single crystal x-ray structure was solved by Dr. J.J. Vittal, formerly of the University of Western Ontario and now located at the National University of Singapore.

X-ray Structure Determination:

Colourless 'block-like' single crystals of suitable size and quality were grown by diffusion method from a mixture of MeOH and water. A crystal with the size 0.54 x 0.20 x 0.19 mm, was chosen, mounted at the end of a glass fibre and used for diffraction experiments. The data were collected on a Siemens P4 diffractometer with sealed molybdenum tube (Mo Kα), scintillation counter and XSCANS[1] software package at 27°C. A total of 5659 reflections were collected in the θ range 2.38 to 30.0° ($-1 \leq h \leq 12$, $-1 \leq k \leq 14$, $-24 \leq \ell \leq 24$) using θ-2θ scans. Four standard reflections were monitored for every 296 reflections collected. The data crystal was face-indexed and the distances between them were measured for absorption correction. *SHELXTL* [2] programs were employed for data processing and the least-squares refinements on F^2. In the monoclinic system, for Z = 4, the space group $P2_1/c$ was determined from the systematic absences. All the non-hydrogen atoms were refined anisotropically. All the hydrogen atoms were located in the difference Fourier routine and were placed in the ideal positions for the purpose of structure factor calculations only. A common isotropic thermal parameter was refined for the H atoms. In the final least-squares refinement cycles on F^2, the model converged at R1 = 0.0532, wR2 = 0.1275 and Goof = 1.066 for 1803 observations with Fo $\geq 4\sigma$(Fo) and 160 parameters, and R1 = 0.1373, wR2 = 0.1536 for all 4353 data. The final difference Fourier synthesis the electron density fluctuates in the range 0.271 to -0.297 e $Å^{-3}$. There were no shift in the final cycles. An extinction coefficient was refined to 0.049(3). The experimental details and crystal data, the positional and thermal parameters, bond distances and angles, anisotropic

thermal parameters, hydrogen atom coordinates and selected torsion angles have been submitted to the Cambridge Crystallographic Data Centre.

References

1. XSCANS, Ver. 2.1, Siemens Analytical X-Ray Instruments Inc. **1994** Madison, USA.
2. SHELXTL Software "version 5.0", Siemens Analytical X-Ray Instruments Inc. **1994** Madison, Wisconsin, USA.

Table A1. Crystal Data

Empirical formula	$C_9H_{18}N_6S_2$
Formula weight	274.41
Temperature	27°C
Wavelength	0.71073 Å
Crystal system	Monoclinic
Space group	$P2_1/c$
Unit cell dimensions	a = 8.678(1)Å
	b = 10.031(1)Å
	c = 17.415(3)Å
	β = 100.13(1)°
Volume	1492.3(3) $Å^3$
Z 4	
Density, calcd.	1.221 $g.cm^{-3}$
Absorption coefficient	0.347 mm^{-1}
Independent reflections	4353 (R(int) = 0.0466)
Refinement method	Full-matrix least-squares on F^2
Data/restraints/parameters	1803/0/160
Goodness-of-fit (GooF) on F^2	1.066
Final R indices [I>2sigma(I)]	R1 = 0.0532, *w*R2 = 0.1275
R indices (all data)	R1 = 0.1373, *w*R2 = 0.1536

$R1 = \Sigma(||F_o| - |F_c||)/\Sigma|F_o|$;
$wR2 = [\Sigma w(F_o^2 - F_c^2)^2/\Sigma wF_o^4]^{1/2}$
$GooF = [\Sigma w(F_o^2 - F_c^2)^2/(n-p)]^{1/2}$
where n is the number of reflections and p is the number of parameters refined.